THE DYNAMIC SAMPLING PLATFORM (DSP) FOR REAL-TIME BIOREACTOR MONITORING

A Dissertation
Presented to
The Academic Faculty

by

Mason A. Chilmonczyk

In Partial Fulfillment
of the Requirements for the Degree
Doctor of Philosophy in the
School of Mechanical Engineering

Georgia Institute of Technology
August 2020

THE DYNAMIC SAMPLING PLATFORM (DSP) FOR REAL-TIME BIOREACTOR MONITORING

Approved by:

Dr. Andrei G. Fedorov, Advisor
School of Mechanical Engineering
Georgia Institute of Technology

Dr. Peter A. Kottke
School of Mechanical Engineering
Georgia Institute of Technology

Dr. David N. Ku
School of Mechanical Engineering
Georgia Institute of Technology

Dr. Robert E. Guldberg
Phil and Penny Knight Campus for Accelerating Scientific Impact
University of Oregon

Dr. Oliver Brand
School of Electrical Engineering
Georgia Institute of Technology

Date Approved: August, 2020

To John “Chil” Chilmonczyk

ACKNOWLEDGEMENTS

I have grown more than I thought possible thanks to the enthusiastic support of Dr. Andrei Fedorov and Dr. Peter Kottke. You ensured that I was my best during some of the hardest times of my life. If I could make one choice again, it would be to work with you both. It has been a privilege and an honor to share this journey and I look forward to more.

My friends and family, for which the list is possibly endless, thank you so much for enduring my wild rants about my research and nodding approvingly all the while. My sister, Samantha, has always and will always be my hero, number one fan, and best friend. Thank you to the entire Georgia Tech cleanroom staff and user base, in no particular order: Mikkel, Vinny, Thomas, Gary, Ben, Todd, Benoit, Anosh, and Joe (note: this is not an exhaustive list). The friendships formed in cleanrooms last a lifetime, particularly those formed on nights and weekends. I would be remiss not to thank the MISC lab for their support professionally and personally. Special thanks to Austin and Joel for sharing stories, laughs, and meals together. To Peter and Curtis, cheers for getting me through my first class at Tech and sticking with me all the way to the end. Thank you to CMaT, MC3M, and especially, Gilad Doron for all the patience and support navigating cell biology.

The work described is supported by NSF ERC (CMaT) Award 1648035, MC3M Collaboration Grant in Cell Manufacturing, The Georgia Tech Foundation, and the GRA. Partial support was also provided by Grant Numbers R21GM103539 and RO1GM112662 from the National Institute of General Medical Science (NIGMS), a component of the National Institutes of Health (NIH). MC was supported by the Renewable Bioproducts Institute Fellowship. Device micro-fabrication was performed using NSF supported NNIN facilities at Georgia Tech's Institute for Electronics and Nanotechnology (IEN).

TABLE OF CONTENTS

LIST OF TABLES

LIST OF FIGURES

LIST OF SYMBOLS AND ABBREVIATIONS

2D	Two-dimensional
3D	Three-dimensional
AA	Acetic Acid
AMI	Acetone, Methanol, IPA Cleaning Protocol
CAD	Computer Aided Design
CAR-T cell	Chimeric Antigen Receptor T Cell
CE	Capillary Electrophoresis
CFD	Computational Fluid Dynamics
$C_{freestream}$	Concentration (mol/m^3) in Free Stream Outside of Boundary Layer
CMC	Chemistry, Manufacturing, and Controls
$C_{membrane}$	Concentration (mol/m^3) on Top Surface of Al_2O_3 Membrane
CMOS	Complimentary Metal-Oxide Semiconductor
CNC	Computer Numerically Controlled
CQA	Critical Quality Attribute
Cyt c	Cytochrome c

D_{ab}	Binary Diffusion Coefficient (m^2/s)
DI	Deionized
DSI	Dynamic Sampling Interface
DSP	Dynamic Sampling Platform
ESI	Electrospray Ionization
FDA	Federal Drug Administration
FTIR	Fourier Transform Infrared Spectroscopy
GMP	Good Manufacturing Practice
h_c	Mass Transfer Coefficient for Conditioner Channel (m/s)
HPLC	High Performance Liquid Chromatography
HUVEC	Human Umbilical Vein Endothelial Cell(s)
I_{avg}	Averaged Intensity Over +/- 0.3 m/z (Section 3.3)
ICP	Inductively Coupled Plasma
$I_{Cyt\ c}$	Intensity of Identified Cyt c Peak (Section 3.3)
IPA	Isopropyl Alcohol
IR	Infrared

$J^{''}$	Convective Flux (mol/m^2)
LC	Liquid Chromatography
LOD	Limit of Detection
mAb	Monoclonal Antibody
MALDI	Matrix Assisted Laser Desorption Ionization
MC3T3-E1	Murine Preosteoblast Cells
m-NBA	3-Nitrobenzyl Alcohol
MRL	Market Readiness Level
MS	Mass Spectrometry
MSC	Mesenchymal Stromal Cell(s)
NHLF	Normal Human Lung Fibroblasts
NMR	Nuclear Magnetic Resonance Spectroscopy
PAT	Process Analytical Technology
PBS	Phosphate Buffered Saline
PCA	Principal Component Analysis
PEEK	Polyether Ether Ketone

Q	Volumetric Flow Rate
RIE	Reactive Ion Etching
SNR	Signal-to-Noise Ratio

SUMMARY

Biomanufacturing for advanced therapies depends on the reliable and reproducible growth of cells. In some cases, the cells produce biomolecules that are the value-added product, while in other workflows the cells themselves are the final product. These cells, whether they are *in vitro* or *in vivo*, secrete biomolecules continuously. These secreted factors may have anti-inflammatory effects, signal neighboring cells for differentiation, or they may even be designer proteins with therapeutic potential that cells are engineered to produce. In most biomanufacturing workflows these secreted metabolites, exosomes, proteins, and other biological factors can also serve as the critical quality attributes (CQAs) that indicate current process state and final product quality. Researchers and industry professionals utilize a suite of sensor technologies to characterize the CQAs, but generally these analysis techniques suffer from a lack generality and granularity in the information they provide. Common approaches are i) unable to provide high resolution transient data for feedback input, ii) targeted, and therefore incapable of discovering which quality attributes serve as CQAs, and/or iii) bulk sensors that average otherwise potentially highly heterogeneous data.

The Dynamic Sampling Platform (DSP) is a technology for real-time analysis of the chemical content of bioreactors. It synergistically combines aseptic, spatially resolved, direct-from-reactor sampling with inline sample treatment and rapid electrospray ionization mass spectrometry (ESI-MS) sensing to fill the void of existing process analytical technologies for real-time biomarker monitoring in biomanufacturing. DSP samples non-invasively from near where cells are growing to capture the rich microenvironment, with high relative concentrations of biomarkers, and subsequently

treats these samples for real-time electrospray ionization mass spectrometry (ESI-MS) analysis. ESI-MS is a powerful analytical technology for the detection of biomolecules, but it is hindered by a need for extensive sample treatment which has made the technique largely an offline approach. The DSP utilizes a novel "active sample treatment" to prepare complex biochemical samples for ESI-MS by conditioning the sample via selective salt removal, MS enhancing chemical infusion, and CQA biomolecule retention. The DSP is produced by employing advanced microfabrication techniques that allow for scalable and reproducible production of the device. The final device utilizes a micro-mass exchanger which replaces time consuming sample preparation steps with a ~1 second flow through reactor.

This thesis outlines the design and system level integration of DSP for advanced biomanufacturing workflows. The batch microfabricated mass exchanger is combined with the dynamic sampling interface (DSI), a fluidic handling system for spatially resolved sample uptake, and an ion transfer interface for transmitting analytes from the DSP system to the mass spectrometer. The result is an analysis system with drop-in readiness for incorporation to existing pharmaceutical grade workflows in good manufacturing practice (GMP) facilities. Important results include the demonstration of active sample conditioning for enhanced ESI-MS performance, such as improved limit of detection, multi-component detection, and high molecular weight protein characterization in real-time. When applied to living cell cultures, DSP reveals that localized sampling is critical to enable detection of the cell status, i.e., cells in their proliferative, confluent, and differentiated state. Offline HPLC ESI-MS is correlated with real-time DSP analysis to demonstrate DSP's value as both a process analytical technology for bioreactor monitoring and as a discovery tool for

identifying the potential target biomolecules serving as CQAs for predicting the cell state. Collectively, this thesis' results demonstrate DSP's utility to help unlock the potential of advanced therapeutic cell manufacturing by providing detailed biochemical information about the process for closed feedback control of bioreactors, allowing for nascent therapies to reach a broad patient population.

CHAPTER 1.
INTRODUCTION: STATE-OF-THE-ART, MOTIVATION, AND RESEARCH OVERVIEW

1.1 Enabling Nascent Biomanufacturing Workflows

In the last 20 years biomanufacturing has seen a drastic increase in the scale of therapeutic production, particularly in the monoclonal antibody (mAb) and biologics space. These molecules are inherently more complicated to manufacture than traditional small molecule drugs, like aspirin, because they are produced by living organisms, i.e., cells. The cells used for biologics generally have their genome edited, or the cells are "engineered", so that they produce the specific protein(s) of interest. In 1998, a problem with the manufacturing process for the drug Enbrel, a recombinant protein produced by Chinese hamster ovary (CHO) cells which are edited with human DNA, led to a shortage of the "miracle drug" used for rheumatoid arthritis. At the time, the company responsible for producing the drug sent a letter to 82,000 patients citing issues with manufacturing-caused delays in production. By 2002 the shortage completely vanished. It was reported that there was an excess amount of capability for biologics production, and the averted crisis can be attributed to a huge expansion of manufacturing facilities.[1] Yet, other nascent cellular-based therapeutics have not seen the same growth trajectory despite having access to the same facilities that enabled the high volume of biologics production prevalent today. While in the biologics industry a medically potent protein produced by the cell is the final product, in the budding cell therapy space the entire cell is the final product, which is comprised of thousands of different biochemicals. This difference makes characterizing and ensuring the safety, efficacy, and potency of cellular therapies far more challenging.

Cellular therapies are transforming how life-threatening ailments are treated with the advent of therapeutic applications (e.g., cancer immunotherapies) to cure diseases; tissue engineered medical products are also used to restore, maintain, and replace damaged organs.[2-5] The outlook for these techniques is exhilarating, with over 900 investigational new drug applications for cell and gene therapy products reported by the FDA as of January 2020. Similar to biologics, these new treatment methodologies depend on the reliable growth of cells (e.g., stem cells) *in vitro*, but a severe lack of scalable cell manufacturing techniques currently limits these treatments' accessibility. This restricted production pipeline also results in low yield manufacturing, which causes excessive product pricing for patients.

Many cellular therapies do not have effective assays for product quality or therapeutic potency, which means that the Chemistry, Manufacturing, and Controls (CMC) standards are not reliable enough for these promising therapies make it through final FDA approval. For those therapeutics that have reached market, such as the CAR-T cell therapy for certain types of leukemia, a lack of feedback control hinders the scale up of production. With the exception of just a few FDA approvals, most advanced therapies fail to reach market because the biomanufacturing processes lack suitable real-time quality control methods capable of monitoring cell bioreactors, and this has resulted in large batch-to-batch variability, with *ad hoc* approaches to cell manufacturing. The lack of process analytical tools for quality control is reported as the main bottleneck to mass-market entry, and contributes substantially to the high patient costs ($0.5M-$2.0M per treatment) associated with the few regenerative medicine techniques approved by the FDA to-date.[6]

1.2 Sensors for Biomanufacturing

Standard approaches to characterizing bioreactors usually exhibit some combination of being off-line, destructive, and/or targeted. These are undesirable properties for analysis approaches when the goal is real-time monitoring to serve as an input to a feedback control for therapeutic cell manufacturing processes. As cell cultures mature and go through developmental stages, the biomolecules they secrete as signaling and paracrine factors can also serve as critical quality attributes (CQAs) for cell biochemical state and therapeutic potency.[7-9] Detecting and identifying these CQAs in real-time, and understanding in what manner they correlate with the cell growth trajectory and final product quality, are key first steps toward unlocking the potential of cellular therapies.

The widely adopted methods for continuous monitoring of bioreactors, including pH measurement, temperature measurement, off-gas mass spectrometry (i.e., monitoring of volatile compounds produced by cells in culture via mass spectrometry), infrared and Raman spectroscopy, all noninvasively capture "bulk" properties of the bioreactor. These bulk values are based on integral averages over the entire content of the bioreactor, and have indirect correlation to cell state. Although these sensors provide temporally sensitive information, they are subpar in offering detailed information such as the secretome's complete biochemical composition or the spatial heterogeneity within the bioreactor.[10-13] Some progress has been made in the implementation of non-invasive technologies that deliver multi-dimensional information about the cell population in a bioreactor. For instance, advanced image processing to track and monitor cell count and distribution on microcarriers in a bioreactor[14] or two-photon microscopy using endogenous fluorophores for monitoring stem cell differentiation[15] provide important insight to the culture status in

terms of cell count and cell differentiation respectively, but do not provide insight to the CQA biomarkers that predict therapeutic potential, safety, or efficacy.

As of yet, the level of quantitative detail required for high fidelity detection of CQAs has only seemed obtainable via offline methods such as liquid chromatography mass spectrometry (LC-MS),[9] microarrays,[16] and enzymatic assays (e.g., ELISA),[12, 17] which have been the main workhorses for the characterization of bioreactor processes and biomarker discovery. These approaches suffer from significant time delays and low throughput that limits their utility for online reactor monitoring. Due to a deficiency in temporal resolution, not only do these approaches miss the transient nature of cell growth, they also are not amenable to incorporation into an online feedback control loop that is key for scaling-up cell manufacturing. Although there have been some successful FDA approvals for cell-based therapies, such as the CAR-T immunotherapy, a lack in process control at each manufacturing step (including the viral vector production, which is also produced via cell-based manufacturing) has contributed to high rates of batch failure that contribute to the exorbitant costs and lack of availability associated with these promising treatments.[18]

Another shortcoming of nearly all current approaches to bioreactor monitoring is that they are limited to monitoring changes in the bulk media. The cell secretome is highly dynamic in nature, dependent on biological context, and spatially variant. As depicted in Figure 1.1, the region directly adjacent to the cell membrane has a rich biochemical environment whereas the region far from the cells has diluted concentrations of secreted

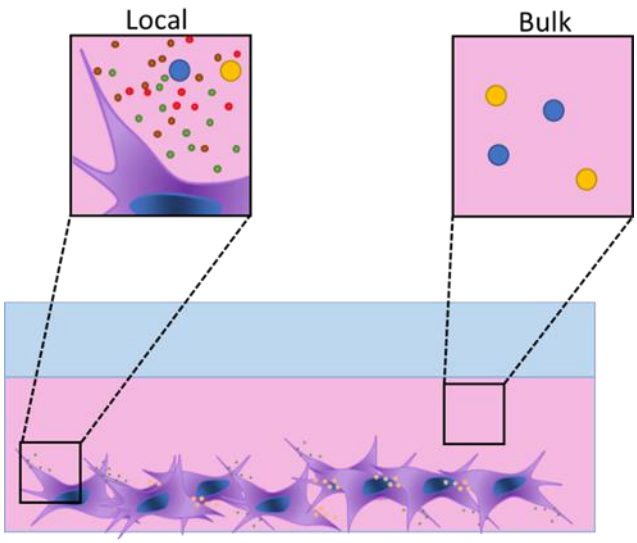

Figure 1.1: While cell cultures mature, secreted biomolecules are in highest abundance near the cells' surface. Traditional analysis techniques analyze bulk media, which includes temporally averaged biomolecular content and higher relative concentrations of molecules contained in stock media (e.g., fetal bovine serum (FBS), salts) that can mask the signature of quality indicating analytes. Rapid, small volume, localized sampling is an advantageous approach because it enables spatial and temporal probing of the cell culture, detecting the molecules when and where they are secreted.

factors and instead is dominated by media components. Furthermore, the local chemical composition can reflect cell heterogeneity, while bulk media loses spatial specificity. Therefore, extraction of large samples that contain secretions from many cells inherently sacrifices potential CQA enrichment as well as key information on local changes that could be important indicators of cell product state. An effective quality control measurement technique should not only be real-time but should also enable localized sampling within

the cell bioreactor: it should sample in close proximity to the cells to capture both spatial and temporal variations within a cell bioreactor.

The benefit of localized sampling is illustrated in Figure 1.2. The left trace represents the time history of species near the cell membrane. The relative concentration of secreted biomarkers, which are the CQAs for cell manufacturing, may vary substantially with time. On the other hand a time history of the bulk, shown in the right graph in Figure 1.2, indicates that high concentration additive biomolecules found in media (e.g. serum) are orders of magnitude higher in concentration when compared to the quality attribute biomarkers. While some CQAs may follow similar trends in both environments, such as "CQA 1" in Figure 1.2, localized sample is advantageous because it captures the cell

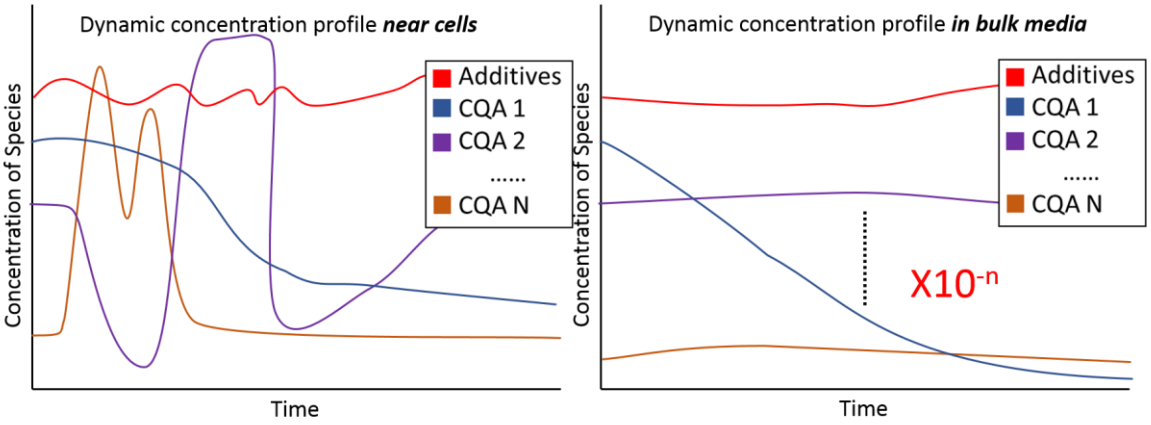

Figure 1.2: Representative time histories of relative species concentration near (left) and far (right) from the cell membrane. Sampling near the cell membrane captures the temporal variation of secreted CQA biomarkers, which are in high relative concentration near the cell. Traditional techniques capture time averaged signals from the bulk that are dominated by media additives that do not correlate with cell state.

microenvironment, which is comprised of low concentration biomarkers that are directly correlated with cell state. Lastly, by capturing quality attributes at their source the time delay between CQA secretion and detection is minimized, which is requisite for any sensor providing input to a feedback loop in biomanufacturing.

1.3 Mass Spectrometry for Biochemical Sensing

1.3.1 Electrospray Ionization Mass Spectrometry (ESI-MS)

Mass spectrometry (MS) is an analytical tool that measures the mass-to-charge ratio of ions. In the biological sciences MS has widespread utility for characterizing biomolecules ranging from small metabolites to entire monoclonal antibodies. The ionization source for a mass spectrometer varies depending on application. In the early applications of MS, electron impact ionization was used to break covalent bonds and produce fragment ions. However, this fragmentation made it nearly impossible to analyze large, complex biomolecules. As MS developed as an analytical tool, new approaches emerged that "softly" ionized molecules including electrospray ionization (ESI) and matrix assisted laser desorption/ionization (MALDI). Both approaches have driven the field of MS forward in a significant manner. MALDI has tremendous utility for analyzing non-volatile species and has broad applicability in the biological sciences. MALDI is particularly well suited to imaging studies, such as defining the spatial distribution of specific compounds on tissues.[19] The MALDI process generally produces ions that are singly or doubly charged. This is an important phenomenon because it enables the identification of molecular ions of proteins, lipids, and carbohydrates and drastically simplifies resulting spectra. However, this limited ionization capability also limits

MALDI's utility for analyzing high molecular weight biomolecules because they are outside of the detectable m/z range on most MS systems. On the other hand, ESI produces ions with multiple charge states and, theoretically, has an unlimited mass range.[20] For this reason, ESI is far more effective at analyzing large molecules such as proteins that must be highly charged for MS detection. Additionally, ESI preserves non-covalent bonds and leaves molecules in a preserved state from the condensed phase to the gas phase, unlike MALDI which suspends analytes in a crystalline solid prior to ionization.[21]

Electrospray ionization mass-spectrometry (ESI-MS) is an excellent approach for biochemical analysis due to its broad molecular weight coverage and capacity for unlabeled biomolecule detection and discovery. ESI-MS maintains the state of large biomolecules, requires no *a priori* labeling of biomolecules, and is very sensitive to low concentrations of chemicals (limits of detection in the nanomolar to even picomolar range).[22] However, direct online ESI-MS of biologically complex samples (e.g., cell media) requires extensive sample preparation prior to the ESI process.[23] One of the most important challenges in the MS field is the detection of ultra-low concentration species. The dynamic range of biomolecules in cell media can range from a few picograms per milliliter to milligrams per milliliter, making it difficult to impossible to detect under-represented proteins.[24] Traditionally, separation techniques such as liquid chromatography (LC) or capillary electrophoresis (CE) are employed when a large number of biomolecules are present in the sample. For example, when analyzing cell culture media, salt must be first removed due to the deleterious effect it has on ESI-MS, and then the biomolecules are separated via LC or CE before MS. This sample preparation reduces chemical noise, simplifies ESI charge

states, mitigates spectral feature overlap from different species, and ultimately enables high-throughput and automated biomolecule identification.[21]

1.3.2 Sample Preparation Requirements for Online ESI-MS Analysis

Although chromatographic methods are widely used to facilitate modern ESI-MS workflows for biochemical analysis, they are not required for ESI-MS analysis. At a minimum, chemicals that are not compatible with ESI-MS must be removed prior to analysis because they interfere with the ionization of biochemicals of interest. Chemicals widely found in lab spaces such as polyethlyeneglycol (PEG, commonly found in detergents), keratin (skin/hair, dust), and some polymers found in labware or commonplace solvents interfere with ESI-MS. In cell biological applications the most common source of interference are inorganic compounds (e.g., NaCl, KCl, etc.) that are not only ubiquitous, but present in far higher concentrations than biomolecules of interest.

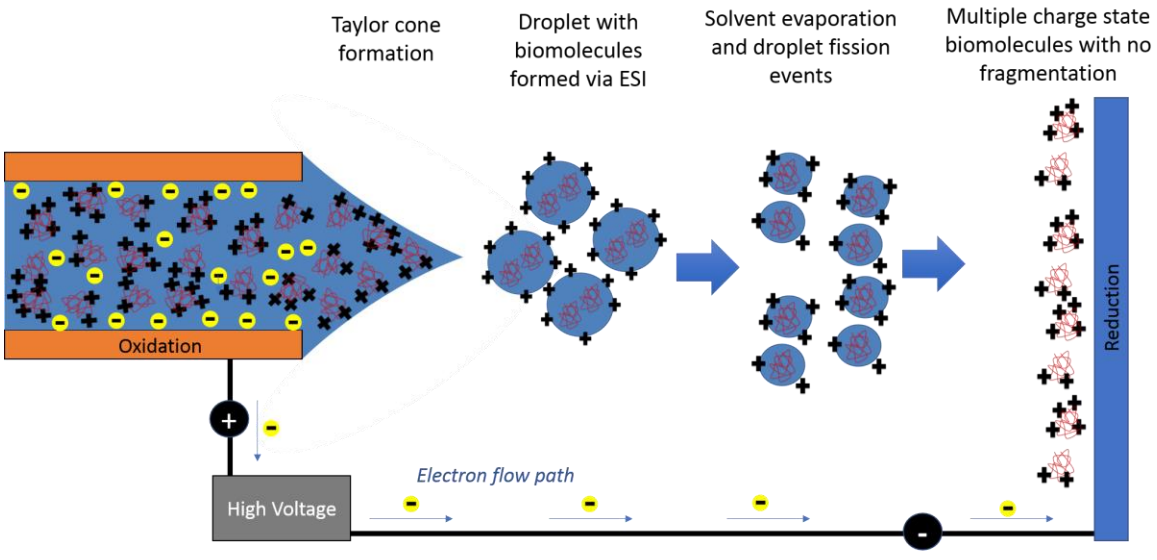

Figure 1.3: Illustration of electrospray ionization (ESI) operating in positive mode.

Figure 1.3 shows the positive mode ESI process, which produces ions with excess protons that are subsequently analyzed by MS detectors (not shown). Although some workflows utilize a negative electric potential on the spray to produce negatively charged ions, positive ESI was the version explored in the work presented here. Positive mode ESI is the most applicable to proteomic workflows (like those that target secreted CQA biomarkers) because negative ions are generally more difficult to analyse using advanced MS techniques like tandem mass spectrometry.[25] During the ESI process, three major steps are involved in bringing analyte molecules from their aqueous state to gas-phase ions that are detected by the mass spectrometer: 1) a strong electric field is applied between the aqueous phase within the ESI source and a counter electrode, causing the production of charged droplets ejected from the Taylor Cone; 2) the charged droplets shrink due to repeated solvent evaporation and Coulombic fission; and, 3) multiply charged ions comprised of the analyte and cations such as H^+, K^+, Na^+, are produced.[26, 27]

For positive-mode ESI-MS workflows, producing "protonated" ions that are charged with only H^+ ions is desirable. When multiple cations are present within the aqueous phase, the ESI process produces both "adducts" and "clusters". Salt adducts are formed when a cation such as Na^+ replaces H^+ during ionization, while clusters are formed when an entire neutral molecule, like NaCl or water (incomplete desolvation), attaches to the analyte during the ESI process. Figure 1.4 illustrates an ion in the +5 charge state in the protonated, adducted, and clustered format. Note that many combinations of adducts, clusters, and protonated ions are produced at each charge state during the ESI process, which causes significant suppression of the protonated state associated with target analytes that is most suitable for unambiguous spectral speciation.

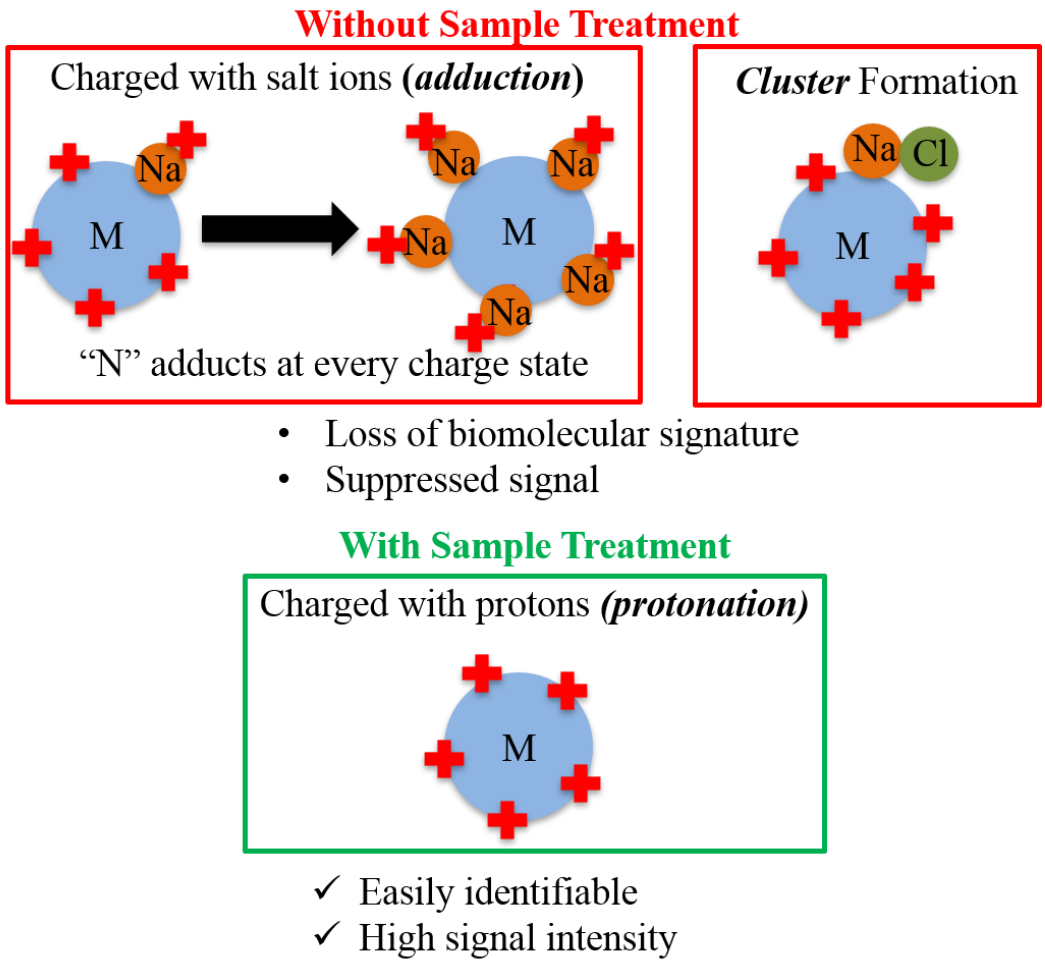

Figure 1.4: Example of +5 charge state of an analyte with mass "M" produced in positive mode ESI. The presence of salt ions (Na^+) results in both adducts and clusters that suppress protonated species. With sample treatment, these salt ions are removed prior to the ESI process, enabling the production of protonated molecules for improved MS identification.

In order to demonstrate the effect inorganic salts have on biomolecule signal suppression, direct ESI-MS analysis of a model protein, cytochrome c (Cyt c, M=12,358 Da), at 5 µM concentration with varying concentrations of inorganic salt KCl (0 to 9,900 µM) was carried out. As shown in Figure 1.5, with no KCl present, a clear signal associated with Cyt c is detected. Charge states ranging from +8 (8 protons with a single Cyt c

molecule) to +19 are highlighted. By increasing the KCl concentration to 250 µM, an adduct peak is detected with a value of ~1550 m/z, indicative of a +8 charge state with 7 H^+ ions and 1 K^+ ion. As the concentration of KCl is increased to 9,900 µM, complete

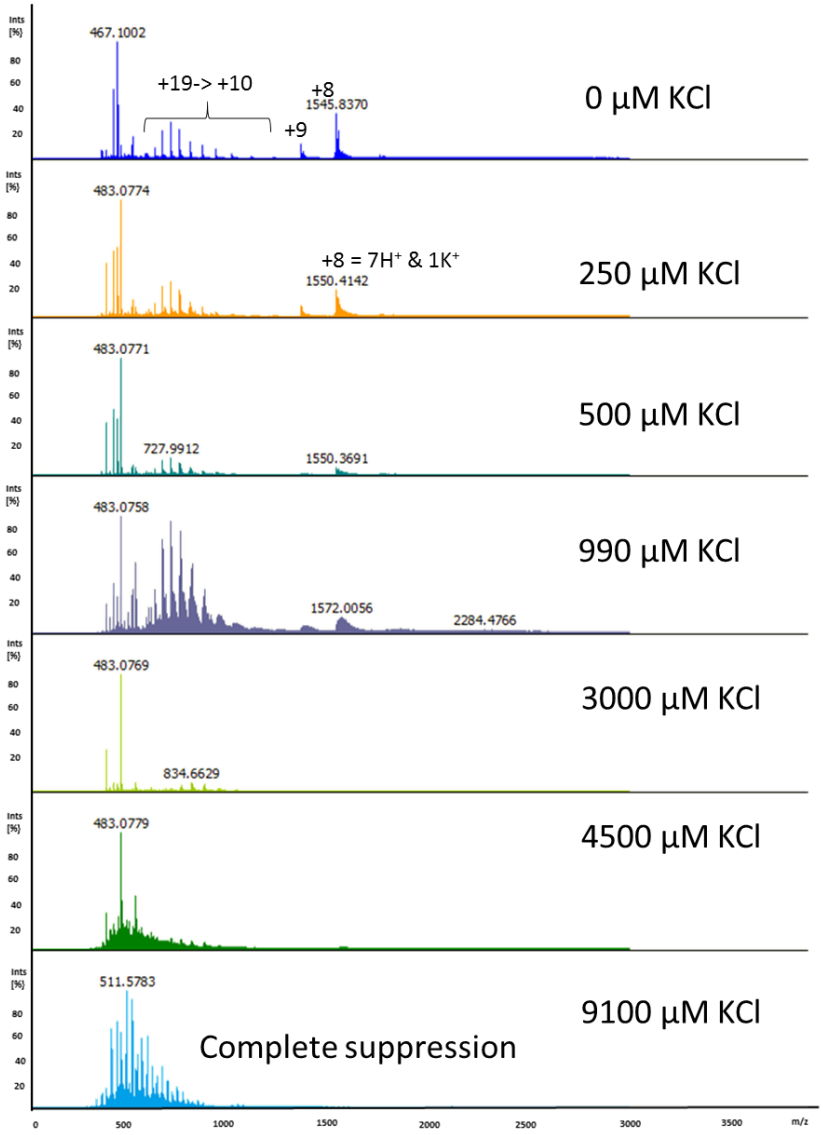

Figure 1.5: ESI-MS analysis of cytochrome c (Cyt c) at the 5 µM level with varying KCl concentrations. Without salt, multiple charge states of the protonated Cyt c are visible. The addition of even moderate amounts of KCl produces parasitic adducts, which can be observed at the 250 µM KCl level. Complete Cyt c signal suppression is observed at the 9100 µM KCl concentration.

suppression of Cyt c is observed. In this experiment identifying the biomolecule is still possible because Cyt c was targeted for analysis. However, in untargeted approaches, not knowing the molecular weight of the target analyte beforehand makes extracting molecular identify challenging. Moreover, in biologically relevant solutions such as cell culture media, the levels of inorganic salts are usually in the ~100 mM range and in many cases more than one type of salt are present simultaneously.[28-30]

The minimum sample treatment requirements for ESI-MS in biomanufacturing workflows can be estimated based on the data presented in Figure 1.5. The signature associated with Cyt c is visible up to the 990 μM level, but the presence of adducts and clusters suppresses the protein's spectral signature above this level. In biomanufacturing applications where cell culture media is to be analyzed, the starting concentration for salts will be at least 100 mM, and therefore at least 99% of the salt must be removed for ESI-MS detection of a single CQA biomolecule. For these experiments, Cyt c was the only biomolecule in solution at the 5 μM level, and only a single species of salt was present (KCl). In cell culture media, the presence of multiple salts and numerous biomolecules introduces the potential for increasingly complex adduct and cluster signatures that further convolute resulting spectra. Importantly, the concentration of CQA biomolecules may be significantly lower than the micromolar level, often in the nano, pico, and even attomolar range, which would necessitate even higher levels of selective salt removal to detect these low concentration biomolecules. Therefore, at a minimum, over 99% of salts should be removed from culture media prior to direct ESI-MS analysis, but for label-free monitoring of multiple secreted CQA biomarkers, the sample treatment requirements are likely to be even more stringent. An effective sample treatment approach should selectively remove

nearly all salt content while retaining CQA biomarkers to enable real-time ESI-MS analysis.

1.4 Prior Real-time ESI-MS Applications

Prior work towards inline sample preparation for ESI-MS applications involved devices with highly variable performance that were hand assembled, low throughput, or without inline ESI-MS analysis. Xiang et al. demonstrated inline dual-dialysis which included high and low molecular weight cut off membranes to isolate target biomolecules within a specific molecular weight range while also removing interfering salts.[31] Although this device demonstrated the ability to successfully remove enough salt for applications to biologically relevant solutions, the large dead volume resulted in poor time resolution of the analysis (~20 min processing time) and large sample size.[29, 32] Additionally, the hand assembled device is not well suited to practical applications where production scale-up would be desirable.

Continuous flow, passive sampling from a pressurized bioreactor with spatially resolved biochemical detection has been demonstrated by Olivero et al. for a 3-D glial cell culture system using a device with inline microdialysis to desalt the sample for direct ESI-MS analysis.[33] The inline salt removal device, which also required hand assembly and used a cellulose dialysis membrane with high mass transfer resistance, enabled detection of moderate concentrations of soluble proteins with a time response of ~1 min. Tibavinsky et al.[34] reduced online sample treatment time down to ~1 s with miniaturization via microfabrication of a mass exchanger with a monolithic ultra-thin nanoporous alumina separation interface for microdialysis.

The device created by Tibavinsky et al. was the inspiration for the work presented here on the Dynamic Sampling Platform (DSP), with significant advances to the fundamental desalination technology. In DSP, a microfabricated mass exchanger is integrated with an aseptic, spatially resolved sampling inlet and an inline ESI emitter, yielding a monolithic device capable of rapid biomolecule identification to meet the needs of online bioreactor monitoring. Additionally, exploration of new operating modes with an active introduction of MS signal enhancing chemicals, in addition to sample desalting, is implemented to enable detection of a broader range of biomolecules.

1.5 The Dynamic Sampling Platform (DSP)

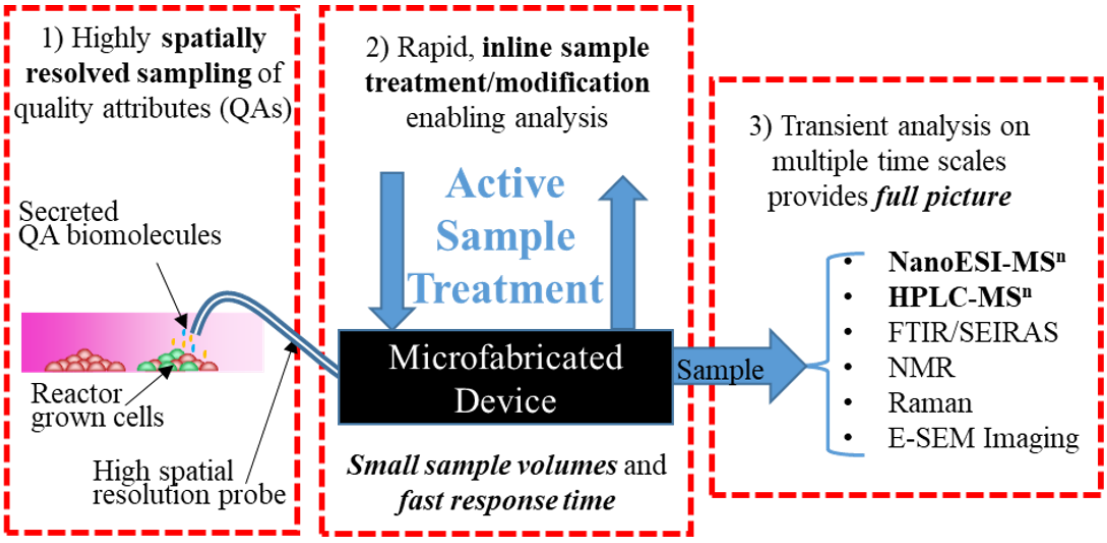

Figure 1.6: The Dynamic Sampling Platform (DSP) incorporates three key elements: 1) spatially resolved, aseptic sampling interface, 2) mass exchanger for inline, rapid sample treatment and, 3) output for real-time analysis. As a platform technology, DSP can be optimized for any analytical output, but is optimized for ESI-MS in this work to enable DSP as both a quality monitoring (targeted) and discovery (untargeted) tool for identifying which quality attributes serve as CQAs.

The Dynamic Sampling Platform (DSP, Figure 1.6) is a technology for real-time chemical analysis comprised of three key components: 1) a spatially resolved sampling probe for aqueous sample uptake 2) a batch microfabricated mass exchanger for rapid, inline sample conditioning including removal of chemicals that interfere with analysis (e.g. salts for MS), exchange of enhancing solvents (e.g., "supercharging" molecules and organic acids for MS), and retention of larger analytes and, 3) an outlet for real-time analysis (e.g., ESI emitter). As a platform technology, DSP is fundamentally compatible with most applications where aqueous samples are to be analyzed. Further, DSP is designed to be compatible with a range of analysis techniques. For each analysis technique the requirements for sample treatment will be different, but the flexible DSP fabrication process can be easily modified for incorporation with other techniques such as Fourier transform infrared spectroscopy (FTIR) or nuclear magnetic resonance spectroscopy (NMR). For the work presented here, DSP was optimized for ESI-MS because this analysis method is appropriate for both quality monitoring and CQA discovery applications in biomanufacturing.

1.6 Research Objectives

The objectives of this research were chosen to establish DSP as a key part of the existing suite of sensor technologies in biomanufacturing. In addition to optimizing DSP for drop-in integration within new and existing workflows, the scientific goals of the work were tailored to enhance fundamental scientific understanding:

1. Design of a robust micro/nanofabrication process for DSP, along with a fluidic interface package for facile integration with mass spectrometers. The result is an

integrated technology for aqueous sample introduction and inline sample preparation for continuous and online ESI-MS of complex mixtures.

2. Development of an optimized DSP mass exchanger based on first-principle analysis of coupled fluid dynamics and mass transfer. Simulation guided design optimization with experimental confirmation of the optimized DSP for improved performance, including fast response time, efficient salt removal, and enhanced sensitivity of ESI-MS analysis of biomolecules.
3. Exploration of the effect conditioning agents have on ESI-MS analysis of i) low concentration biomarkers, ii) multi-component systems, and iii) high molecular weight proteins.
4. Development of a microfluidic sampling interface for localized sample uptake directly from cell bioreactors that matches biological timescales; integration of DSP with clinically relevant workflows where cell culture and analysis take place in different locations.
5. Demonstration of the localized sampling from a cell culture in combination with DSP-ESI-MS analysis to capture the CQA biomarkers that allow the secretome-based identification of the cell state (e.g., differentiated, proliferative, confluent) during a complete cell development cycle.
6. Exploration of DSP as a discovery tool for identifying biomarkers in a cell growth bioreactor to establish the DSP utility as a biological discovery tool aiming at detection and identification of potential CQA biomolecules with no a priori knowledge.

1.7 Thesis Organization and Overview

The presented work is divided into three chapters covering the DSP technology development and relevant applications of the prototype systems, followed by concluding remarks and recommendations for future work. Chapter 2 is comprised of a detailed description of the DSP system design. First, the design requirements for any sensing system operating within biomanufacturing are outlined. The DSP solution is comprised of a sampling interface, a microfabricated mass exchanger, and an ion transport interface. The Dynamic Sampling Interface (DSI) is the engineered solution presented for providing localized, aseptic samples from directly within bioreactors. The microfabricated mass exchanger is central to DSP, not only treating samples in real-time, but also integrating the DSI and an ESI-MS outlet for inline analysis. An overview of the microfabrication process is given in this chapter, along with salient features which enable DSP. For drop-in integration to clinically relevant workflows, an ion transfer interface is incorporated with the DSP and the features and limitations of the technology are explored. Finally, a computational-model guided approach to estimate the relevant mass-transport in the DSP mass exchanger is employed. A simple change in the fluidic package is implemented to significantly improve device performance for treating chemically complex samples.

In Chapter 3 the integrated DSP system is applied to proxy cell culture solutions comprised of soluble biomolecules in high salt content solutions. With constant sample composition (5 μm Cyt c, 100 mM KCl) different types of active-conditioning and their effects on real-time ESI-MS are explored. Conditioners, including acetic acid, methanol, ammonium acetate, and, notably, super-charging molecule 3-nitrobenzyl alcohol (m-NBA), are shown to improve the real-time ESI-MS detection of Cyt c. The effects of

supercharging molecules are further probed and shown to improve sensitivity to low concentration biomarkers and to enable multicomponent detection. Finally, the improved crossflow orientation DSP is utilized to facilitate high weight protein detection. The superior conditioner orientation, along with optimized conditioner composition, enables the detection of these difficult-to-detect monoclonal antibody fragments, which is an important application for the already established biologics industry.

DSP use for live cell analysis is presented in Chapter 4. The crossflow design, with integrated localized sampling capability, is applied first to three types of clinically relevant cell types (hMSC, HUVEC, NHLF) for fingerprinting. For this exploratory work localized sampling is shown to reveal a significantly different MS signature when compared the bulk media samples, demonstrating that the resulting ESI-MS analysis of a cell culture is highly dependent on where the sample is taken from. These results suggest that by sampling from near the cell membrane secreted molecules are captured for analysis that correlate with the cell state directly. These results also motivated the longitudinal study of a culture of MC3T3-E1 cells (murine preosteoblasts) throughout their entire cell cycle. *Post hoc* analysis using a principal component analysis (PCA) approach reveals that localized sampling is key to detecting cell state, including differentiation, proliferation, and confluence. Lastly, a workflow for applying DSP with complimentary approaches such as high performance liquid chromatography (HPLC) is presented.

In the final chapter, conclusions are presented and future work is outlined. One major area of interest is optimizing sample conditioning for high/low molecular weight cutoff applications. Filtering out high molecular weight proteins that are found in high abundance in cell media, such as albumin, is important for clinical applications because

these molecules dominate during MS analysis and mask the signal of lower concentration CQA biomolecules. In addition to filtering out high molecular weight species, retaining smaller biomolecules is also of interest. Optimizing the integrated nanoporous membrane for reduced pore size can help retain smaller biomolecules of interest. Potential cell therapy testbeds of immediate clinical relevance, such as interferon-gamma primed mesenchymal stromal cells and IL-2 primed T-cells, are discussed as candidate systems for DSP-based monitoring.

CHAPTER 2.
DSP SYSTEM LEVEL INTEGRATION

The DSP was developed for integration with cell bioreactor monitoring in compliance with Good Manufacturing Practice (GMP) standards. The rules and regulations associated with GMP necessitate that industrial grade biomanufacturing processes adhere to stringent operating conditions that govern the entire process, including the integration of process analytical technologies (PAT). The DSP as a PAT system was developed with a holistic design approach to create an integrated analytical approach supported by tools capable of sample uptake, treatment, transport, and analysis. It incorporates a sampling interface for aseptic, spatially resolved sample uptake from a bioreactor followed by an inline sample treatment protocol for chemical modification and subsequent real-time ESI-MS analysis. At the core of the DSP system is the batch microfabricated device which integrates clog resistant counterbores for the inlet and outlet capillaries with a ~20 nL micro-mass exchanger that contains the sample channel and the active conditioning region. The DSP fabrication process uses state-of-the-art MEMS foundry techniques that are highly repeatable and scalable to meet high volume demand in future biomanufacturing workflows. The fabrication was carried out in the shared-user facility at the Georgia Tech Institute for Electronics and Nanotechnology (GT IEN). While the microfabricated exchanger is central to the DSP system, the auxiliary systems allow for GMP drop-in integration capability. The fluidic interface package, dynamic sampling interface (DSI), and ion transfer interface are each critical technologies for enabling clinical workflows operating under GMP standards where the cell culture, analysis instrument (e.g., mass spectrometer), and DSP system may each be in spatially disparate locations. Design and

integration of all aspects of DSP result in a robust system for deployment into new and existing biomanufacturing workflows.

2.1 Good Manufacturing Practice Integration

The DSP approach to bioreactor monitoring was developed with the end-use application in mind. Therapeutics produced from biomanufacturing workflows, like biologics and advanced cellular therapies, must adhere to strict standards that govern their production. Good manufacturing practices (GMP) or current good manufacturing practices (cGMP) are a set of guidelines and operating principles set forth by governing bodies such as the FDA to ensure that the final therapeutic product is consistent, safe, and efficacious. GMP regulations span every aspect of the production including record keeping, cleanliness, sanitation, equipment verification, air purity, raw material quality, etc.[35] Most GMP requirements are relatively open-ended, and therefore the approaches from each manufacturer to meet these standards differ. Between processes there is some consistency in that biomanufacturing processes related to cell culture take place in clean (e.g., low particle count, sterile) environments following strict protocols where contamination is unacceptable. Analysis of the cell culture, on the other hand, most often takes place in a separate location/lab with different standards for cleanliness and ambient conditions. Any biomanufacturing sensor system must be designed to remove the risk of introducing contamination to the culture while still providing valuable information on measured process parameters. For instance, sensors that measure pH, temperature, dissolved oxygen, or glucose usually are embedded into the bioreactor in a manner that prevents contamination.[36] For assays that are not *in situ*, every step from sample uptake to sample analysis must be minimally invasive and completely compatible with GMP requirements.[35]

The GMP facility at the Georgia Tech's Marcus Center for Therapeutic Cell Characterization and Manufacturing (MC3M) is a proxy for industrial environments. This facility was used as a test bed for the DSP prototype deployment. The layout for the MC3M GMP facility is shown in Figure 2.1. The areas relevant to the integration of DSP are

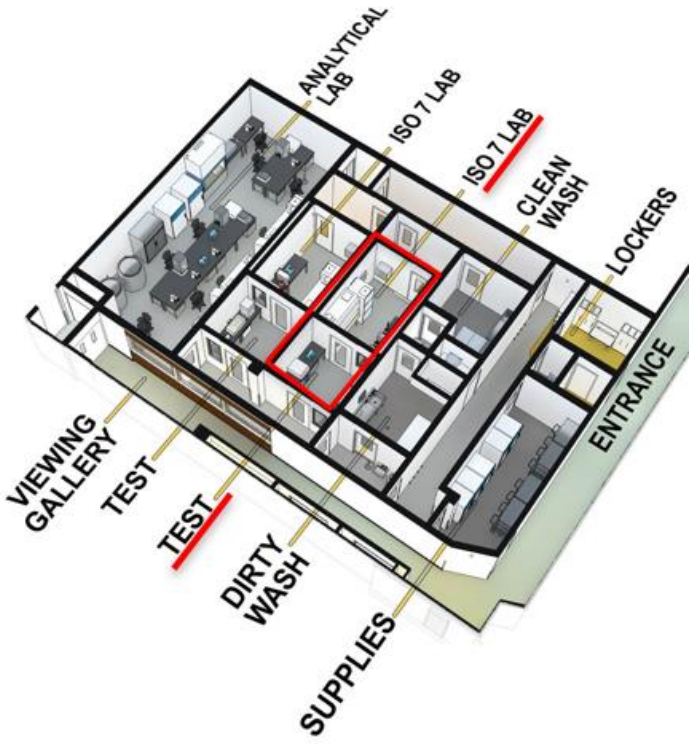

Figure 2.1: The GMP facility at Georgia Tech's MC3M Center serves as a proxy to industrial environments for cell therapy manufacturing. Importantly, low particle count (ISO 7) suites where the cells are cultured are separated from test suites where analysis occurs. For effective application of DSP, sample uptake, treatment, and transfer for analysis must occur in a manner that does not affect any of the GMP requirements. Image courtesy of FLAD Architecture.

highlighted in red, namely, the ISO 7 and test suite. The ISO 7 suite is a cleanroom environment. Within this area there is a biosafety hood and an incubator, and this is where

cells are cultured. Adjacent to the ISO 7 suite is the test suite, where an analysis instrument is kept. For the work presented here, a Thermo Fisher™ Q-Exative Plus mass spectrometer is housed in the test suite. For any real-time coupling between the culture and the analysis system, a sample must be transported from the ISO 7 suite (where cells are cultured) to the analytical suite (where analysis takes place) without affecting the sterility of the cell culture or violating GMP protocols. For example, in the facility shown in Figure 2.1, an operator can only walk in one direction, from the ISO 7 suite to the analysis suite, because the higher ambient pressure in the ISO 7 suite reduces the chance of contaminants traveling from the analysis suite to the ISO 7 suite. The DSP system was designed for flexible integration into restrictive environments similar to the GMP facility at Georgia Tech to enable aseptic sampling, inline treatment, long distance sample transport, and real-time ESI-MS analysis.

The DSP sample treatment mass exchanger is central to the DSP technology. This device is fabricated using a robust microfabrication process that reduces batch-to-batch variability and provides precise control over feature size. The DSP mass exchanger has monolithic fluidic interconnects that are designed for facile integration with a sampling inlet and an ESI outlet. Restrictions on aqueous sample transport, i.e., sample dilution and mechanical pump limitations, motivated the integration of a small-dead volume sampling system and a long-distance ion transport interface to couple the DSP with an MS system for real-time analysis. The layout of the DSP analysis system for GMP integration is illustrated in Figure 2.2. The dynamic sampling interface (DSI) enables aseptic, spatially resolved sample uptake from a cell growth bioreactor. The microfabricated portion of DSP

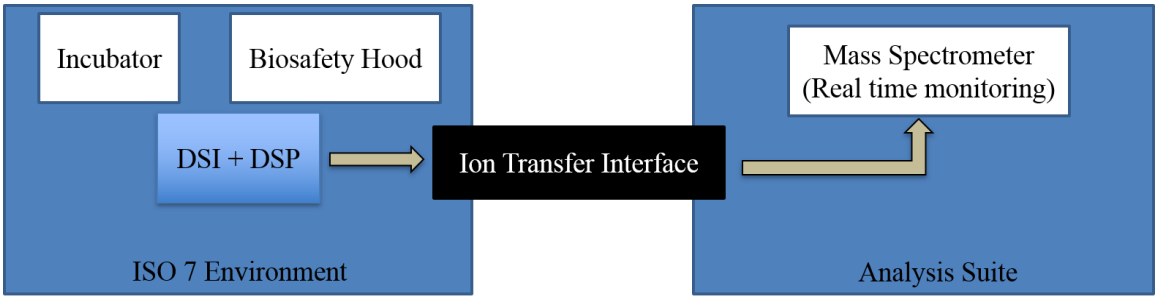

Figure 2.2: Layout of the constituent technology for the DSP analysis system, including the dynamic sampling interface (DSI) for sample uptake, the DSP mass exchanger/ion source for inline sample treatment and analyte ionization, and the gas phase ion transfer interface to the MS for real-time analysis.

integrates the sample interface with a mass exchanger and an ESI source, which treats complex cell culture media and produces ions for MS analysis inline. The ion transfer interface transports the analyte ions in gas phase from the ISO 7 suite to the MS for real-time analysis.

2.2 Dynamic Sampling Interface (DSI)

Secreted biomolecules from cells growing within a bioreactor can be correlated to cell health, propagation, and differentiation.[7, 8, 23, 37-39] As cells secrete, the released biomolecules rapidly become less concentrated as they diffuse away from the cell membrane. As a result, bulk sampling away from the cells will uptake the target biomolecules at significantly reduced concentrations. These bulk samples also capture a temporally averaged media composition, which makes time dependent monitoring impossible. Further, the presence of high abundance molecules such as albumin (contained in serum) commonly found in cell cultures provide an overwhelming background for ESI-MS detection of low abundance secreted analytes. Therefore, spatially and temporally

resolved sampling is essential for high sensitivity monitoring of cell secretomes to enable 1) the mitigation of spatial dilution and time averaging of secreted biomolecules by analyzing the secretome in the immediate vicinity of cells or cell carriers, 2) the capability for capturing the transient cell secretion events as online sample treatment by DSP affords a nearly real-time ESI-MS analysis, and, 3) the probing of spatial heterogeneity of secretomes within the bioreactor environment in correlation with the spatial distribution of 2D and 3D cell cultures.

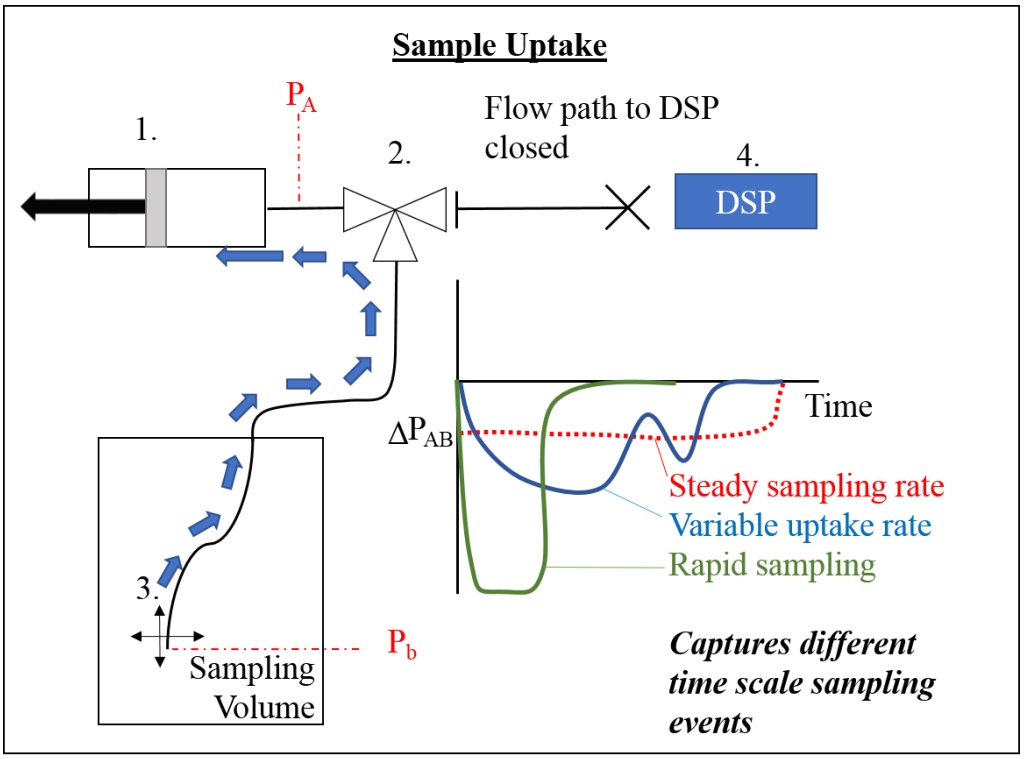

Figure 2.3: The dynamic sampling interface (DSI) consists of 4 components: 1) a bi-directional, variable flow rate pump with sample for uptake/infusion; 2) a switching valve or quick disconnect fitting for isolating sampling/infusion steps; 3) a sampling probe for localized secretome intake; and, 4) interconnecting tubing for sample transport to DSP. Sample uptake can be carried out with dynamic pressure profiles tuned for rapid, low dilution sampling.

Figure 2.3 and Figure 2.4 depict the key components of the Dynamic Sampling Interface (DSI) for integration of DSP with a bioreactor. These include 1) a pump for bi-directional sample uptake/infusion, e.g., syringe pump, 2) a switching valve or quick disconnect fitting for isolation of flow during uptake and infusion, 3) a flexible capillary terminated with a small size orifice to capture small volumes of the reactor content locally, i.e., near cells for probing the secretomes, and, 4) capillary connection to DSP for online ESI-MS analysis. During sample uptake, the flow rate can be tuned to match the rate and duration of the chemical secretion of the cells, thus capturing transient events in the reactor. On the other hand, during infusion, the flow rate should be tuned for matching the optimal flow rate required by DSP for desalting, active sample conditioning, and subsequent ESI-

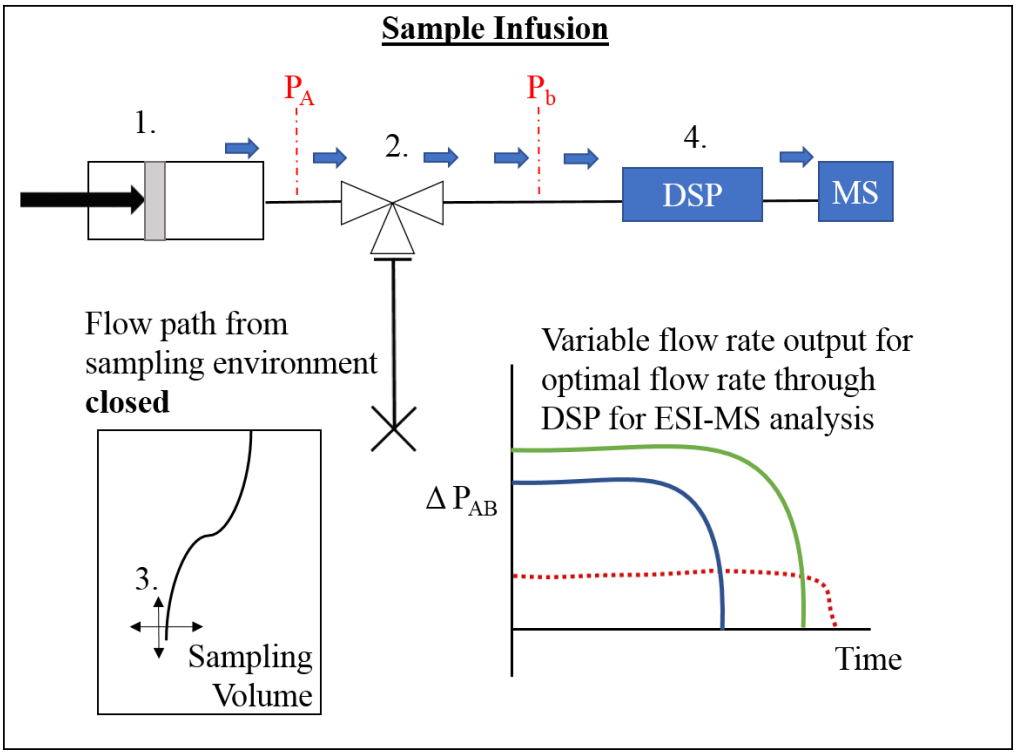

Figure 2.4: The dynamic sampling interface (DSI) separates sample uptake from sample infusion. During infusion, constant flow rate matches that necessary for consistent ESI-MS.

MS analysis. For a given ESI spray capillary size (i.e., emitter tip inner diameter), only a small range of flow rates will produce stable spray, and therefore the sampling interface should infuse to match this optimal range. In Figure 2.3, the difference in pressure between ports A and B illustrates that sample uptake can be dynamically changed to capture the secretion dynamics using small extracted liquid volumes, whereas during infusion (Figure 2.4) the pumping pressure difference is constant for sustaining an optimal, steady flow rate during DSP infusion to ESI-MS.

The sampling interface should be able to uptake volumes as small as necessary to capture the molecular release during the localized cell secretion event, which is expected to be in the few nanoliter range. However, the dead volume of the DSP mass exchanger (20 nL) is about 10X above this level. Therefore, the entire sampling interface and DSP dead volume was initially filled, or "primed", with a non-interfering liquid prior to sampling from the bioreactor to enable only a small volume sample to be extracted without the introduction of air bubbles into the system. This is illustrated in a simplified diagram shown in Figure 2.5.

As a small sample is taken up into the system, a liquid "plug" will flow through the piping and valves of the primed sampling interface (Figure 2.3, Figure 2.4). As the liquids are assumed to be miscible, dispersion of the sampled liquid plug will dilute the sample as it advances through the sampling interface and to the DSI outlet/inlet to DSP. According to Taylor's dispersion theory,[40, 41] lower flow rate and smaller capillary diameter will result in reduced dispersion effects. However, as velocity, transit time, and system dead volume are related to the dispersion phenomenon, the design requires careful optimization, balancing the reduction in the device response time with improved sensitivity that comes

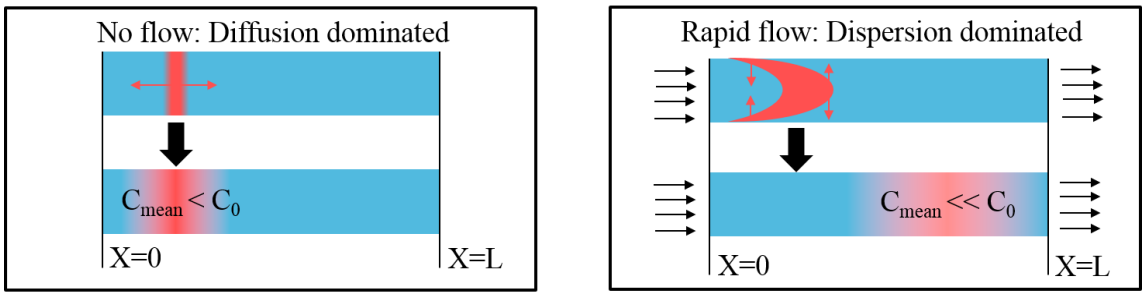

Figure 2.5: During sample transfer, a small liquid plug is transmitted through the primed fluidic interface. The plug dilutes due to both diffusion and dispersion effects that reduce the average concentration of the sample. At one extreme, diffusion dominates the dilution while sample transmission time increases (Pe = 1). In the other extreme (Pe>>1), dispersion effects dilute the sample although sample transmission time is reduced. A reduced mean concentration, taken as the integral average of species over plug volume, will affect the ESI-MS detection of already low concentration species.

with a less dispersed sample. Another consideration is that as flow rates become smaller, axial diffusion will become significant as the Peclet number approaches unity. Both extremes are illustrated in Figure 2.5. In this simplified representation of the sampling interface, a small plug of a homogenous sample (e.g., cell culture media) is assumed to have an initial concentration of C_o as it enters a tube which is filled with a miscible liquid (e.g., water). Diffusion or dispersion will cause the initial plug to spread along the length of the tube, and the species are now diluted in a larger volume. The mean concentration, C_{mean}, can be estimated as an integral average of the total species over the new volume. The same amount chemicals that were present in the initial plug are now in a larger volume, hence C_{mean} is always less than C_o. In both cases, a lower mean concentration will affect

detection of the sample, so a design criterion for the DSI is to preserve the initial plug concentration during transmission.

Figure 2.6 illustrates the effect that flow rate and capillary diameter have on the mean concentration of a liquid plug within a 25 cm long capillary. In the flow regime where DSP operates (10-50 µL/hr) the output concentration of a small plug is nearly linearly proportional to flow rate and independent of inner diameter. One solution is to minimize the inner diameter the capillaries as a smaller total volume will transmit samples faster. However, the pressure drop in a capillary scales inversely with tube diameter raised to the fourth power for a given volumetric flow of incompressible fluid, and therefore the tradeoff is high operating pressures. It was found that longer fluidic paths between the pump and

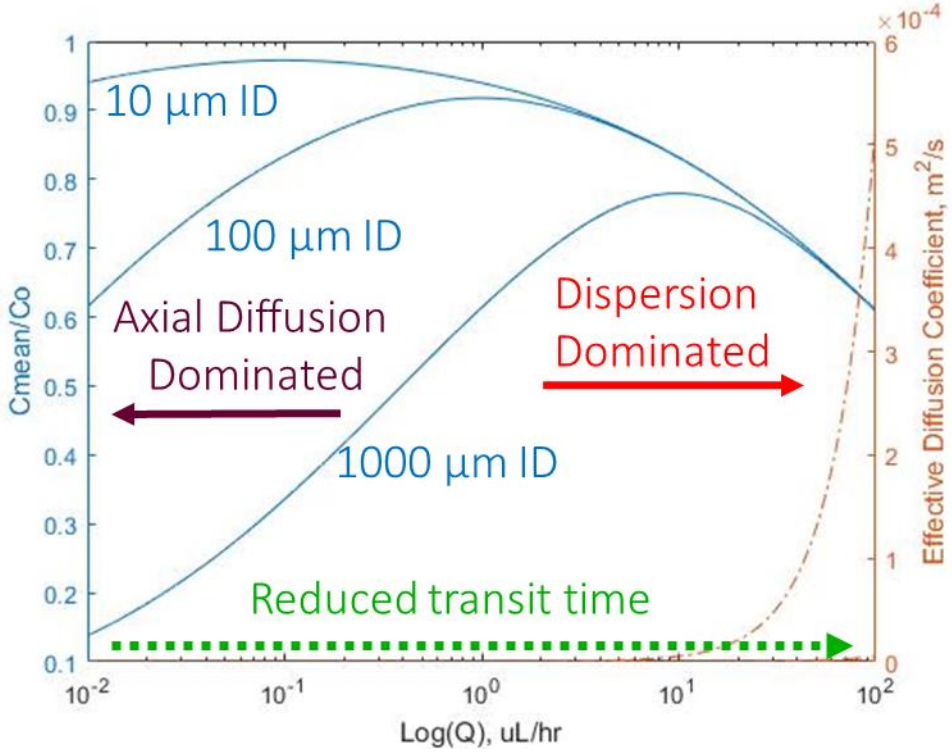

Figure 2.6: Mean concentration versus flow rate for a 25 cm capillary (left) and effective diffusion coefficient (right) based on Taylor-Aris dispersion effects.

sampling inlet caused leaks and bubbles that interfered with both sample uptake and DSP operation during infusion. The optimal operating mode for DSI was to uptake enough volume to fill the entire sampling interface and to then infuse directly through DSP for immediate ESI. Two operating modes were found to function well: 1) drawing enough liquid through the inlet to fill past the switching valve, or, 2) replace the switching valve with a quick disconnect fitting and sampling directly from the culture before reattaching the sampling inlet to the quick disconnect fitting. In either case, minimizing sample fluidic transmission lengths reduced the effect of dispersion. This mode of operation was found to function well for prototype experiments where the mass spectrometer, sampling volume, and DSP system were in close proximity. For GMP integration (Figure 2.1) it is more appropriate to transfer dry ions from the DSP outlet to the MS inlet via an ion transfer interface instead of transferring the samples in their liquid state because of a significant separation length between the sampling point in the cell culture and analytical suite where MS analysis is performed.

2.3 Ion Transfer Interface

The ion transfer interface is a technology for transferring dry ions over a long distance (~1-8 meters) from their source to the mass spectrometer.[42] Instead of ionizing directly in front of the mass spectrometer, a cascaded pressure glide system from atmospheric conditions at the ion source to the reduced pressure (vacuum) near the inlet to the mass spectrometer is established to transfer the ions over long distances. Figure 2.7 demonstrates the operating principal of the ion transfer interface.[42] A vacuum, generated by an auxiliary vacuum pump, is drawn on a customized MS vacuum box mounted on the front of the MS. The pressure within the vacuum box is higher (~10^2 Torr) than the pressure

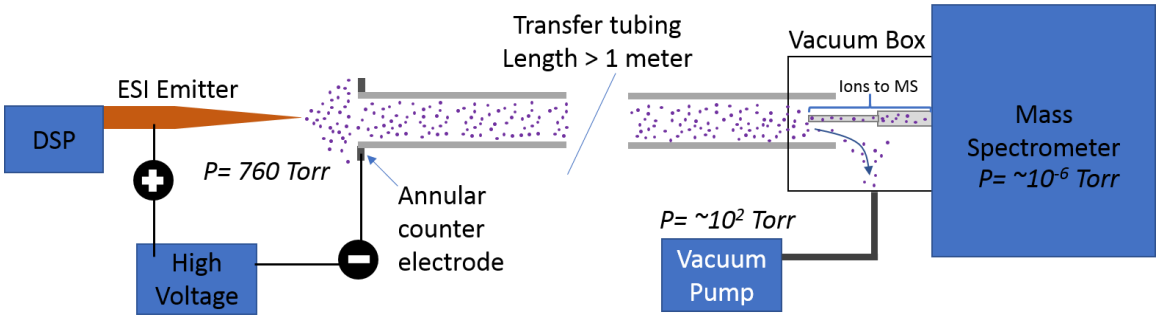

Figure 2.7: The gas phase ion transfer interface uses a multistage vacuum system to transfer ions from their source (DSP) to the MS inlet. A vacuum drawn on the MS vacuum box drives ions from the ESI emitter to the MS inlet, while the vacuum inside the MS draws the ions from the MS vacuum box to the MS for analysis.

generated by the MS internally (~10^{-6} Torr), which enables a multistage ion transfer between different evacuated zones. Ions are generated in ambient pressure at their source, in this case the DSP outlet, and transferred through a 3/8" OD, 5/16" ID Tygon^{TM} tube by the high flow rate vacuum applied the MS vacuum box. Once the ions reach the vacuum box at the intermediate pressure, the internal MS vacuum draws them into the instrument for analysis.

A prototype design was first developed for a Bruker MicrOTOF MS with a 1-meter transfer distance. A CAD model of the ion transfer interface for this geometry is shown in Figure 2.8. In this design, the MS inlet had to be modified to extend the inlet within the ion transfer tube for ions to be detected. The vacuum drawn by the Bruker was found to be too weak to overcome the vacuum of the bench-top pump used for ion transfer. Increasing the pressure within the vacuum box was found to be an inadequate solution because ions failed to reach MS the vacuum box with a smaller pressure differential between the ESI outlet and the MS vacuum box. For this reason, a custom MS inlet was designed to extend into

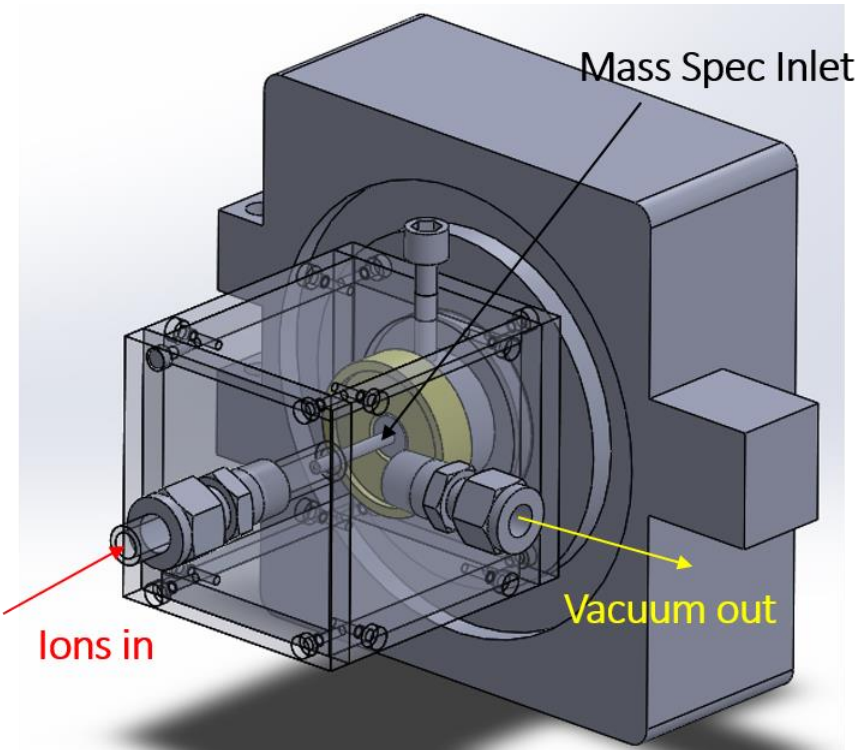

Figure 2.8: Ion transfer interface design for the Bruker MicrOTOF MS. A vacuum generated by a bench-top vacuum pump draws ions from approximately 1 meter away to the modified MS inlet, which is extended ~5 mm into the ion transfer tube.

the ion transfer tube, which improved ion transfer efficiency. Other MS systems, like the Thermo Fisher system used to demonstrate GMP integration, were observed to have sufficient pressure drop from the MS vacuum box to the MS system such that no modifications to the MS inlet were necessary.

To test ion transfer efficiency in the prototype system on the Bruker MS, 5 μm cytochrome c (Cyt c) with 1% AA was infused directly to the MS and then infused through the 1-meter ion transfer tube of the ion transfer interface. Figure 2.9 shows the comparison of the resulting spectra for the two methods, and in both cases a clear signal associated with

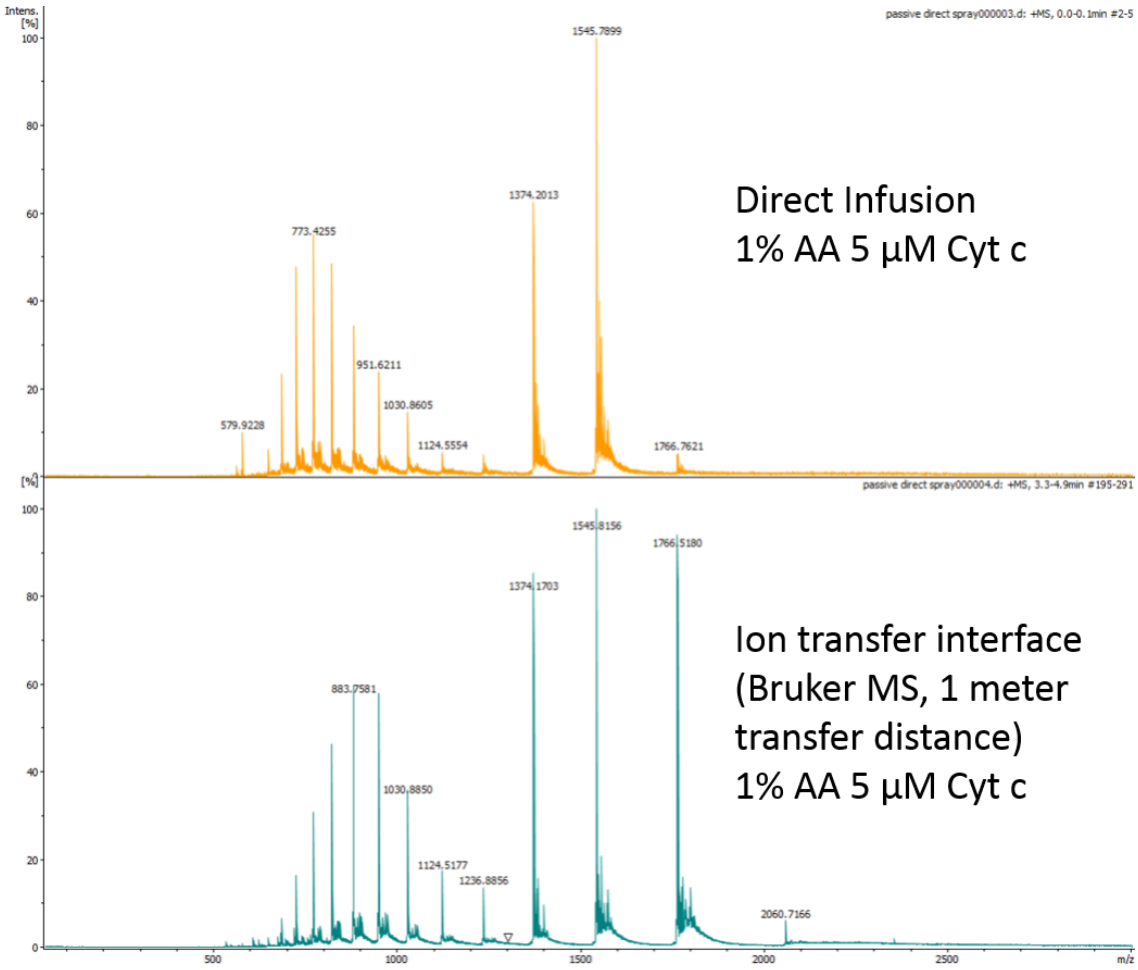

Figure 2.9: Comparison of direct infusion and ion transfer of 1% aa, 5 µM Cyt c. The higher intensity of lower charge states in the ion transfer spectra is likely due to enhanced droplet desolvation in the ion transfer interface, although it is reported that lower charge state ions transfer more efficiently.

Cyt c is obtained. It has been reported that the trend for ion survival in the interface is dependent on ion size and charge state. Larger ions, with lower charge states, are observed to transfer more efficiently through the length of the interface because they have lower bulk diffusion coefficients and are affected by space charge repulsion to a lesser degree.[42] In the MS spectra corresponding to ion transmission through the interface shown in Figure 2.9, lower charge states (i.e., +7 and +6 states, m/z ~1766 and ~2060 respectively) are present

in higher abundance, which may be due to the increased transfer of low charge state ions through the ion transfer, but can more likely be attributed to enhanced desolvation as none of the other charge states appear to change in relative intensity. The ion transfer design was not required for experiments with the Bruker MS, where direct ESI-MS was possible. The MS within the GMP facility (Figure 2.1), on the other hand, required the integration of the ion transfer interface to enable real-time ESI-MS of samples which could not be infused directly to the instrument.

The next iteration of the ion transfer interface was designed for a ThermoFisher™ Q-Exactive Plus mass spectrometer located in a GMP-level facility on GT campus (Figure 2.1). The ion transfer interface was designed for ion transmission over a ~3.5 meter distance. This length was selected to transfer ions from the ISO-7 suite, where cells are cultured, to the mass spectrometer isolated in the analytical suite to meet GMP requirements. This facility serves as a proxy to pharmaceutical/clinical grade biomanufacturing, where it is expected that cell cultures in production lines will be separate from analytical suites. Therefore, demonstrating that the ion transfer interface is capable of transferring ions from a remote bioreactor to the MS is important for enabling drop-in integration of DSP into GMP workflows.

A CAD model of the ion transfer interface implemented in the GMP cell manufacturing facility is shown in Figure 2.10. The design was similar to the baseline used for the Bruker mass spectrometer, with a major change to the system support and a different vacuum pump for generating flow. The front-end design of the Thermo Fisher MS was reverse engineered to create an adjustable latching system that was used to tune the

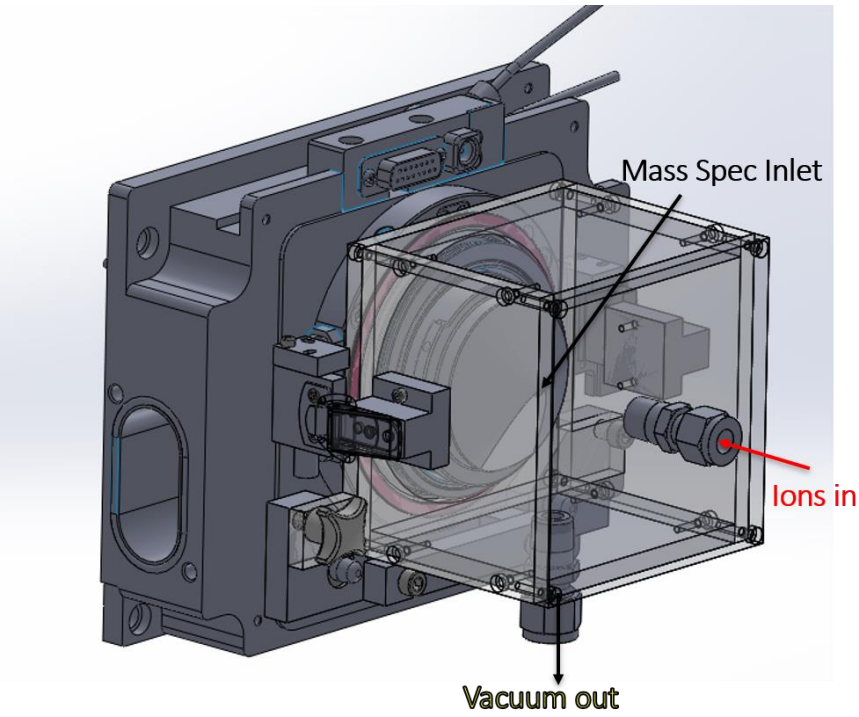

Figure 2.10: Thermofisher Q-Exactive Plus ion transfer interface CAD model.

clamping force between the MS front end and the vacuum box. This design reduced leaks at the MS/vacuum box interface, which ultimately resulted in better ion transfer efficiency and longer distance transport compared to the Bruker system, which was attached to the MS via elastic bands (i.e., rubber bands). Instead of a bench-top vacuum pump, a high flow rate ShopVac^{TM} was used to generate flow from the ion source to the MS inlet. The ShopVac provided high flow rate suction with moderate pressure drops. In agreement with reported data, higher flow velocity within the ion transfer interface improved ion transfer efficiency. For this iteration of the ion transfer interface, no modifications to the MS inlet were required, and it was observed that ion transfer efficiency was unaffected by the relative position of the transfer tube and the MS inlet, unlike the Bruker design where it was critical that the customized MS inlet extended into the ion transfer tube. It is expected

that the Thermo MS is less sensitive to the relative positioning of the ion transfer tube exit for two reasons: i) the inlet orifice to the MS is larger and ii) the difference between the pressure in the interface box and the MS is greater because the ShopVac operated at relatively high pressure (~100 Torr). These factors increased the relative flow rate into the MS system and therefore more ions were drawn into the MS for analysis compared to the Bruker system.

To determine the impact of ion transfer on MS limit of detection, a comparison was performed using the commercial nanoESI source provided by ThermoFisher (direct ion infusion to the MS) and via the ion transfer interface. Varying levels of Cyt c in a 50/50 acetonitrile/H_2O solution with 0.1% formic acid were used as the test samples. For direct infusion to the mass spectrometer with the commercial source, the limit of detection was found to be 15 nM Cyt c, while for the 3.5 meter long ion transfer interface it was 100 nM. Additionally, intensity dropped approximately 2 orders of magnitude, from 10^6 counts to 10^4 counts as measured by the MS due to ion losses during the long distance transport. As reported in literature, only the lower charge states of Cyt c were observed in the ion transfer interface (+9 and lower) whereas in the direct infusion case a full range of charge states was detected. This confirms prior reports that the ion transfer interface preferentially transmits lower charge state ions, which may have implications for MS/MS which benefits from highly charged species.[42] As the loss of some sensitivity as a result of ion transfer will impact CQA biomarker detection in cell culture, the ion transfer interface has been identified as an area requiring further improvement

2.4 DSP Mass Exchanger

The DSP is designed for continuous flow sample treatment in a tangential flow mass exchanger. Figure 2.11 illustrates a cross section of the DSP mass exchanger. Sample flows through the sample channel at 10-50 µL/hr to match the appropriate flow rate of the ESI

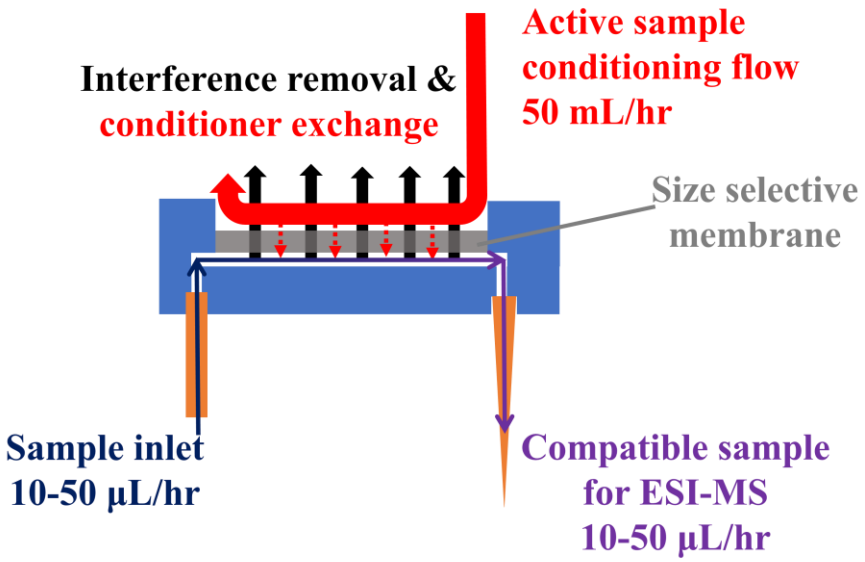

Figure 2.11: The DSP mass exchanger integrates a size selective membrane to separate a sample channel from a conditioner channel. Sample flows through the sample channel at 10-50 µL/hr, whereas the conditioner flow operates at 50 mL/hr. During sample treatment, species which interfere with ESI-MS analysis diffuse from the sample channel to the conditioner channel through the membrane. Simultaneously, chemical "conditioners" the enhance ESI-MS sensitivity to CQA biomarkers diffuse from the conditioner channel to the sample channel. Target CQA biomarkers are retained in the sample channel because their large size hinders diffusion through the membrane, resulting in a compatible sample for real-time ESI-MS analysis.

emitter for real-time MS analysis. Active conditioning flows at 50 mL/hr and is separated from the sample channel by a size selective Al_2O_3 membrane which fluidically couples the sample and conditioner channel. The nanoporous membrane allows small molecules, for example, salt ions that interfere with MS analysis and/or acids providing protons for ionization, to diffuse freely into or out of the sample. Larger molecules, such as target CQA biomolecules, diffuse through the membrane at a reduced rate because their transport through the nanopores is restricted in proportion to their molecular weight. Therefore, larger size biomolecules are preferentially retained in the sample channel during treatment, while the smaller salt molecules readily diffuse out to the salt-free conditioner channel driven by the concentration gradient. The monolithic mass exchanger enables DSP's "active sample treatment" protocol, which refers to the simultaneous infusion of signal enhancing molecules from the conditioner channel to the sample channel, removal of small molecular weight interfering species (primarily salts) from the sample channel, and retention of large biomolecules in the sample channel. The pore size is 50 nm in the membrane, which retains most signaling and paracrine factors, but can lead to inadvertent removal of some smaller CQAs as explored in CHAPTER 3.[34]

A representative CAD model of the DSP mass exchanger is shown in Figure 2.12. In this figure, the inlet and outlet are represented by 1.5 cm long, 360 μm OD cylinders for visualization purposes. In practice, the DSP inlet is 360 μm OD PEEK tubing with an extended length (5-20 cm) while the outlet is a fused silica ESI emitter. The conditioner channel is 4.5 mm wide and 11 mm long, defined in a 500 μm thick silicon wafer. Conditioning flow is introduced via a fluidic interface package (section 2.6) and flows along the bottom of the conditioner channel, tangentially to the size selective Al_2O_3

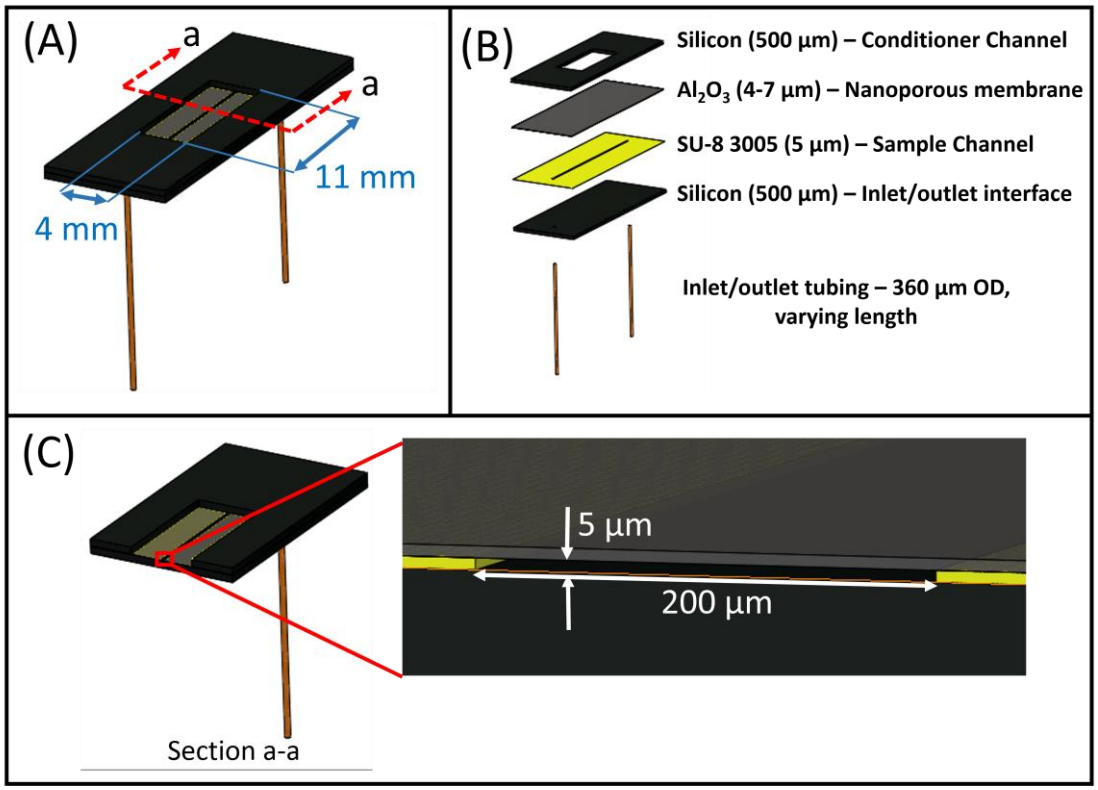

Figure 2.12: A) A CAD model of the DSP illustrates the final mass exchanger geometry as well as the dimensions of the active conditioner channel and the section line used for visualization in C. B) The DSP conditioner channel is separated from the sample channel by a thin (<10 µm) nanoporous Al_2O_3 membrane which fluidically couples the two channels. An SU-8 layer defines the sample channel geometry (5 µm tall, 200 µm wide, 2.2 cm long) and a silicon base layer enables monolithic integration of 360 um OD tubing via through hole counterbore geometries. C) The section view from part A is used to visualize the sample channel cross section to scale.

membrane. The sample channel is below this membrane. The DSP sample channel is 5 µm deep, 200 µm wide, and 2.2 cm long. The sides of the sample channel are defined by SU-8 3005, the bottom is SiO_2 on Si, and the top is Al_2O_3. The active portion of the sample channel, where treatment occurs, runs parallel to the length of the 11 mm long active

conditioner channel. The inlet and outlet interfaces for the DSP mass exchanger are identical counterbores (inset image, Figure 2.13) for inserting the 360 μm OD capillaries for the sampling probe inlet and electrospray tip outlet. The counterbore design allow for precise alignment of the inner through channels within the capillaries with the ~60 μm through holes in the wafer for sample transfer in and out of mass exchanger, while mitigating potential clogging at the interconnection joints due to epoxy overflow, silicon chipping or fused silica tubing fracture. The total volume of the DSP mass exchanger, from inlet to outlet, is merely 22 nL, a very small value which is essential for minimizing the dead volume and in turn reducing the sample size and the transit time of the sample analysis.

2.5 Microfabrication Overview

The DSP microfabrication (detailed process information, lessons learned, and process parameters are described in APPENDIX A) incorporates aspects of prior work by

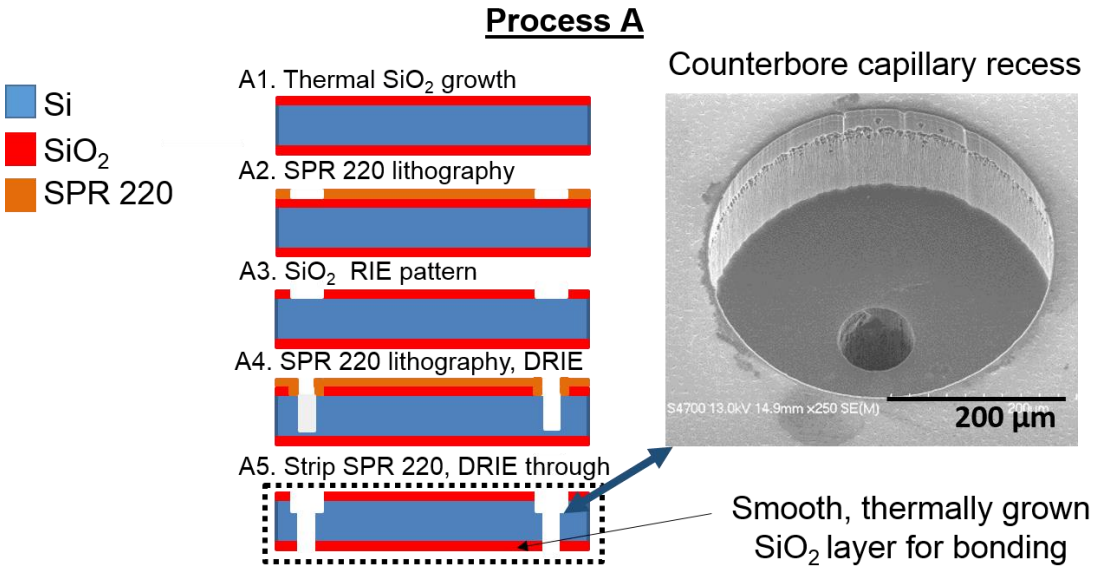

Figure 2.13: Process A for microfabrication of the counterbore capillary recess.

Tibavinsky et al. but extends the processing capabilities and introduces new steps into a microfabrication process to produce a robust microfluidic mass exchanger for flexible integration to ESI-MS workflows.[34, 43] The DSP microfabrication process is divided into three main stages: process A, B, and C (Figure 2.13, Figure 2.14, and Figure 2.15 respectively). These processes were intentionally designed to place wet etching steps before the sample channel was enclosed during bonding (process C). Once bonded, only dry etching steps were carried out on the device stack. This significantly improved device reproducibility and reduced the chance of clogs in the final device.

A novel feature of the DSP system is the clog resistant counterbore geometry (inset, Figure 2.13). This feature is used for precise alignment of the fluidic inlet/outlet and mitigates the risk of clogs caused by fractured silica from the ESI outlet or epoxy used to

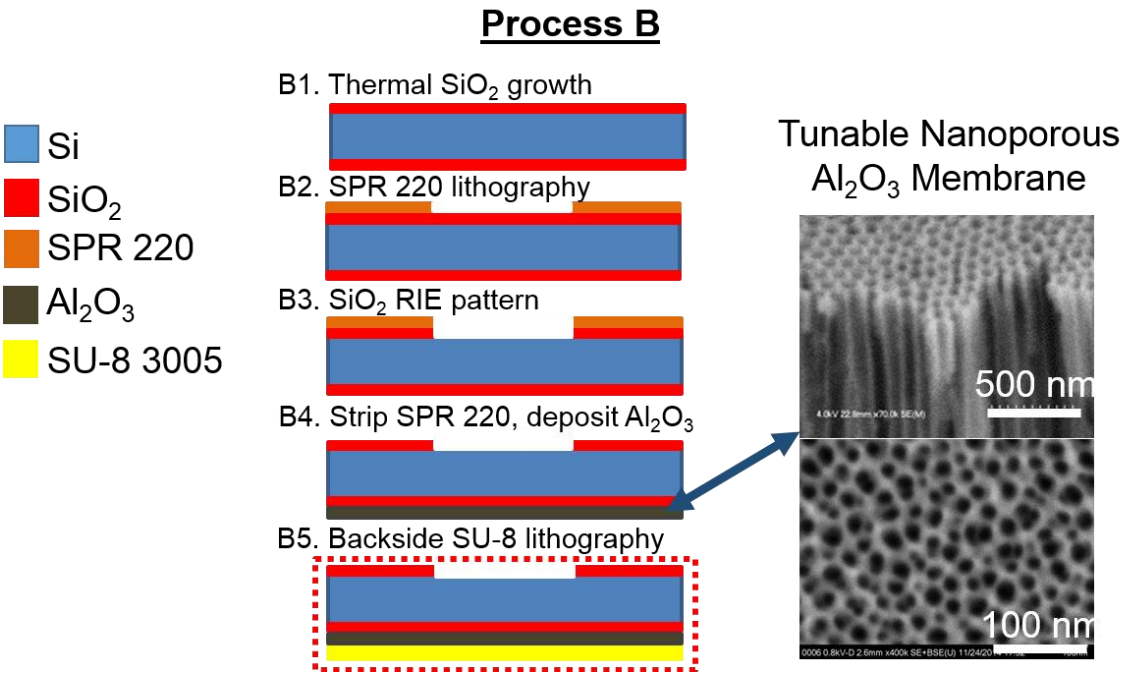

Figure 2.14: Process B microfabrication for integration of the nanoporous membrane and definition of the sample channel in SU-8.

secure the DSP to the tubing. Importantly, the process A workflow was intentionally developed to only incorporate Si/SiO_2, does not rely on backside alignment, and only etches one side of the wafer. In other words, process A was designed as a CMOS compatible process (i.e., SiO_2 on Si), and therefore the final wafer could be cleaned in aggressive piranha bath after through etching was completed. This cleaning step was significant as it removed residue within the through holes to mitigate any clogs in the final device. Finally, process A enabled device bonding. One side of the wafer was left with a

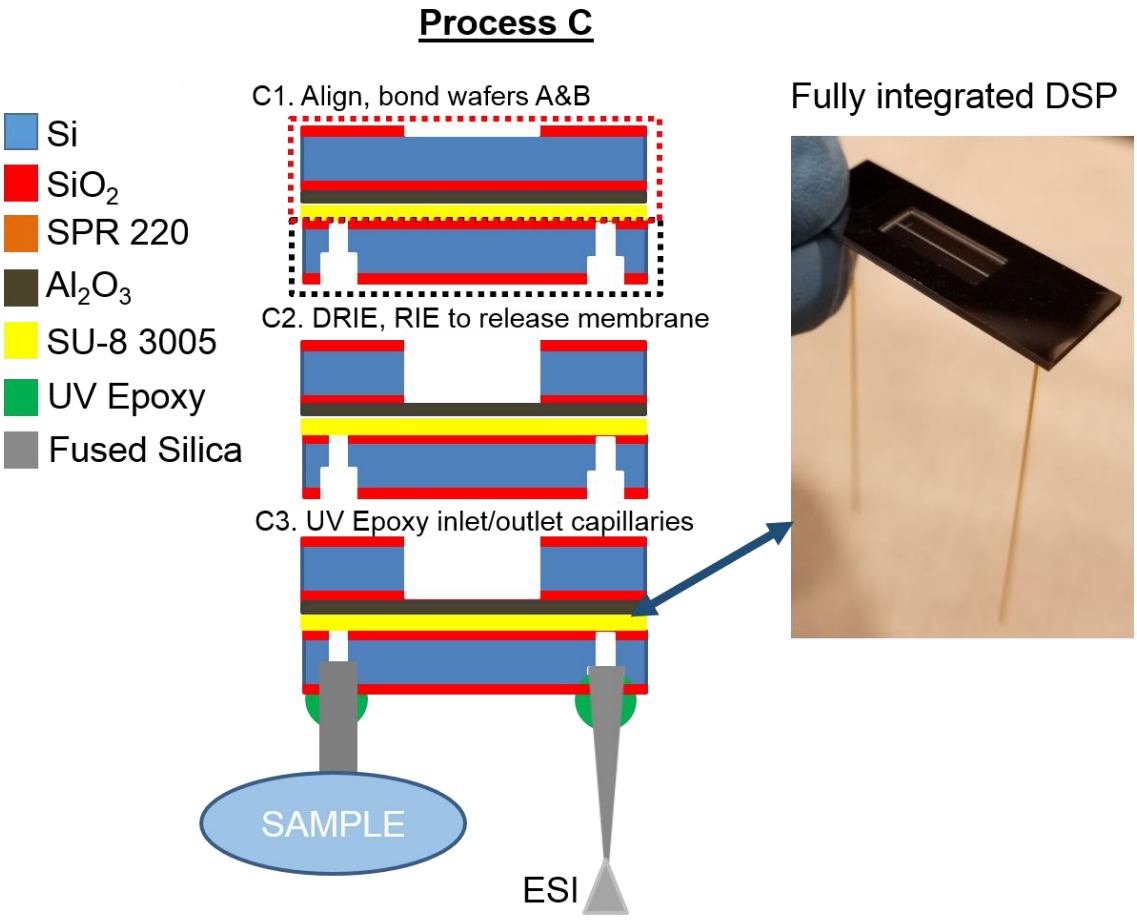

Figure 2.15: Process C microfabrication for wafer level bonding, membrane release, and inlet/outlet integration.

smooth, thermally grown SiO_2 layer which served as a suitable interface for the bonding procedure in process C.

The infrared (IR) transmissibility of silicon was exploited to enable the wafer level alignment of the process A and B wafers in process C (Figure 2.15). Early iterations of the DSP microfabrication process deposited SU-8 on the inlet wafer (process A) to align the sample channels with the inlet holes. However, the rough Al_2O_3 layer did not adhere to the smooth SU-8 layer which resulted in batch delamination of the final devices. Modifying the process to deposit SU-8 on the Al_2O_3 enabled bonding, which motivated the use of a back-lit IR microscope to align the sample channels and inlet holes. This modification to the process demanded that the first pattern deposited on each process wafer was centered, hence the utilization of a maskless aligner to center each pattern on the wafers.

2.5.1 Microfabrication Process in Brief

The DSP mass exchanger is produced via batch microfabrication with three separate process flows, the first two accomplished in parallel on individual wafers and then a final process flow with processing steps carried out on the bonded wafer stack, including the incorporation of an inlet capillary and an outlet ESI emitter. Both process A and B (Figure 2.13 and Figure 2.14) begin with thermal oxidation of double side polished p-type <100> orientation silicon wafers (1-20 ohm-cm, Polishing Corp of America) resulting in a 3μm thick SiO_2 mask layer on both sides of each wafer. Process A begins as 380 μm diameter holes are patterned in a layer of SPR 220 photoresist with photolithography Figure 2.13 A2), and then in the SiO_2 layer with a reactive ion etch (RIE) step (Figure 2.13 A3). Concentric 60 μm diameter holes in a layer of SPR 220 are patterned above the larger SiO_2

patterned holes, followed by a deep reactive ion etching (DRIE) "Bosch" process carried out on the wafers for ~400 microns (Figure 2.13 A4). The photoresist is stripped, and another DRIE etch is carried out on the unmasked 360 μm patterned SiO_2 layer with concentric partially etched 60 μm inlets until a through etch is achieved, resulting in the clog resistant counterbore capillary recess depicted on the inset image (Figure 2.13 A5). Process B begins as the active conditioning channel is patterned in SPR 220 (Figure 2.14 B2) followed by a subsequent RIE etch in the SiO_2 masking layer (Figure 2.14 B3). Afterwards, the wafer is cleaned and a ~5 micron thick film of aluminum is deposited on the side opposite the patterned SiO2, and subjected to an anodization process which creates a nanoporous alumina film with tunable pore diameters in the 10-50 nm range (Figure 2.14 B4).[44] Following the anodization, backside photoresist patterning of SU-8 3005 is carried out to define the sample channels (Figure 2.14 B5). Process C begins as the two wafers are bonded at 130 ^{o}C and 10 bar for 30 minutes (Figure 2.15 C1). A DRIE process is carried out on the patterned conditioning channels down to the layer of SiO_2, followed by two RIE steps (CHF_3 followed by CF_4) to open the barrier layer in the nanoporous membrane to allow fluidic transfer between sample and conditioning channel (Figure 2.15 C2). Between the first and second RIE step for opening pores, the devices are diced. Finally, inlet and outlet capillaries are positioned and glued into place within each counterbore capillary recess using a UV activated epoxy (Figure 2.15 C3).

2.6 Fluidic Interface Package

The DSP is packaged in a CNC machined polycarbonate or PEEK package which is designed to introduce a uniform flow of conditioning liquid across the top of the DSP

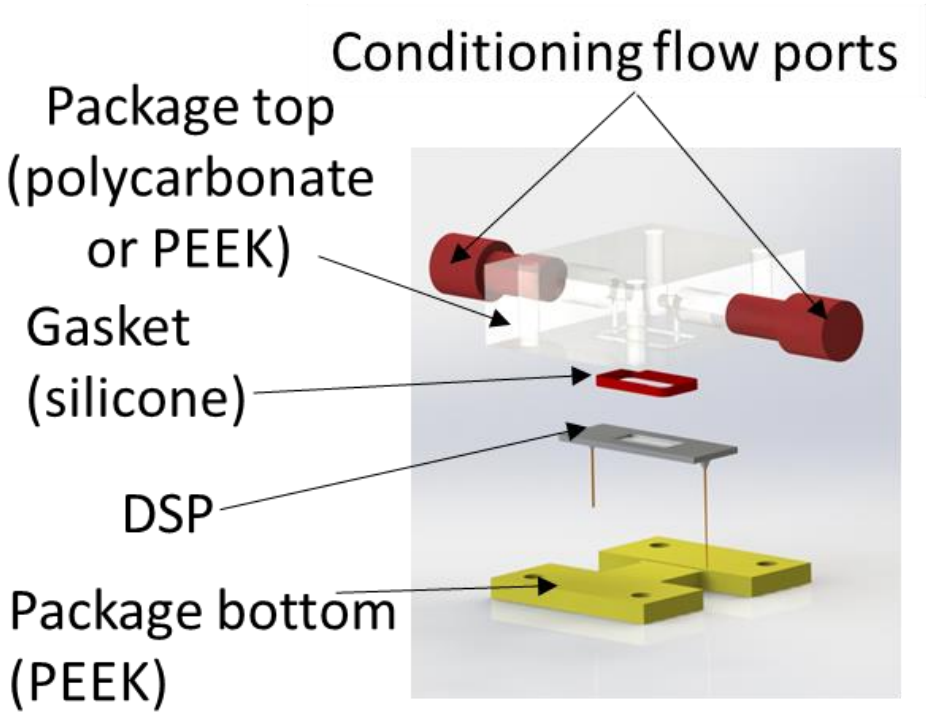

Figure 2.16: An exploded view of the DSP fluidic interface package.

device at a relatively high flow rate (μL/hr of the sample flow vs mL/hr of the conditioner solution). As shown in the exploded view in Figure 2.16, a self-adhesive silicone gasket placed between the package and DSP sealed the conditioning flow against the topside of the DSP for continuous flow through the package. For superior chemical resistance when exploring conditioners such as acetonitrile, a PEEK package top was used, but for most applications a transparent polycarbonate package proved to be beneficial for identifying bubbles within the conditioning channel. Bubbles within the conditioner channel stop the diffusional transfer of species from the sample channel to the conditioner channel and render DSP conditioning ineffective.

The fluidic interface package underwent two design iterations for improved mass exchanger performance. In the initial design, the conditioner flow and sample flow were

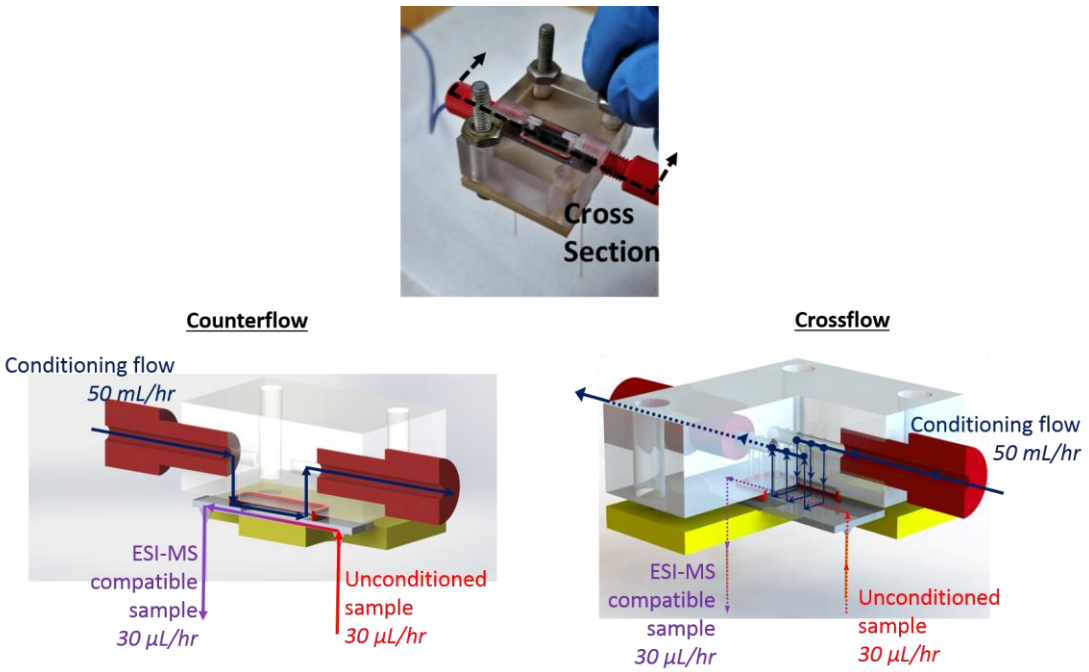

Figure 2.17: Cross section of DSP in the fluidic interface package with CAD schematics of both counterflow (first generation) and crossflow (second generation after performance optimization) flow configurations.

oriented in parallel but opposite directions, or in the "counterflow" orientation used for DSP prototyping (CHAPTER 3). CFD modeling guided an improved design in which the conditioner and sample flow paths are perpendicular to each other, i.e., in "crossflow" orientation which has improved DSP performance as discussed in section 2.7. Figure 2.17 shows an isometric view of the assembled fluidic package along with CAD models of both orientations. For both iterations, a peristaltic pump provided conditioner flow at 50 mL/hr while a separate syringe pump forced flow through the sample channel in the 10-50 µL/hr range.

2.7 Model Guided Mass Exchanger Optimization

During sample treatment, species within the sample channel are transported through the size selective membrane into the conditioner channel (or vice versa in the case of MS enhancing chemicals). Prior work reported that the transmembrane velocity in the mass exchanger was 9.2 μm/s within the 50 nm pores in the Al_2O_3 membrane. Based on the characteristic length of transport, i.e., a 5 μm membrane thickness, and this transmembrane velocity, the Peclet number for a species with a diffusion coefficient of 10^{-9} m^2/s within the nanopores is ~0.022.[34, 43] This indicates that within the nanopores, diffusion is the dominant transport mechanism. In both the sample and conditioning channels, the average velocity can be estimated as V=Q/A where Q is the flow rate and A is the cross-sectional area. Within the sample channel, with a length of 2.2 cm and a characteristic velocity of 8 mm/s, the Peclet number is ~10^5. The conditioner channel Peclet number is ~10^4 using the length of 11 mm and a characteristic velocity of 3 mm/s. Advection is dominant within both the sample and conditioner channels based on these large Peclet numbers, and therefore increasing the bulk mass transfer coefficient in either channel will enhance transport in the mass exchanger. However, increasing the mass transfer coefficient in the sample channel comes at a significant operational cost. Assuming the flow is fully developed (from both a hydrodynamic and mass transfer perspective) within the sample channel, the Sherwood number is constant, and only by reducing the characteristic length of transport can mass transfer efficiency improve. The sample channel height (5 μm) can be reduced to improve the resulting mass transfer coefficient, but the tradeoff is increased hydrodynamic resistance, which can lead to membrane failure due to an increased pressure loading across it. From a practical standpoint, reducing the sample channel height may also result in more

clogging events from debris with critical dimensions (i.e., minimum length dimensions) above the reduced height dimension. Further, prior work indicated that the dominant resistance to mass transfer in a similar mass exchanger geometry was convection within the conditioner channel.[34, 43] The conditioner channel is easily modified without affecting device reliability, and therefore the flow structure within the conditioner channel was studied to reduce mass transfer resistance in the entire system.

In order to improve device efficiency in terms of salt removal and MS enhancing species infusion, the conditioner flow orientation was changed from a counterflow to a crossflow orientation relative to the sample channel, as shown in Figure 2.18, to reduce the characteristic length over which the mass transfer boundary layer grew. The design was qualified with simulations, and experimental validation of the improved device performance was carried out prior to applying the optimized DSP to more complex samples, e.g., those taken directly from a cell culture.

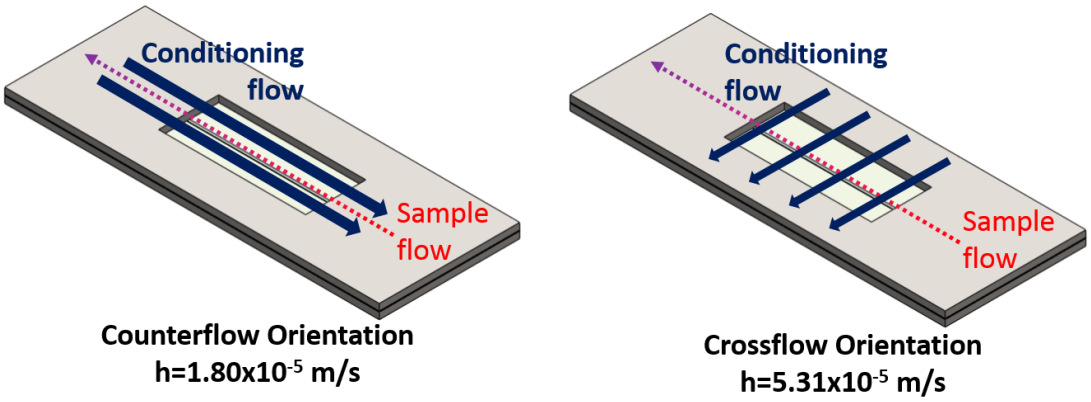

Figure 2.18: Counterflow and crossflow orientations for the DSP mass exchanger. A simple change in package geometry modified the flow orientation to enhance the mass transfer coefficient by over 150%.

The short distance between the conditioner flow inlet along with a step change in geometry upon entering the conditioner channel creates a system in which the flow is developing from both a hydrodynamic and mass transfer perspective, necessitating the use of simulations to accurately predict the mass transfer coefficient. Both two-dimensional (2D) and three-dimensional (3D) simulations were carried out, and it was determined that a full domain simulation was necessary for effectively estimating the mass transfer coefficient, especially in the counterflow orientation. Figure 2.19 shows the growth of the concentration boundary layer by plotting the surface corresponding to the 99% free stream

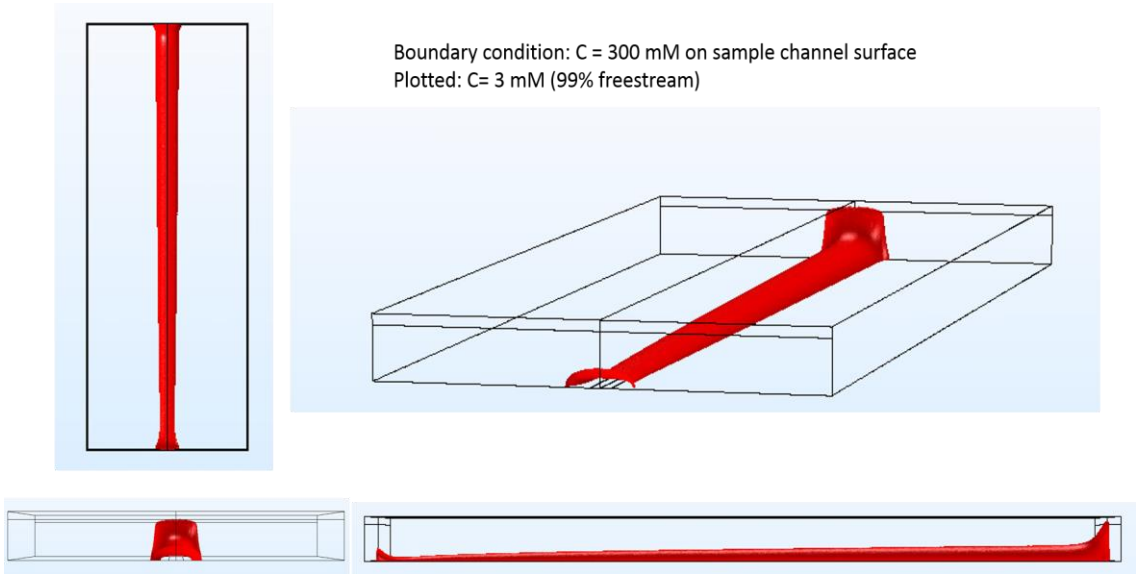

Figure 2.19: Simulation domain and iso-surface (red) corresponding to 1% of the boundary value of concentration (proxy for the upper edge of the concentration boundary layer) for the counterflow orientation with a constant concentration (C=300 mM) boundary condition at the top (facing the conditioner flow) membrane surface. The 3D nature of the boundary layer growth confirmed that 2D simulations would not capture the relevant phenomena nor estimate the mass transfer coefficient accurately.

concentration value. The three-dimensional nature of the boundary layer affects the local mass transfer coefficient, motivating the use of a full domain simulation to effectively estimate the mass transfer effects.

The convective flux can be estimated within the conditioner channel using equation (2.1):

$$J_c'' = h_c(C_{membrane} - C_{freestream}) \tag{2.1}$$

where J_c'' (mol/s/m^2) is the flux from the sample channel into the conditioner channel, h_c (m/s) is the convective mass transfer coefficient in the conditioner channel, $C_{membrane}$ (mol/m^3) is the analyte concentration on the top surface of the membrane, and $C_{freestream}$ (mol/m^3) is the analyte concentration far from the membrane in the free stream outside of the concentration boundary layer. The concentration far from the membrane surface was assumed to be 0 mol/m^3, and this was confirmed with the simulation result. The position where *C*=3 mM (1% of the surface value) is shown in Figure 2.19 (red) is taken to be the location of the concentration boundary layer edge. The boundary layer does not reach the top edge of the domain, therefore it is reasonable to assume that *C* approaches 0 mol/m^3 and the convective mass transfer coefficient can be approximated by equation:

$$h_c = \frac{J_c''}{C_{membrane}} \tag{2.2}$$

The simulations were carried out in the COMSOL™ software using coupled modules of Laminar Flow and Transport of Dilute Species. For each simulation, the conditioner channel was simulated with the following depth x width x length dimensions: 600 μm x 4.5 mm x 11 mm. A plane on the bottom of the channel with width x length dimensions of 200 μm x 11 mm represented the area of the membrane where active analyte exchange occurs with the sample channel. Along this plane, either a constant flux or a

constant concentration boundary condition was implemented to establish a range of potential mass transfer coefficients. A total of four simulations were carried out to estimate h_c: two in counterflow orientation with either a constant flux or constant concentration boundary condition, and again two in crossflow with the same boundary conditions. For each simulation the inlet and outlet to the conditioner channel were modeled as 100 μm tall strips spanning the entire width of the appropriate side walls to represent the area between the compressed silicone gasket within the fluidic package and the Si top plate of the mass exchanger, where conditioning flow enters or exits the package (Figure 2.17). At the inlet, species concentration was set to 0 mol/m^3 and the flow was introduced as a uniform plug with the average velocity calculated as V=Q/A where Q is the conditioner flow rate (50 mL/hr) and A is the inlet cross-sectional area, 100 μm x 11 mm in crossflow and 100 μm x 4.5 mm in counterflow. At the outlet, pressure was set to ambient and species were free to transport out of the domain. Water at 25 ^{o}C was used as the working fluid, and the binary diffusion coefficient (D_{AB}) was set to 1x10^{-9} m^2/s to capture a representative value of the diffusion coefficient for relevant species transport, e.g., salts and biomolecules. A mesh convergence study showed that directly over the sample channel, elements of a maximum size of 5 μm were required with a growth rate of 1.03 for the rest of the domain. The maximum element size in the entire domain was set to 30 μm. Values of the average mass transfer coefficient were used to confirm mesh convergence.

Figure 2.20 shows the resulting mass transfer coefficient calculated according to equation 2.2 along the center of the sample channel as a function as sample channel length. The surface average value from each simulation is written above the respective trace. In counterflow, the mass transfer coefficient increases to a maximum within 500 μm of the

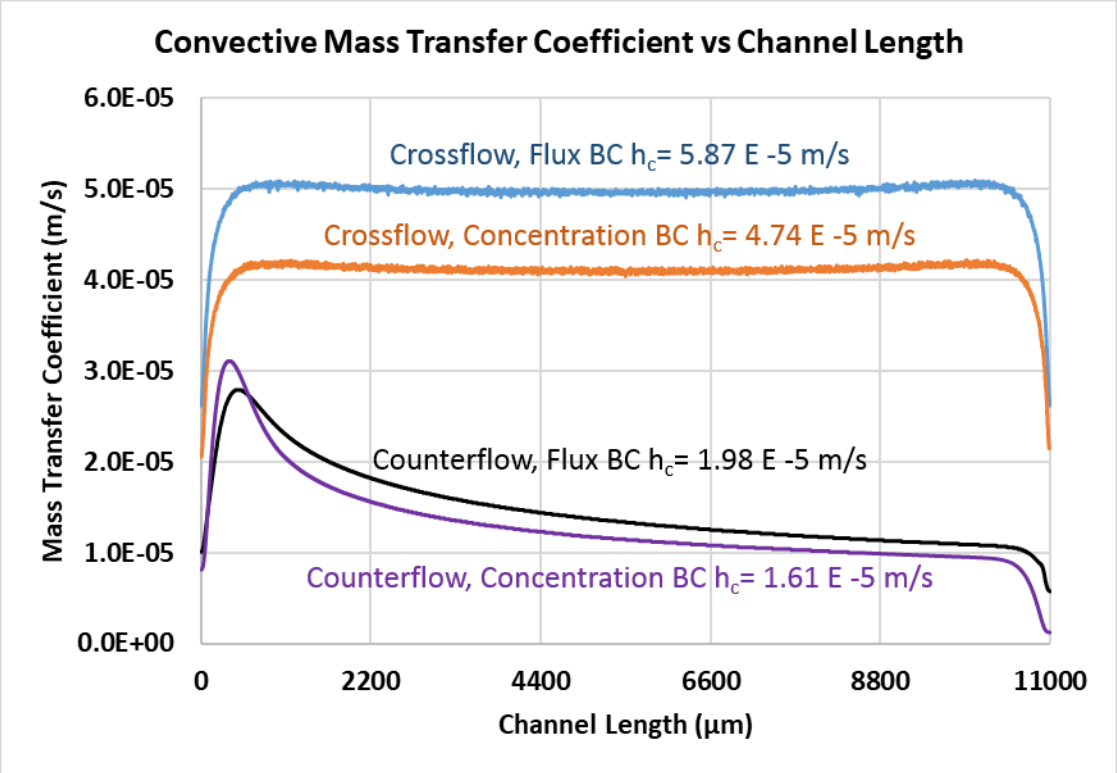

Figure 2.20: Mass transfer coefficient as a function of channel length along the centerline of the sample channel. Note that the displayed mass transfer coefficient value is an average across the entire sample channel area.

entrance and then continuously decreases along the sample channel. The step change geometry at the entrance results in a stagnation zone at the entrance of the channel, but as the velocity just above the membrane increases, the mass transfer boundary layer thickness reaches a minimum and the mass transfer coefficient reaches a maximum. The mass transfer boundary layer then grows along the length of the channel, causing the mass transfer coefficient to decrease continuously. The profile of the mass transfer boundary layer in the counterflow orientation is shown in the side view in Figure 2.19. The minimum thickness of the boundary layer corresponds to a maximum mass transfer coefficient. In the counterflow geometry at the edges of the sample channel, the mass transfer coefficient is on average higher than at the center because the boundary layer is thinner towards the

edge. Due to the 3D nature of boundary layer growth in counterflow, the edge regions of the sample channel have lower resistance to mass transfer and therefore a higher average mass transfer coefficient.

Crossflow orientation results in a 200 to 300% increase of the surface averaged convective mass transfer coefficient. Although the average flow velocity within the channel is actually lower in crossflow (3 mm/s in crossflow vs 8 mm/s in counterflow) because of a much greater cross sectional area for the same volumetric flow rate, the average thickness of the mass transfer boundary layer is smaller across the entire sample channel resulting in a higher mass transfer coefficient. The reason for this is twofold: 1) the small stagnation zone at the entrance region in counterflow is no longer in an active mass transfer area in crossflow 2) the mass transfer boundary layer is much smaller across the active transport area due to a shorter development length in crossflow (200 μm in crossflow vs 11 mm in counterflow).

A design change in the fluidic package allowed for crossflow orientation mass exchanger operation with no other changes to the system (Figure 2.17). The enhanced mass transfer was confirmed by comparing treatment of control samples consisting of phosphate buffered saline (PBS) and cytochrome c (Cyt c). Comparison of MS spectral signatures for treatments of 2xPBS (274 mM NaCl, 5.4 mM KCl, 20 mM phosphate buffer) with 2.5 μM Cyt c treated with 1% acetic acid (AA) in both the crossflow and the counterflow orientations clearly indicates the superiority of mass transfer (and thus enhanced interfering salt removal) in crossflow. In counterflow, the Cyt c signal is masked by adducted peaks while the crossflow treatment reveals multiple charge states associated with Cyt c with reduced background noise as shown in Figure 2.21.

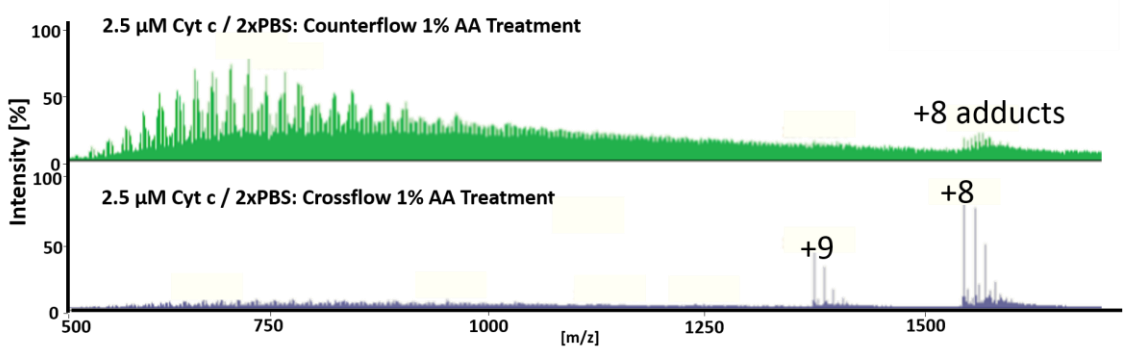

Figure 2.21: MS spectra comparison of counterflow and crossflow DSP treatment for sample with 2.5 µM Cyt c in 2xPBS. Counterflow treatment reveals a cluster of heavily adducted peaks around the expected +9 protonation state and overall a very noisy spectrum with significant background due to salt in the sample. Mass spectra for crossflow treatment are much cleaner with less background chemical noise and two distinct protonated +8 and +9 charge states associated with Cyt c, indicating higher levels of salt removal during treatment.

Throughout the rest of this thesis DSP is employed in both the counterflow and the crossflow orientation. The counterflow orientation DSP is used to demonstrate the advantageous effects that active sample conditioning has on real-time ESI-MS analysis in most of CHAPTER 3, but the later results in this chapter (Section 3.5) and all of the results in CHAPTER 4 are from DSP in the optimized crossflow orientation. The reason that a sub-optimal design was applied in CHAPTER 3 is because the evidence of insufficient salt removal in the results presented in Sections 3.2-3.4 are what motivated the detailed study of the DSP mass exchanger. In other words, the model guided optimization presented here was carried out after the experiments presented in the early sections of CHAPTER 3.

CHAPTER 3.
DSP ANALYTICAL CHARACTERIZATION

Inline, rapid analysis is important to enable *in operando* feedback and process control for quantitative monitoring methods in the biomanufacturing field. Electrospray ionization mass spectrometry (ESI-MS) is a suitable candidate for inline analysis due to its broad molecular weight coverage, sensitivity, and a possibility for preserving structure/folding and non-covalent interactions of biomolecular complexes through "soft-ionization".[22, 45, 46] ESI-MS requires no labeling of biomolecules, allowing not only monitoring of target biomolecules, but also identification of unknown bio-analytes. However, direct ESI-MS analysis of biological samples is difficult due to the need for sample preparation prior to analysis. Inorganic salts found in high abundance in cell cultures suppress the signal associated with biomolecules, reducing ESI-MS measurement sensitivity and making identification challenging. Typically, techniques such as high performance liquid chromatography (HPLC) are employed upstream of ESI-MS both to remove compounds that interfere with the analysis and to separate and assist in identifying components of complex biomolecule mixtures. Due to the large time delay associated with these separation methods, real-time ESI-MS monitoring of cell cultures has been largely unexplored.

In this chapter, real-time DSP ESI-MS analysis is explored and its performance metrics are defined and assessed under different conditions. The experiments were designed to probe active sample conditioning for enhanced MS analysis. Organic acids and supercharging molecules are of particular interest as conditioning agents for improving the DSP approach for ESI-MS analysis.[47-49] A prototype DSP with counterflow orientation

sample treatment is applied to a range of high salt-content solutions that served as proxies to biologically relevant solutions. These results demonstrate that in addition to removing salts during treatment, transferring conditioners into the treated sample can improve limit of detection (LOD) by an order of magnitude and enable multicomponent detection, a key milestone for monitoring bioreactors which have a range of soluble biomolecules present in low abundance. In the improved crossflow design, varying the concentration of organic acids is shown to improve protonation effects and enable the detection of high molecular weight (~50 kDa) monoclonal antibody (mAb) fragments, emphasizing that active conditioning improves the ability to detect a broad range of biomolecules.

3.1 Experimental Setup for Real-time ESI-MS

The experimental configuration used for qualification of the DSP for real-time ESI-MS is shown in Figure 3.1. A sample of known composition was drawn into a 50 μL syringe (Hamilton™ Gastight 50 or 100 μL) and infused with a syringe pump at 35 μL/hr through a length of fused silica capillary with a 75 μm inner diameter, which is attached to the inlet capillary of the DSP with Upchurch fittings in a Valco™ union. On the tip of the syringe, an electrical connection is made to the probing end of a picoammeter. The ground end of the picoammeter is then attached to the ground of the mass spectrometer for continuous ESI current monitoring. The DSP in the fluidic interface package was positioned 3-5 mm away from the Bruker micrOTOF MS inlet, which is held at a negative bias to complete the circuit. During all experiments, spray current was kept between 10 and 20 nA at a steady value to ensure similar ESI conditions at the MS inlet.

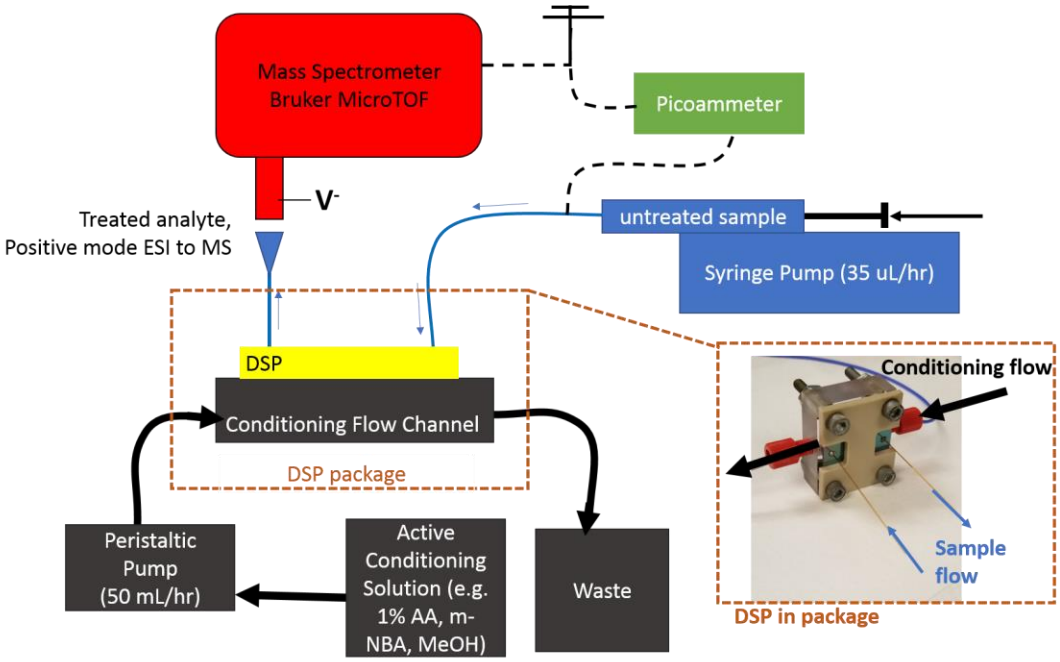

Figure 3.1: The DSP experimental setup for analysis with the Bruker MicrOTOF MS. This system was used for all experiments using this MS, including those in CHAPTER 4.

Conditioning flow is delivered at 50 mL/hr with a peristaltic pump, which draws from a liquid reservoir through silicone tubing. Conditioning liquid then travels to the device package, where the connection is made with Upchurch fluidic fittings into the DSP package (section 2.6). For the counterflow experiments in sections 3.2, 3.3, and 3.4 conditioning solution travels in the opposite direction of sample flow along the top side of the etched conditioning channel, separated from the sample channel within DSP by the size selective nanoporous membrane. For some results in this chapter (section 3.5) the crossflow orientation fluidic package was used. More details on the packages are provided in section 2.6.

3.2 Salt Removal and Active Sample Conditioning

Inorganic salts interfere with positive mode electrospray mass spectrometry (ESI-MS) by suppressing the MS signal associated with analyte molecules. Removal of salts promotes charging of molecules with only protons, i.e. protonation, instead of charging molecules via metal cation adduction. In addition to cation adduction, neutrals (e.g. KCl, NaCL, H_2O molecules) can attach to the ionized analytes, forming "clusters" (see section 1.3.2). The signal at any fully protonated charge state associated with a given biomolecule becomes masked by the signal of the same or other molecules whose ions carry adducted and clustered species, making it impossible to identify the biomolecule via MS.[31, 33, 34, 50-52]

DSP enhancement of ESI-MS analysis was explored through comparison of the effect of four different active conditioning solutions. Each conditioning solution contained 1% acetic acid (AA) to facilitate the protonation of compounds[53] and three of the conditioning solutions contained one additional ESI-MS enhancing chemical: ammonium acetate, 3-nitrobenzyl alcohol, or methanol. Ammonium acetate has been reported to increase the acidity in the electrospray plume for enhanced protonation[54] and reduced formation of salt adducts.[55, 56] While acetic acid and ammonium acetate enhance protonation, the other conditioners were explored for their charge state shifting effects. A shift (increase) in the charge state distribution was expected to increase sensitivity in ESI-MS analysis while also enhancing advanced tandem mass spectrometry applications.[47-49, 57] Supercharging molecule 3-nitrobenzyl alcohol (m-NBA) in concentrations from 1-20% has been reported to increase charge state distribution in non-denaturing solutions. Although the mechanism is not completely settled, it is suggested that supercharging occurs

due to the low volatility and low surface tension of the super charging agent, a combination that promotes the Coulombic droplet fission process.[57, 58] Finally, methanol (MeOH) can shift charge state distribution towards a lower m/z spectral range due to a denaturing of biomolecules which results in exposing more locations for protonation.[49]

A solution of 100 mM KCl with 5 μM cytochrome c (Cyt c) was used to carefully characterize the effect of active sample treatment. In order to maintain relevance to cell manufacturing, the salt level used is similar to that expected in a bioreactor,[29] and Cyt c is an appropriate model protein in the mass range (~12 kDa) of signaling molecules secreted from cells, such as cytokines, that are expected to be CQAs for cell state.[8, 23, 37, 39] When untreated, the spectra obtained for ESI-MS of 100 mM KCl with 5 μM Cyt c (Figure 3.2) has no peaks associated with Cyt c, indicating that the added KCl levels are high enough to render MS analysis incapable of identifying the protein. This result demonstrates that the high salt content in bioreactors will mask biomolecule signals in direct ESI-MS analysis. As discussed in CHAPTER 1, (Section 1.3.2, Figure 1.5) salt concentrations need to be reduced to below about 1 mM for identification of Cyt c at a concentration of 5 μM.

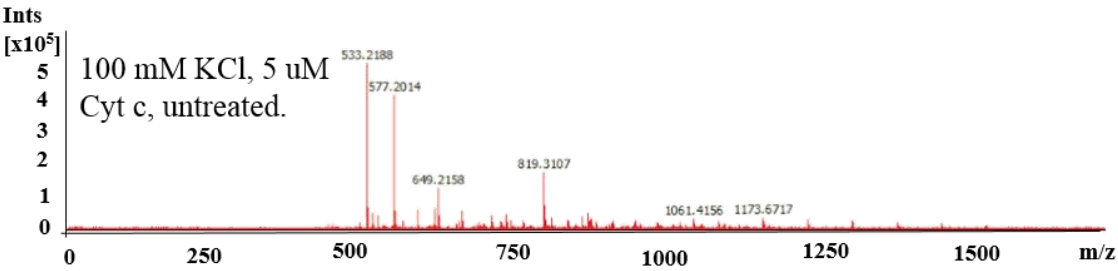

Figure 3.2 Resulting mass spectra from direct infusion ESI-MS through DSP of a solution with 100 mM KCl and 5 μM cytochrome c without treatment, i.e. empty conditioning channel. No characteristic cytochrome c peaks are visible due to salt which causes adduction and clustering that masks the signal of the protein.

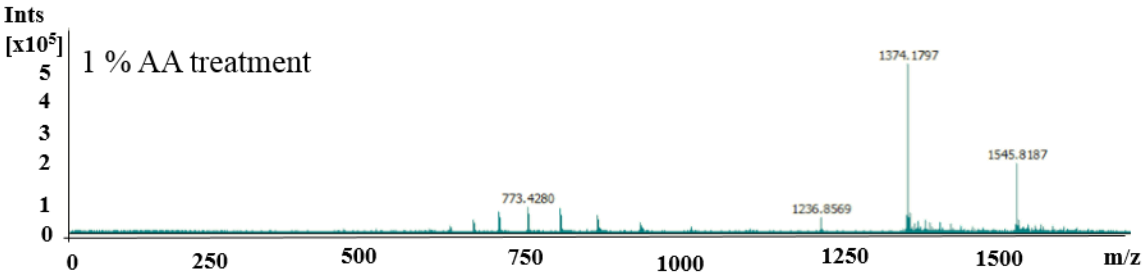

Figure 3.3 Resulting mass spectra from direct infusion ESI-MS treated by DSP of a solution with 100 mM KCl and 5 µM cytochrome c with 1% AA treatment reveals a strong cytochrome c signal.

Therefore, at least 99% of the KCl in the solutions tested here were removed by DSP. In cell monitoring applications, analyte concentrations could be lower than 5 µM which is why a highly selective mass exchanger, such as DSP, is necessary to remove salt to a sufficient degree while retaining biomolecules of interest through size selective separation.

The benefit of DSP online active sample treatment is made evident by comparing the spectra of an untreated sample (Figure 3.2) and a sample with treatment (Figure 3.3) using a 1% acetic acid (AA) conditioning solution. The mass spectra shown in Figure 3.3 is characteristic of Cyt c ionized in low salt content solutions. The most intense peak (m/z ~ 1374) is associated with Cyt c molecules charged via addition of nine protons, referred to as the +9 charge state. The appearance of Cyt c spectral peaks in online analysis of a high salt solution occurs as a result of several mechanisms. First, the removal of salt reduces metal cation adduction of the protein, so that the protein is charged via protonation. Salt removal also eliminates the formation of cluster peaks, reducing charge competition and corresponding signal suppression. Finally, addition of AA into the sample further

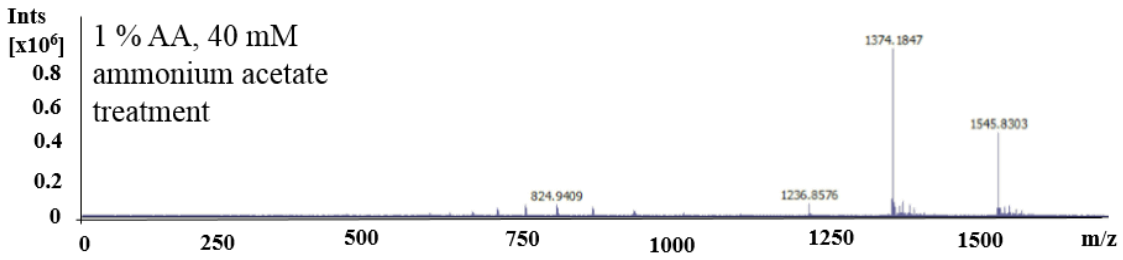

Figure 3.4 Resulting mass spectra from direct infusion ESI-MS treated by DSP of a solution with 100 mM KCl and 5 μM cytochrome c with 1% AA, 40 mM ammonium acetate treatment reveals a strong cytochrome c with improved signal intensity.

increases the rate of protonation due to the increased proton concentration in acidified solution.

Adding 40 mM ammonium acetate to the conditioning solution increases the intensity of the largest Cyt c associated peak from ~10^5 with AA only treatment (Figure 3.3) to ~10^6 with no shift in charge state distribution (Figure 3.4). While addition of ammonium acetate further enhances protonation[54] and mitigates salt adducts,[56] ammonium acetate does not change the surface tension and has little to no denaturing effect on the protein so there is no apparent impact on the charge state. For this experiment it is also unclear whether intensity is an indication of improved sample conditioner efficacy. With Cyt c at the 5 μM concentration level, later experiments show that MS signal intensity varies while signal to noise ratio remains the same, suggesting that the signal is saturated at the 5 μM level and that signal intensity may be a poor metric for DSP performance (see section 3.3).

In contrast, adding supercharging molecule m-NBA at 2% to the conditioning flow results in a significantly shifted charge state distribution (Figure 3.5). This shift in charge state reveals Cyt c with 15 protons attached as the most dominant, referred to as the +15

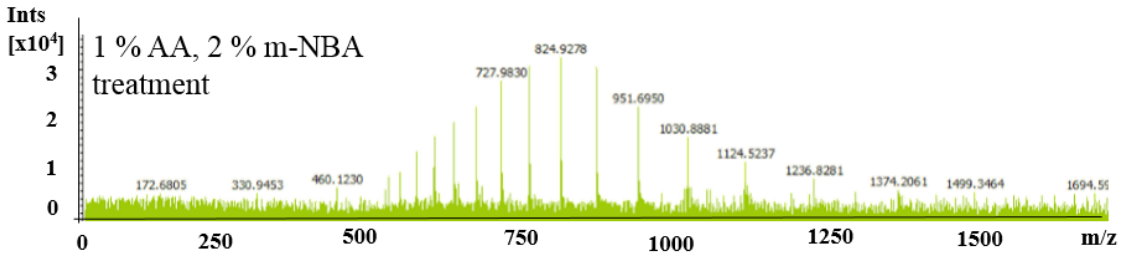

Figure 3.5 Resulting mass spectra from direct infusion ESI-MS threated by DSP of a solution with 100 mM KCl and 5 µM cytochrome c with 1% AA, 2% m-NBA treatment shifts to a higher charge state distribution.

charge state, at about m/z 824. For non-denaturing/super-charging treatment types like AA or ammonium acetate (spectra shown in Figure 3.3 and Figure 3.4) the +9 charge state is most dominant, at approximately m/z 1374. Although not producing the same maximum peak intensity as ammonium acetate, m-NBA causes a marked increase in the prevalence of peaks corresponding to the highly charged protein. This suggests the possibility of using m-NBA treatment for higher molecular weight proteins that would usually be outside the range of a given mass spectrometer. For instance, the Bruker MicrOTOF time-of-flight mass spectrometer used in these experiments has a mass to charge ratio (m/z) range of 30 – 5000 m/z. Thus, increasing the maximum number of charges placed on a protein from 10 to 20, for example, would raise the size of the largest detectable protein from 50 kDa to 100 kDa. The impact of supercharging is also seen in its potential for improved sensitivity. This is because tuning the ion transfer voltages in a mass spectrometer to acquire signals over the entire available m/z range sacrifices sensitivity compared to that obtainable when tuned for a smaller m/z range. As seen in Figure 3.5, super charging compresses the range of m/z values for Cyt c peaks enabling better use for the instrument capabilities for biomolecular detection.

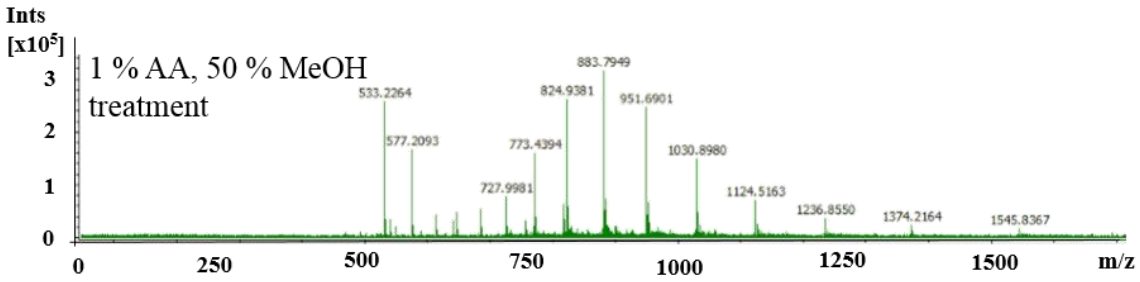

Figure 3.6 Resulting mass spectra from direct infusion ESI-MS treated by DSP of a solution with 100 mM KCl and 5 µM cytochrome c with 1% AA, 50 % methanol also increases the average charge state, but long term operation is hindered due to increased inorganic salt precipitation clogged DSP.

Addition of 50% methanol (MeOH) also has a significant effect on the charge state distribution (Figure 3.6). This treatment results in a spectra in which the +14 charge state (m/z ~883) is most abundant, which suggests that the effects of m-NBA and MeOH are not identical. Methanol denatures the protein, revealing more sites for protons to attach, which results in a shift in the spectrum to a higher charge state distribution. Although MeOH, like m-NBA, has a lower surface tension than H_2O, it is also more volatile than H_2O. Therefore it does not yield the same increase in droplet fission events that m-NBA produces.[49, 58] Further, due to a lower solubility limit of inorganic salts within MeOH, continuous flow analysis is difficult using MeOH as an active conditioner.[59] As MeOH is exchanged into the sample, salt precipitates form. These precipitates eventually clog the sample channel or the ESI emitter, causing the DSP to cease operation.

3.3 Signal to Noise Ratio and Limit of Detection Enhancement

To quantify the impact of DSP active sample treatment, MS signal to noise ratio (SNR) and limit of detection (LOD) were studied. Samples containing varying Cyt c

concentrations (0.25, 0.5, 1.0, 2.5, 5, and 10 µM) in 50 mM KCl were treated with two conditioning solutions, 1% AA or 1% AA, 2% m-NBA, to explore what effect active conditioning has on DSP-MS in terms of SNR and LOD. These experiments were designed to investigate if supercharging molecules enhance ESI-MS detection of proteins at low concentrations because the effect of ammonium acetate on resulting ESI-MS was subtle, and methanol hindered continuous DSP operation.

The addition of m-NBA to the active conditioning solution increases SNR across multiple charge states. Figure 3.7 illustrates this point by plotting the highest and fifth highest SNR as a function of Cyt c concentration (there are multiple SNRs associated with

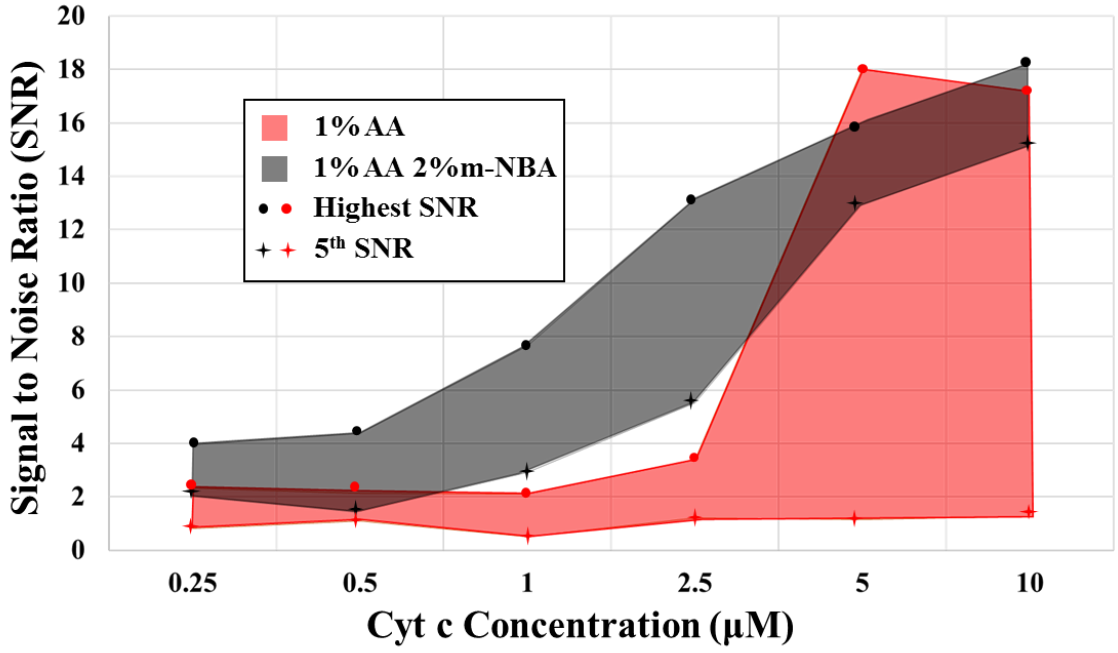

Figure 3.7: Highest across all peaks and 5th highest signal-to-noise ratio (SNR) values of identified Cyt c peaks within samples (50 mM KCl with: 0.25, 0.5, 1.0, 2.5, 5, & 10 µM Cyt c) treated with 1% AA vs 1% AA 2% m-NBA. The m-NBA treatment reveals multiple charge states at all concentrations.

Cyt c due to existence of multiple charge states). Here, signal to noise ratio is defined as $SNR=I_{Cyt\ c}/I_{avg,}$, where the $I_{Cyt\ c}$ is the intensity (%) of an identified Cyt c peak and I_{avg} is the averaged intensity (%) of all peaks within a window +/- 0.3 m/z of the identified peak. This definition gives a local SNR value for every protonated Cyt c peak. An SNR above ~2.5 corresponds to a distinguishable, fully protonated Cyt c peak. These results are presented in this manner to demonstrate that m-NBA treatment improves the LOD and increases the SNR for detected molecules *across multiple charge states*, which enables easier identification of low concentration biomolecules in complex mixtures.

Active treatment with m-NBA drastically improves the LOD, i.e., the lowest concentration for which the SNR of a peak associated with fully protonated Cyt c is greater than 2.5. For Cyt c in 50 mM KCl, this LOD is improved by an order of magnitude, from 2.5 µM to 250 nM. To illustrate the qualitative effect that m-NBA has on the resulting

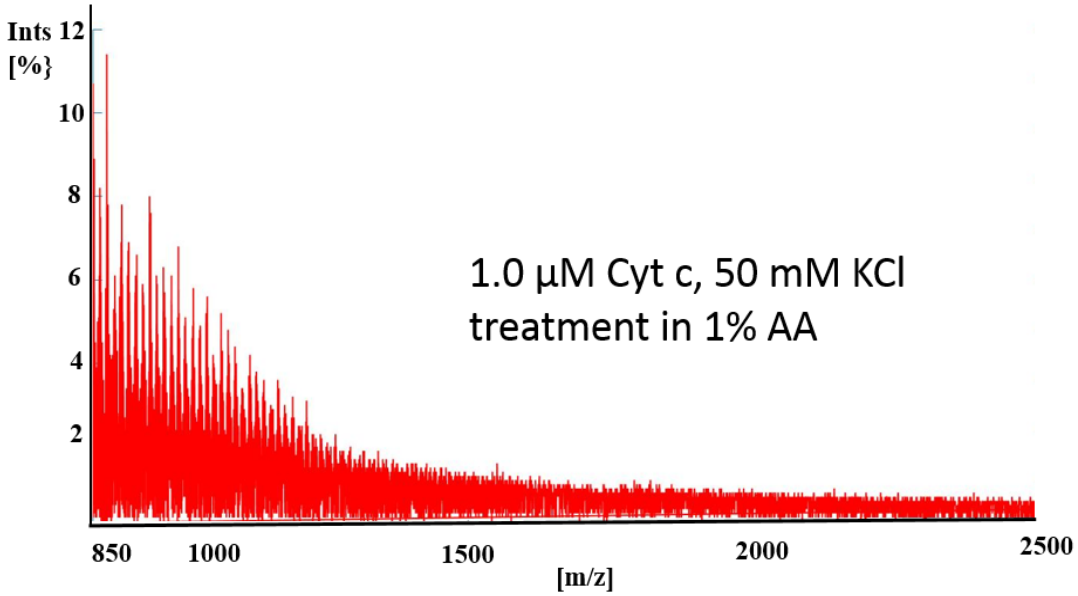

Figure 3.8: DSP 1% AA treatment -ESI-MS of 50 mM KCl with 1 µM Cyt c shows no characteristic Cyt c spectral features. The protein is unidentifiable after standard desalination without active sample conditioning.

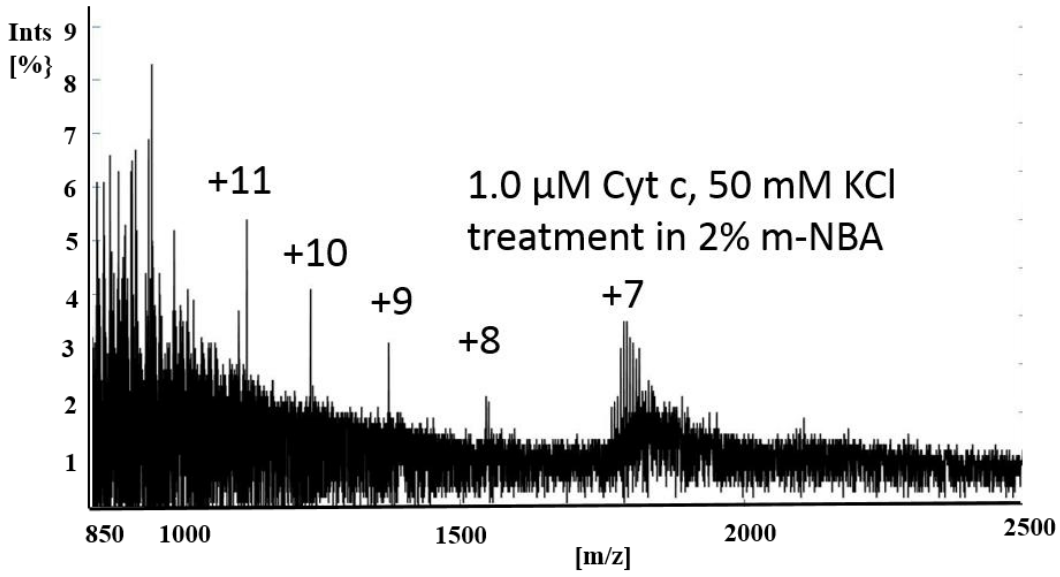

Figure 3.9: DSP 1% AA, 2% m-NBA treatment-ESI-MS of 50 mM KCl with 1 µM Cyt c reveals multiple charge states for identification of the protein, which shows that the active sample conditioning can improve both signal to noise ratio and limit of detection (sensitivity).

spectra, DSP nanoESI-MS analysis of 1 µM Cyt c in 50 mM KCl with 1% AA conditioning solution (Figure 3.8) and 1% AA and 2% m-NBA (Figure 3.9) is shown. The difference in the two spectra highlights the significant effect addition of m-NBA has on LOD. With 1% AA treatment (Figure 3.8), no distinguishable protonated Cyt c peaks are visible, while treatment with 1 % AA 2% m-NBA produces five distinct peaks associated with completely protonated species (Figure 3.9).

At 2.5 µM Cyt c conditions, where use of both conditioning solution compositions in DSP successfully reveal the protein signature, m-NBA treatment enhances SNR across multiple charge states far above the levels obtained with AA only treatment. With very high SNR peaks across a range of multiply charged states, identification of biomolecules is easier, and applications which can benefit from biomolecule structural information are

enabled through the use of tandem (MS/MS) mass spectrometry that performs best with highly charged species.[48] Although for both 5.0 and 10.0 μM Cyt c concentrations 1% AA treatment produces a very high SNR for the highest intensity peak, m-NBA treatment again creates higher average SNR values. These levels of Cyt c concentration (5, 10 μM) are approaching the point where signal saturation was observed, such that MS measurements of abundance is not dependent on treatment type, muting the impact of active sample conditioning. However, the ability to detect low concentration biomolecules (i.e. <2.5 μM Cyt c) through DSP's active sample conditioning with m-NBA is the most important conclusion of these experiments. The results emphasize that DSP has the capability for detection and/or discovery of low concentration biomolecules because of active sample treatment via inline introduction of ESI-MS enhancing compounds. This type of detection is usually only possible with offline methods like HPLC-MS, rendering DSP a unique and powerful tool for *in operando* cell-health monitoring.

The concentration of some CQAs in bioreactors is significantly lower than those explored here. Therefore, the ability to detect even lower concentration biomolecules enabled by DSP treatment is critical for ESI-MS application to cell manufacturing quality monitoring. Importantly, these experiments were performed on a Bruker MicroTOF MS which was available for device development and testing. Unfortunately, this MS does not possess the capabilities or sensitivity of more advanced MS instrumentation available for bioanalysis. For example, an improved dynamic range on updated instruments enables lower concentration species to be detected, especially when in the presence of higher concentration biomarkers. On the Bruker instrument the LOD for a Cyt c solution is roughly 10 nanomolar, while on advanced instrumentation picomolar and even femtomolar

sensitivity is expected. Furthermore, improved resolution and tandem mass spectrometry would also enable more complete CQA characterization. The Bruker micrOTOF MS only allows accurate mass predictions of species. This system does not possess isotopic resolution for resolving charge state or protein conformation which makes untargeted identification of CQAs challenging. Updated mass spectrometers also utilize tandem mass spectrometry for protein sequencing and biomolecular identification, which are key to enabling biomolecular discovery. In other words, extrapolation of LODs with the Bruker MS illustrates the power of the active sample conditioning protocol, but in cell culture applications more advanced MS instruments will improve the DSP enabled ESI-MS characterization of CQAs significantly. In advanced therapy applications the limitation may be on the analytical instrument, not on the DSP sample conditioning protocol.

3.4 Simultaneous Identification of Multiple Proteins

In any bioreactor there are a multitude of dissolved biomolecules which are difficult to detect simultaneously without chromatographic separation or other sample preparation techniques such as digestion. To assess the DSP's capability for multiple biomolecule detection, experiments were performed with a high salt content buffer mixture, phosphate-buffered saline (1xPBS: 137 mM NaCl, 2.7 mM KCl, 1.0 mM Na_2HPO_4, and 1.8 mM KH_2PO_4), containing 5 μM of interleukin 6 (IL-6), interleukin 8 (IL-8), and Cyt c. This multi-component mixture was then treated with the two different active sample conditioning strategies described in the prior section (3.3) to investigate the effect that super charging molecules have on multi-component detection. With molecular weights of ~8 kDa (IL-8), ~12 kDa (Cyt c), and ~21 kDa (IL-6), the mixture of these molecules is a realistic proxy for cytokines, which are known to be indicative of cell health,[37, 39] in a

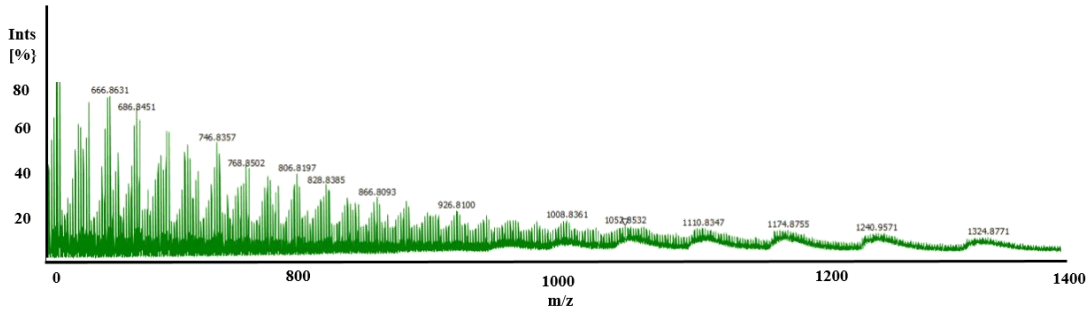

Figure 3.10: Mass spectra produced via direct infusion ESI-MS treated by DSP of untreated 1xPBS with 5 µM Cyt c (12 kDa), 5 µM IL-6 (21 kDa), and 5 µM IL-8 (8.4 kDa) shows no identifiable peaks associated with protonation of biomolecules.

solution that has multiple inorganic compounds in concentrations representative of a bioreactor environment.[29] As expected, the baseline ESI-MS of 5 µM IL-6, IL-8, and Cyt c in 1x PBS without DSP treatment produces no meaningful detection of any biomolecules (Figure 3.10). When 1% AA treatment was used, only IL-6 was detected (Figure 3.11), whereas treatment with 1% AA 2% m-NBA yielded detection of both IL-6 and Cyt c (Figure 3.12).

During treatment with 1% AA as the conditioning solution, removal of inorganic compounds and acidification of the sample reduces chemical noise associated with salt adducts and clusters, and IL-6 can be detected (Figure 3.11). The highest concentration of salt in PBS is NaCl at 137 mM, which is higher than the salt levels explored in the experiments described in earlier sections (100 mM Figure 3.2-Figure 3.6, 50 mM Figure 3.7-Figure 3.9). Again, referring to the minimum sample treatment requirements for ESI-MS explored in CHAPTER 1 (Section 1.3.2, Figure 1.5), it can be estimated that the DSP is removing over 99% of the salts present in order to reveal the signal associated with IL- 6. However, the SNR is low, and peaks formed via salt adducts are visible at higher m/z

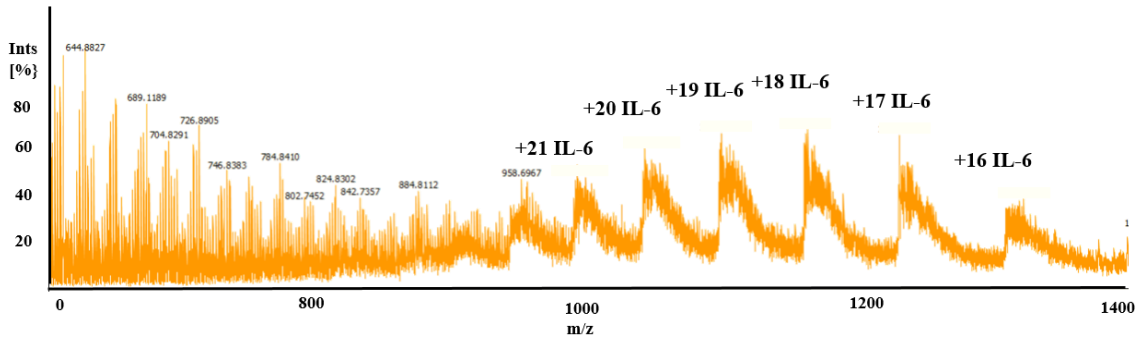

Figure 3.11: Mass spectra produced via direct infusion ESI-MS through DSP with 1% AA treatment of 1xPBS with 5 µM cytochrome-c (12 kDa), 5 µM IL-6 (21 kDa), and 5 µM IL-8 (8.4 kDa) reveals multiple charge states associated with IL-6 only.

values along with each protonated peak, indicating not fully sufficient salt removal with DSP operating in counterflow. These results motivated the optimization of DSP from a mass transfer perspective as discussed in Section 2.7.

Treatment with 1% AA, 2% m-NBA reveals high SNR, fully protonated Cyt c and IL-6 peaks, but IL-8 is not observed (Figure 3.12). As the smallest of the analytes, IL-8

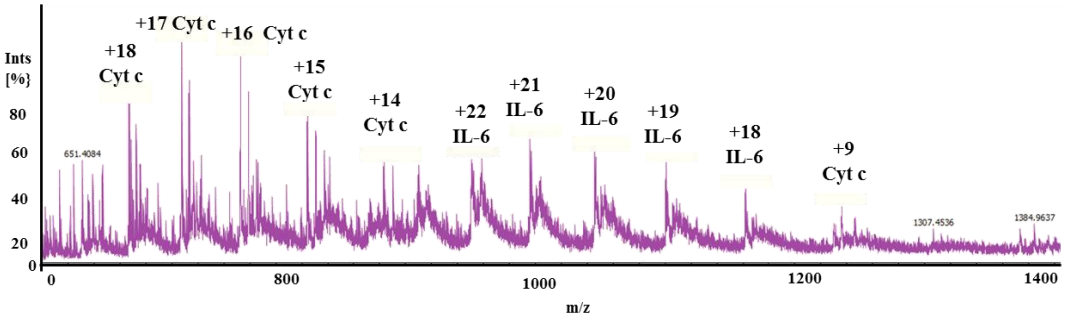

Figure 3.12: Mass spectra obtained via direct infusion ESI-MS through with 1% AA, 2% m-NBA treatment of 1xPBS with 5 µM cytochrome c (12 kDa), 5 µM IL-6 (21 kDa), and 5 µM IL-8 (8.4 kDa) reveals fully protonated charge states of cytochrome c and IL-6. IL-8 is not detectable, likely due to its unintended removal through the membrane due to low molecular weight (small size).

may have suffered more parasitic loss (cross-over to the conditioner flow) in the DSP mass exchanger than larger in size Cyt c and IL-6.[34] This result further emphasizes that active sample treatment with m-NBA is a very useful for reducing chemical noise due to metal cation adduction and salt cluster formation. These promising results demonstrate that DSP with active sample treatment enables the detection of multiple biomolecules in a high salt content mixture, at the concentration levels relevant to cell manufacturing applications.

3.5 High Molecular Weight Tuning

Detecting high molecular weight biomolecules has important applications in nascent cellular therapy workflows because some of the CQA biomolecules or paracrine factors that signal therapeutic responses are well above the 21 kDa (IL-6) upper limit explored in section 3.4. Additionally, well established fields such as pharmaceutical biologics rely heavily on the ability to detect and characterize large, complex proteins such as monoclonal antibodies (mAbs). Preserving the state of these proteins to capture non-covalent interactions or post translational modifications is a key advantage of ESI-MS as an analysis technique, but these molecules can be difficult to detect in their intact state due to the limited m/z ranges on mass spectrometers. As discussed, supercharging molecules like m-NBA are effective for improving signal to noise (SNR) and limit of detection (LOD), but these benefits are limited. It was observed that when increasing the concentration of m-NBA above 2% in the conditioner channel that the resulting spectra was dominated by m-NBA and associated clusters, although it has been reported that m-NBA has advantageous effects and concentrations well above this level.[47-49, 57, 60] The negative effect of m-NBA clusters was even more drastic in the later iteration of DSP with crossflow orientation sample treatment, which not only improved removal of parasitic species, but also improved

the transfer of conditioning agent m-NBA to the sample. The presence of m-NBA clusters was not observed in the initial proof-of-concept, SNR, and LOD experiments presented in previous sections 3.2, 3.3, and 3.4 where DSP was operated in counterflow orientation at the 2% m-NBA conditioner level. However, as it was observed that m-NBA at levels above 1% in the conditioner was found to have a negative effect in crossflow, other means of improving MS sensitivity to high weight molecules were explored.

As shown with MeOH active treatment (Figure 3.6), the denaturing of a protein enhances the protonation efficiency because more sites for ionization are revealed. However, most organic solvents are not compatible with DSP due to salt precipitates formed when the solvent transferred into the sample channel and interacted with untreated media. Another common method used to denature a protein is changing the solution pH. In positive mode ESI, reducing the pH also improves ESI-MS analysis as lower pH solutions are inherently more likely to produce protonated species due to a higher prevalence of free protons. For these reasons, the concentration of acetic acid (AA) was varied in the conditioner channel to observe the results on biomolecule detection.

Figure 3.13 shows the treatment of 50 mM KCl, 5 μm Cyt c with varying levels of AA in the conditioner channel. For these experiments, DSP was operated in the crossflow orientation which improved salt removal and, importantly, AA transfer to the sample. As expected, signal associated with Cyt c is visible with the "baseline" 1% AA treatment (top) in Figure 3.13. Increasing the AA to 5% shifted the spectra to higher charge states and improved the SNR of the observed charge states in the m/z range below 1300. Increasing from 5% to 10% did not result in any notable qualitative or quantitative changes in the spectra. The increased AA concentration from 1% to 5% improves biomolecular detection

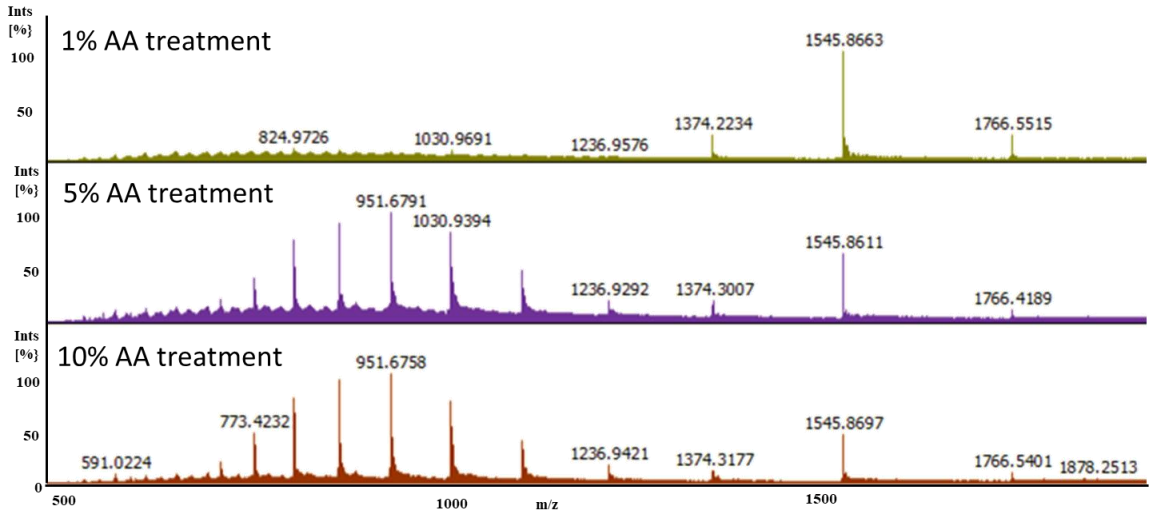

Figure 3.13 DSP-ESI-MS analysis of 50 mM KCl, 5 µM cytochrome-c with varying concentrations of acetic acid (AA). Increasing the concentration of acetic acid in the conditioner channel from 1% v/v to 5% enhances the protonation of the protein, producing a very clear charge state distribution. Increasing the concentration from 5% to 10% does not appear to affect the signal.

due to a combination of improved ionization from higher relative concentrations of protons and moderate protein denaturing in the low pH solution. However, this trend has diminishing returns at 10% AA where solid precipitates formed in the sample channel which hindered continuous operation of DSP. In addition, the higher acidity also caused material compatibility issues. Notably, the self-adhesive gasket used for sealing the conditioner channel was visibly damaged after ~2 hours of use.

To demonstrate the effect that tuning the conditioner composition has on practical applications a monoclonal antibody (mAb) fragment with a molecular weight of ~50 kDa was used as a testbed. This antibody fragment is part of the OMG 18 RV anti-frizzzled mAb which has been shown to have important roles in the WNT signaling pathway with

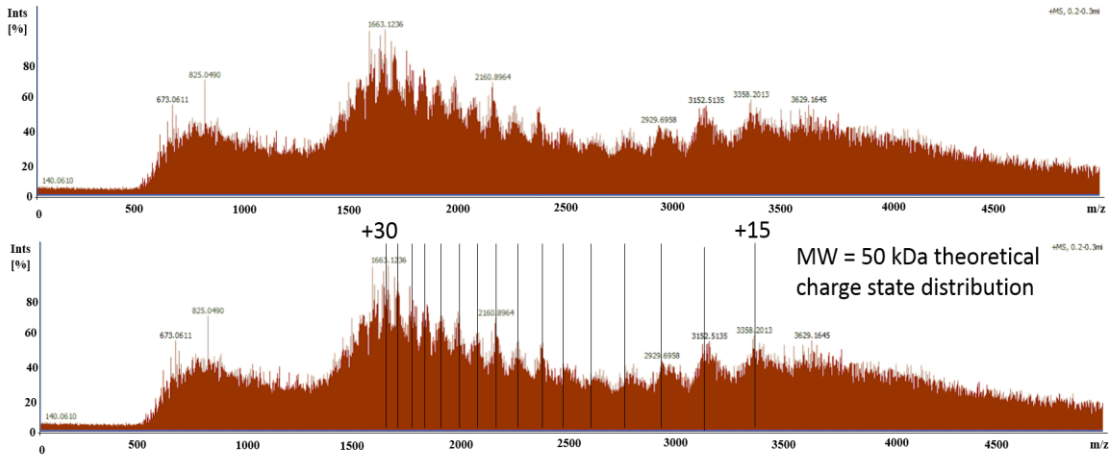

Figure 3.14: 5% AA, 1% m-NBA treatment of 1X PBS, 2% glycerol, 800 nM OMP 18 RV anti-frizzled mAb fragment (50 kDa). The theoretical charge state "ruler" for a 50 kDa protein is overlaid on top of the spectra for visualization purposes.

strong anti-tumor properties.[61] The protein was obtained in an isolated format in 1X PBS at approximately 800 nm concentration with 2% glycerol to aid in suspension. This solution was treated with DSP in the crossflow orientation using a conditioner solution of 5% AA, 1% m-NBA. The resulting spectrum from direct DSP-ESI-MS analysis of the protein is shown in Figure 3.14. As these experiments were conducted on the Bruker MicroTOF instrument, detecting a protein of this size proved to be challenging. The lack of isotopic resolution made it impossible to determine the charge state associated with each peak. It is also unclear if the peaks associated with each parent peak are associated with adducts, clusters, or protonated species. To aid in visualizing the MS spectra appearance of incompletely resolved protein, a theoretical charge state distribution for a completely protonated 50 kDa protein is overlaid on the spectra in Figure 3.14. The spectral peaks align well with the predicted charge states for a completely protonated species, indicating

that the protein was detected. However, this "semi-targeted" approach is only possible if the identity of the protein is known *a priori,* but these results demonstrate that the active conditioner composition plays a key role in aiding in the detection of a broad range of biomolecules. The analysis of larger mAbs is commercially and clinically relevant as these molecules already have substantial use by pharmaceutical industry unlike nascent advanced therapeutics (e.g. cell therapies). Already there are real-time approaches for mAb monitoring using Raman spectroscopy, but DSP provides a unique ability to characterize these molecules as they are produced using MS sensing. Raman requires significant data training to detect a known molecule, and subtle aspects of the molecules' structure (e.g., oxidation) and folding are not always captured in the data output.[10] On the other hand, ESI-MS when coupled with tandem mass spectrometry enables complete mAb characterization including structural conformation and sequencing. Therefore, the DSP approach enables a highly detailed analysis of mAbs in real-time that as of yet has not been realized.

CHAPTER 4.
DSP APPLICATION TO CELL STATE ANALYSIS

Cell cultures and bioreactors are transient and heterogenous environments. Probing spatial variation is critical to understanding the cell state but is challenging because the microenvironment is comprised of CQA biomarkers that are masked by other types of biomolecules in cell culture media. These biochemicals are necessary for culture health but are also present in high abundance in the bulk. This poses a hurdle for direct ESI-MS without any type of offline chromatographic separation, as direct analysis is more likely to detect only higher concentration biomolecules. While monitoring bulk media may be useful for detecting the downregulation of species like glucose or oxygen, the complete culture state is not captured by these measurements. Monitoring the local cell environment is therefore critical to understanding the underlying mechanisms or parameters that correlate with final therapeutic product quality, potency, efficacy, etc.

This chapter explores the application of DSP to monitoring live cell cultures. First, DSP is applied to three human cell types to demonstrate the ability of the system to utilize localized sampling to generate unique fingerprints associated with each cell type. Next, a longitudinal study demonstrates that DSP can detect important aspects of cell state, such as proliferation, confluence, and differentiation. For these experiments DSP sampled directly from culture aseptically throughout the entire ~21 day growth cycle, validating the system's capability for providing insight to cell state without affecting final product quality. Localized sampling from these cultures is shown to be required to detect cell state using *post hoc* analysis. Finally, a new workflow for enabling DSP as an orthogonal

approach to detect CQA biomolecules is presented, laying the groundwork for DSP as a discovery tool in cell manufacturing.

4.1 Localized Sampling for Cell Fingerprinting

Commonly used methods to characterize cell cultures or their conditioned media, for instance ELISA or HPLC-MS, analyze bulk samples. In the case of ELISA, the approach is highly sensitive and targeted, whereas HPLC is sensitive but mostly untargeted. In both cases the assay cannot pinpoint biomolecules' point of origin nor identify the moment of secretion; the assays reveal spatially and temporally averaged CQA content. DSP seeks to address the shortcomings of these approaches by sampling directly from where the CQA biomolecules are secreted, i.e., the cell microenvironment adjacent to the cell membrane, and immediately processing the sample for real-time feedback.

In order to maintain clinical relevance, DSP was first applied to three different types of human based cells. These cells were cultured with different medias and were from different source materials, thus they were expected to exhibit clear differences in the resulting DSP-MS spectra. First, DSP-MS analysis of a single normal human lung fibroblasts (NHLFs) cell culture was performed to compare bulk and local sampling effects with results presented in Figure 4.1. The first and third spectra are from a localized sample, taken ~100 μm above the cell membrane, while the second and fourth spectra are the result of bulk media analysis. The red boxes on the localized samples highlight spectral features that differ from bulk samples. The presence of highly resolved peaks in the local samples indicates that the cell microenvironment contains higher concentrations of biomolecules that are not detectable in bulk samples. For these experiments, no species identification

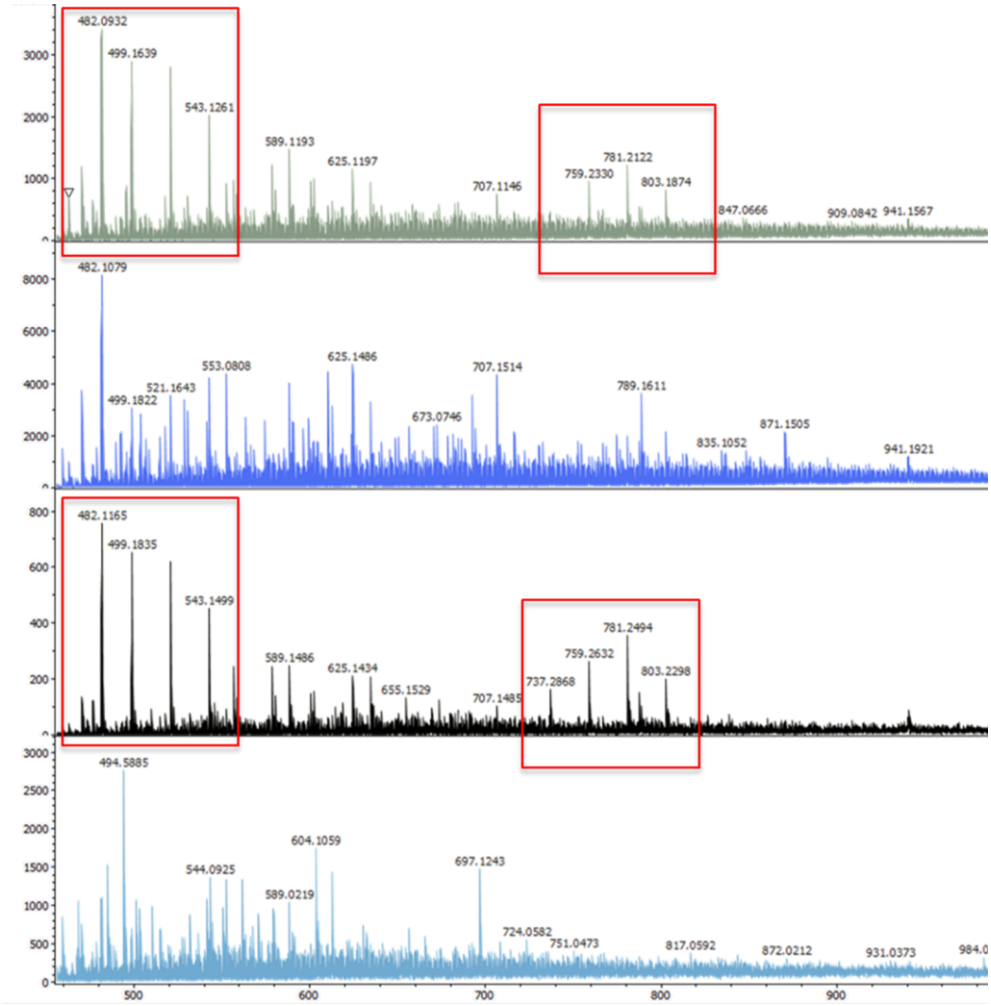

Figure 4.1: Localized sampling (first and third spectra) from normal lung fibroblast cells (NHLF) reveals a drastically different spectra than those of bulk samples (second and fourth spectra) indicating that the region near the cell membrane contains biochemicals that become diluted below limit of detection in

was carried out, as the Bruker MicroTOF MS is not capable of performing MS-MS analysis for protein sequencing or database matching.

DSP was then applied to two other cell groups, human mesenchymal stromal cells (MSCs) and human umbilical vein endothelial cells (HUVEC) to fingerprint each cell type

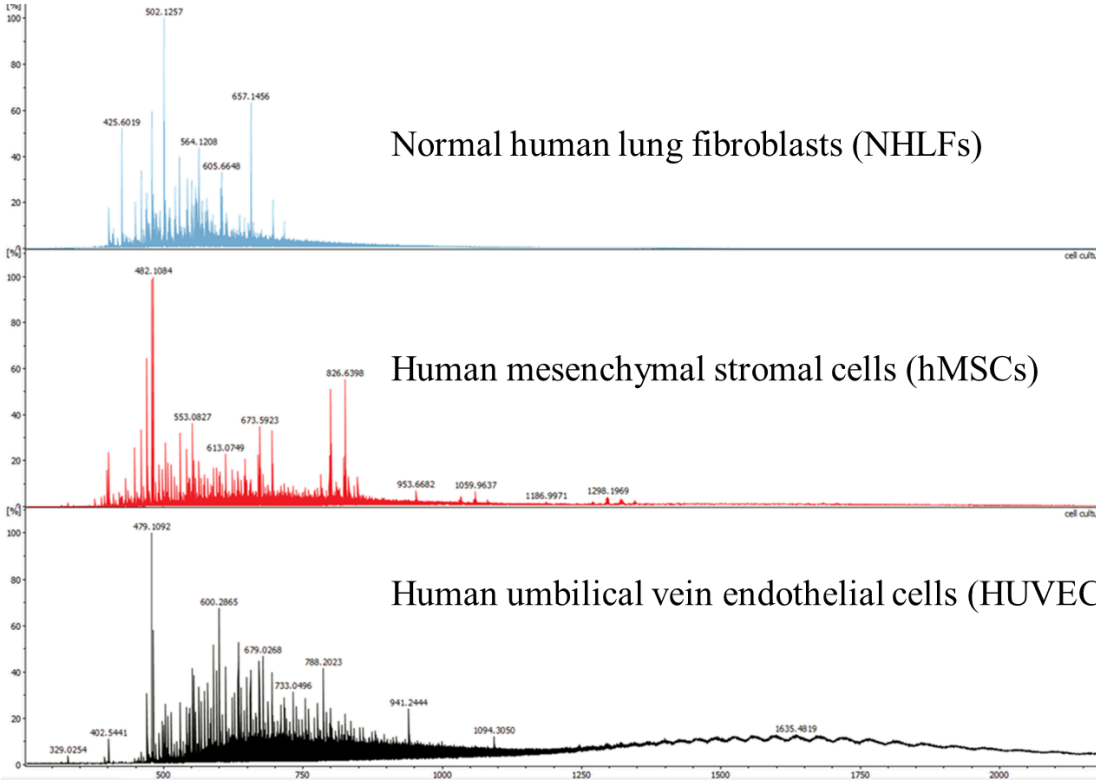

Figure 4.2: DSP application to three types of cell cultures with localized sampling demonstrates key ability to "fingerprint" different cell types.

with localized sampling. Figure 4.2 shows the resulting spectra for each cell group. Each spectra differs significantly; however, because each cell is phenotypically unique and the media used to culture the cells is different, it is not clear whether the qualitative differences in each spectra are due to secreted factors associated with cell type or due to bulk media composition differences. Nevertheless, the complex spectrum for each cell type is not dominated by a common signal, such as a frequently used serum additive like albumin. In the HUVEC spectra, some indication of heavy protein content is shown in the m/z 1200-2000 range, but the fact that this signature it is not present in each spectra suggests that

local sampling mitigates the effects that high weight proteins found in additive serums, like albumin, have on detecting locally secreted CQA biomarkers.

From a clinical perspective, MSCs have shown some promise for their anti-inflammatory potential and their role in producing tissue engineered medical products for regenerative medicine.[15, 62, 63] MSCs, like most stem cells, naturally differentiate into different phenotypes depending on their biological context. Whether *in vivo* or *in vitro*, determining MSC differentiation state is important for predicting the cell's therapeutic potential. Therefore, predicting cell state at each developmental stage, from proliferation to confluence to differentiation, is a critical area for DSP application. To this end, an experiment was designed with a cell type with well understood differentiation properties, i.e., MC3T3 preosteoblasts. While MSCs, IPSCs, and T-cells may differentiate into a range of sub-types the MC3T3 cell type differentiates controllably from preosteoblast to osteoblast. Additionally, the assay used to detect differentiation is well documented and only two additives are used to induce differentiation, which enables more control over the cell growth cycle and reduces the sources of experimental noise that more complex cell types inherently possess.

4.2 Cell Culture Method

Murine preosteoblastic cells MC3T3-E1 (ATCC CRL-2593) were obtained and expanded according to established protocols.[64] Gilad Doron (Guldberg/Temenoff lab) carried out all of the cell cultures as described here. Cells were seeded on T-150 flasks (Corning) at 5000 cells/cm2 and expanded in a growth media consisting of MEM α with nucleosides (Gibco) with 10% fetal bovine serum (Atlanta Biologicals, Lot #E15052) and

1% penicillin/streptomycin (Corning). Media was replenished with clean growth media every 2-3 days until cells reached 80% confluence. Once confluent, cells were washed with phosphate-buffered saline (PBS, Gibco) and detached from flasks with 0.25% trypsin-EDTA (Gibco). Dissociated cells were counted and replated onto 6-well plates at $5x10^5$ per well (53,000 cells/cm^2). After overnight adhesion, MC3T3s were separated into two groups, one group subjected to osteogenic differentiation (i.e., differentiated group) using the In Vitro Osteogenesis Assay Kit (ECM810, EMD Millipore) and the other cultured in growth media (i.e., undifferentiated group). For cells undergoing osteogenic differentiation, media was aspirated and replaced with 2.5 mL growth media supplemented with 0.2 mM ascorbic acid 2-phosphate (EMD Millipore), and 10 mM glycerol 2-phosphate (EMD Millipore) while non-differentiated cells were aspirated and given 2.5

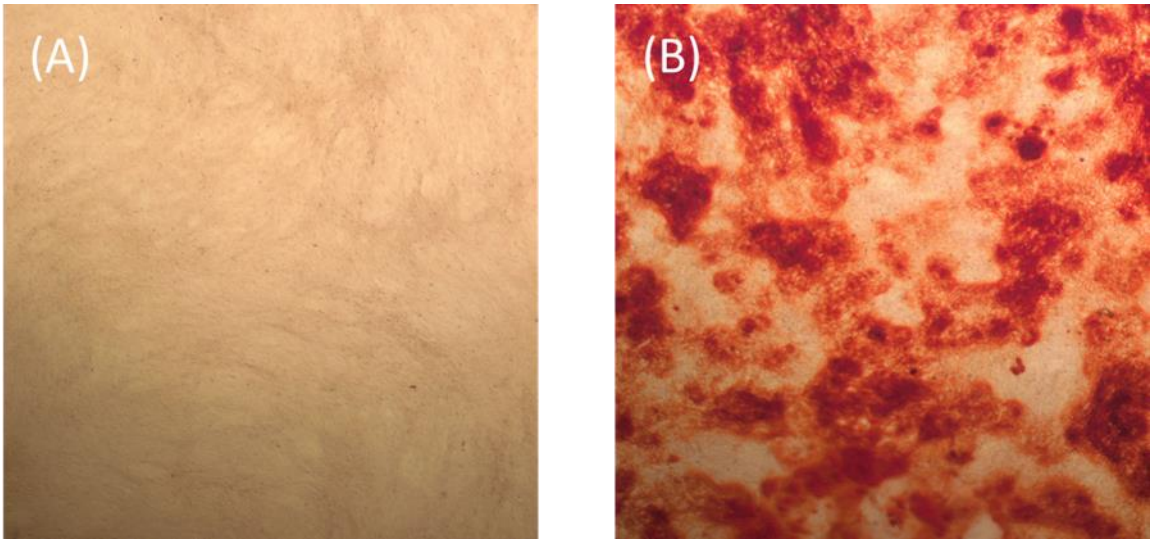

Figure 4.3. Representative images of the two cell culture groups after alazarin red staining A) In the undifferentiated group, which was not given additives to induce differentiation, no staining is evident B) In the differentiated group, red staining is seen throughout the culture indicating the presence of calcium deposits which are a byproduct of MC3T3-E1 differentiation. Image taken by Gilad Doron.

mL growth media with no additives. Every 3 days, media was replaced after DSP sampling. Immediately after sampling, conditioned media from both differentiated and non-differentiated MC3T3s was aliquoted for layer analysis and replaced with their respective fresh media. After 6 days in culture, the differentiation media was also supplemented with 50 nM melatonin (EMD Millipore). Both cell groups were cultured for 18 days total, being sampled 6 times total. After the final DSP experiment (day 18) cells were washed with PBS and fixed with 4% paraformaldehyde (Sigma Aldrich) in PBS at room temperature for 15 minutes. Fixative was removed and the cells were carefully rinsed three times with distilled water. Next, differentiated and non-differentiated MC3T3s were incubated in 2 mL alizarin red staining solution (EMD Millipore) for 20 minutes. Staining solution was then removed and cells were washed 4 times with deionized water. Osteogenic differentiation was confirmed in the differentiated group by red staining of calcium deposition, while no staining was observed in the non-differentiated group, as shown in Figure 4.3 (photo credit: Gilad Doron).

4.3 DSP Application to 2D Cell Culture

The MC3T3 cells were cultured in the Guldberg/Temenoff lab (IBB) by Gilad Doron. The DSP and MS systems were located in the Fedorov lab (Love) approximately 10 minutes walking from where the cells were cultured. Moreover, the Fedorov lab was not equipped with sterile space for culture manipulation (i.e., biosafety hoods) which increased the chance that the culture would become contaminated. To overcome these limitations, a method for sample transport and direct-from-culture sampling outside of a biosafety hood was developed. This protocol was designed to preserve the cell growth processes throughout the entire culturing period. When ready for sampling, the cells were

removed from the incubator and placed into a sterile fume hood. The 6 well plate cover was removed and replaced by autoclaved aluminum foil, which was taped down in a manner that allowed for visual inspection through the side of the culture plate. During sampling, a digital microscope was positioned orthogonally to the cell culture plate, allowing for visual confirmation of sampling mode (i.e., local or bulk) as shown in the Figure 4.4 inset images. After the cells were ready for transport, they were placed in a Styrofoam cooler and brought to the Fedorov lab, where they were immediately placed on a hotplate to maintain the media at ~37 ^{o}C throughout the entire sampling process for DSP-ESI-MS analysis.

Direct from culture DSP-nanoESI-MS analysis was carried out every 3 days, immediately before media changes, allowing for the highest concentration of biomolecules to be secreted between time points. The MS was tuned and calibrated using Bruker^{TM} tune mix at the start of each experiment to facilitate accurate mass identification. To remove all air bubbles, which interfere with continuous ESI, the entire sampling interface and DSP system was primed with sterilized DI water. To allow access to the cell media through the aluminum foil a 22 gauge sterilized hypodermic needle was used to puncture the foil and the sampling inlet was inserted through the hole. Directly before each sampling event, 2 μL of the sterilized water was pumped out of the sampling inlet at 100 μL/hr to purge the sample inlet line, reducing sample carry over effects. Samples of 1 μL volume were drawn into the sampling interface at 50 μL/hr and subsequently infused through the DSP for direct ESI-MS analysis at 30 μL/hr. Conditioning flow (1% acetic acid, 1% m-NBA) was run continuously at 50 mL/hr in crossflow orientation throughout the entire experiment. The

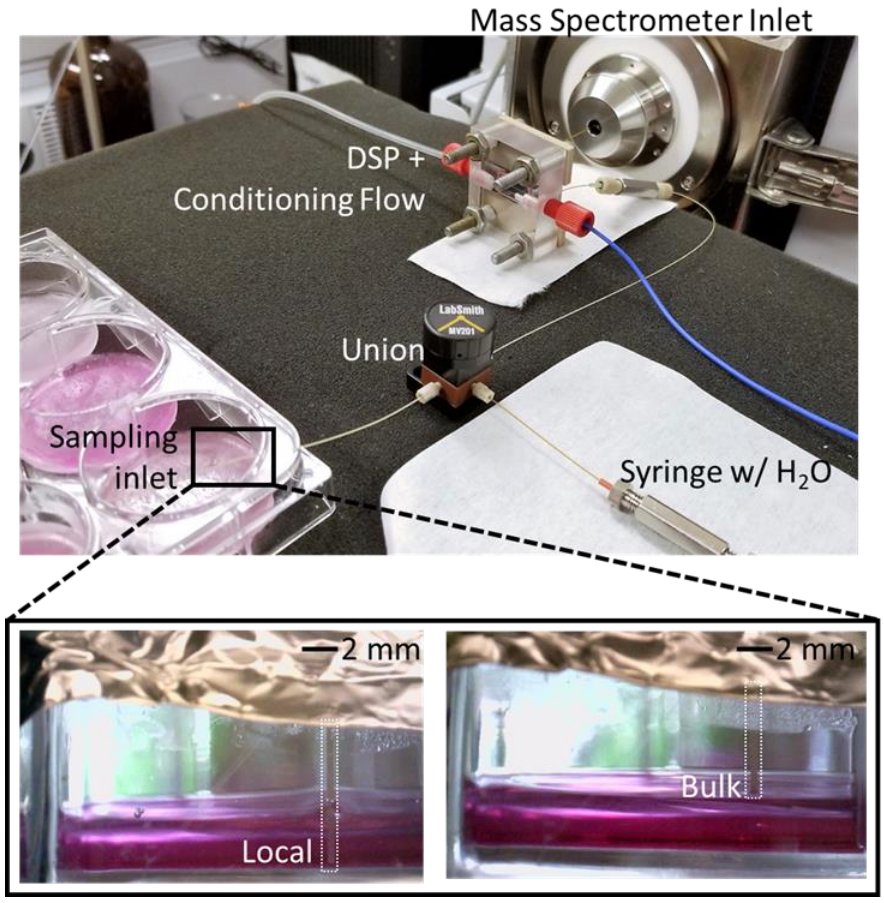

Figure 4.4. Dynamic Sampling Platform (DSP) setup for direct 2D cell culture analysis. The DSP, in the fluidic package, is positioned so that the ESI emitter is directly in front of the MS inlet. The DSP is connected to the sampling interface, which consists of a 50 µL syringe, union, and sampling inlet. Localized sampling is carried out by positioning the inlet directly above the bottom of the cell culture, in close proximity to the cells, while bulk sampling is carried out by submerging the capillary just below the media surface (inset images).

conditioning flow channel also served as the electrical connection for a picoammeter, which was connected to a stainless-steel wire submerged in the conditioning liquid reservoir. The electrospray current during all experiments was maintained at 10-20 nA so that the ESI characteristics remained consistent between experiments. Between each

sample, DI water was infused through the DSP and into the MS via ESI to remove residual media from the fluidic system and to reduce MS signal carryover before starting another sampling event. A total of 6 samples were captured from each cell group (i.e., differentiated/undifferentiated) at each time point. At each sampling event, 3 local and 3 bulk (Figure 4.4, inset) samples were taken with each sample taken at a spatially disparate locations to probe heterogeneities throughout the volume.

The resulting spectra from DSP application to the MC3T3 cell cultures (Figure 4.5) are not distinguishable without careful analysis. To analyze this data, principal component analysis (PCA) was used. PCA is an unbiased approach to data analysis that was used to identify features in the data which are hypothesized to correspond with known cell states. Raw data from the first and last time points is shown in Figure 4.5. Note that most of the salient signal is in lower m/z ranges which was confirmed to contain the features most

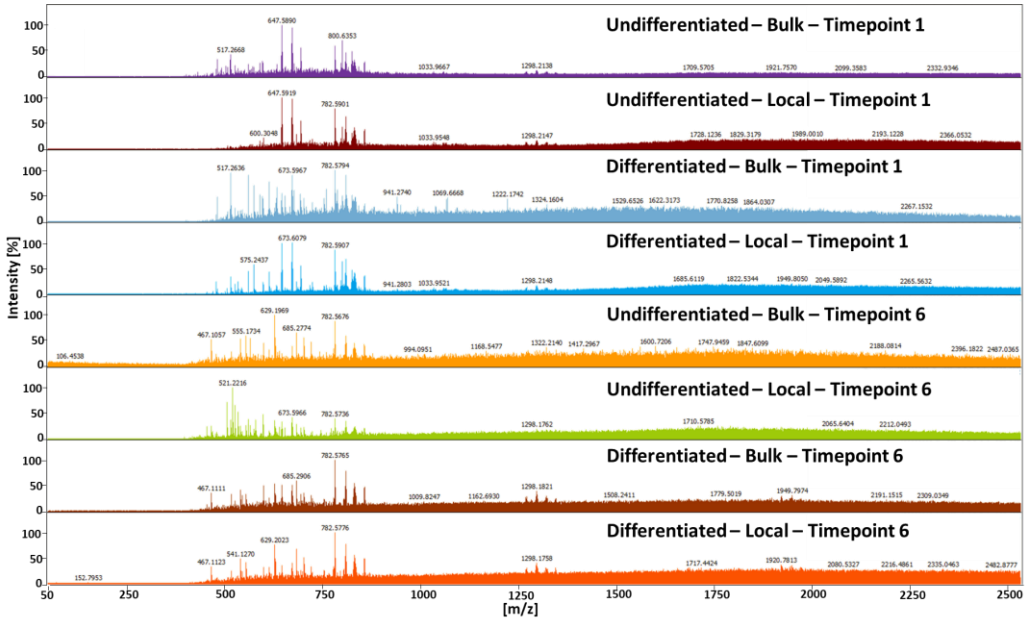

Figure 4.5 Raw data from the first and last timepoint for both cell groups. No clear differences are observed between the data, necessitating the use of an unbiased data analysis to identify features indicative of cell state.

indicative of cell state. Preprocessing of the resulting spectra, mostly in the form of smoothing and winnowing, was used to tease out features in the large (72 spectra total) data set that contributed to differences between the groups.

4.4 Raw Data Preprocessing

Bruker MicrOTOF output files gathered for each of the 72 samples were parsed and converted to "mzML" file type using the open source data conversion software, *ProteoWizard.*[65, 66] Principal component analysis (PCA) was completed using two open source software utilities. The first was *ms-alone*, a python-based utility for preprocessing and peak extraction used on the raw mzML files prior to importing the data to the second utility, *multiMS-toolbox*, an R based software for PCA analysis.[67] Preprocessing was accomplished using *ms-alone* on the raw data including baseline subtraction and peak smoothing. Within *ms-alone*, the signal to noise ratio threshold of data was set to 0.5, and a Savitzky-Golay smoothing method was used to reduce noise.[68] The parameters used for these steps of pre-processing were recommended by the developers and implemented to enable data transfer between the different software utilities. The final PCA results did not depend on these steps, but the results did depend heavily on the winnowed range of m/z values used for comparing the time points.

PCA is used for a range of applications, but for the DSP results it was used to determine if differences between the cells in their different differentiation states are reflected in the spectra. Therefore, the input to the PCA was the entire spectra and the outputs are principal components and associated "loadings" which reveal which features in the spectra that contribute most to differences between the groups. Each principal

component has a percentage value assigned to it and a loading plot associated with it. The loading plots are simply reconstructed spectra comprised of m/z values and contribution to variance. Therefore, principal components with high percentage values assigned to them are more likely to have spectral features in the loading plots that correspond to actual differences between the raw spectra.

Before conducting PCA, each data point was tagged with properties such as time point, differentiation status, and whether it was a bulk or local sample. An entire spectra is represented as a single point on the output PCA scatter plots. The PCA protocol groups the data based on how similar the input data is. PCA is unsupervised, and therefore groups data based on their principal component loadings which are assumed to be due to the tagged properties, but unlike other supervised methods, PCA does not force the separation of

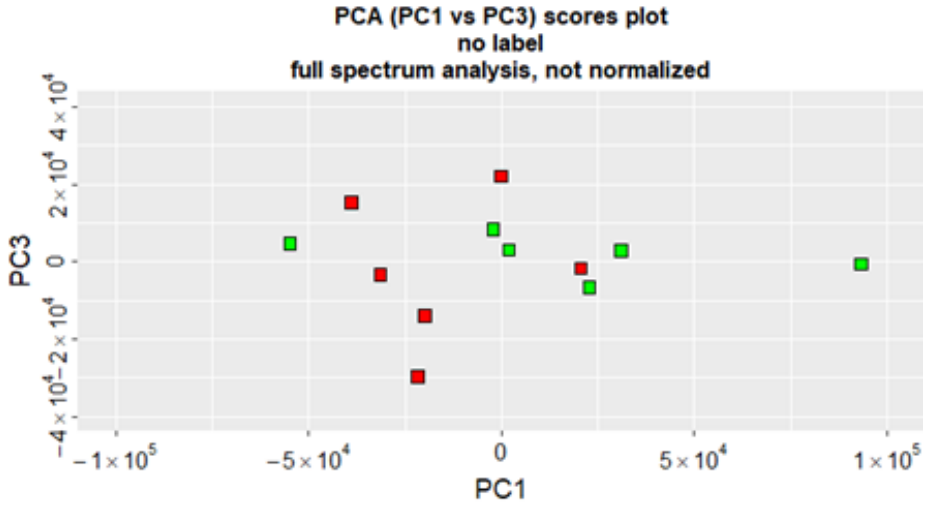

Figure 4.6: Resulting PCA scatter plot for unwinnowed data from localized sampling done on cells in their undifferentiated (red dots) and differentiated (green dots) states. The lack of separation between the different colored points indicates there is no consistent difference between the two groups.

groups based on these tags. When the different groups separate well, this indicates that there is a variable responsible for this difference that may not be directly measured, which in this case was cell state. A large swath of each spectra had low intensity signal, and this reduced the effectiveness of PCA in revealing differences between the data sets. Therefore, the spectra were winnowed prior to the final analysis. To demonstrate the effect that winnowing had on PCA results in this chapter, a sample workflow is presented here.

First, intensity based (i.e., no data normalization) PCA was run on the entire spectrum (m/z 0-2500) of cells in an undifferentiated and differentiated state. To increase the count of data points in each group, multiple points were grouped such that each group (e.g., undifferentiated, differentiated, proliferative, etc.) had at least 6 spectra to represent it. The specific groupings, and the reasoning behind them, are discussed in detail in section 4.5. The data used for this demonstration is for the local samples taken from time points 5 and

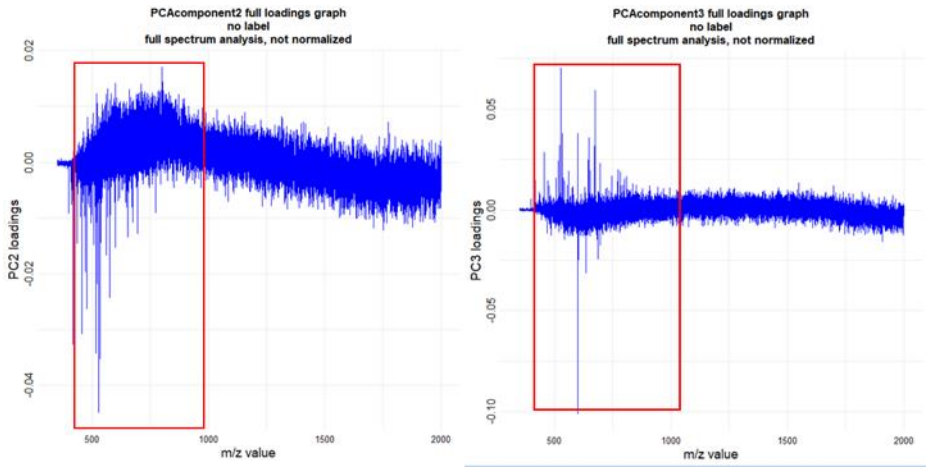

Figure 4.7: Loading plots for PCA in Figure 4.6: reveals a large part of the input spectra does not contribute to variance between the groups. A threshold value of 20% of the maximum was used to winnow the data.

6 from the differentiated and undifferentiated groups. The green dots represent cells which were differentiated, while the red dots represent cells that maintained their undifferentiated state. Without any data winnowing, the groups do not show any separation (Figure 4.6:). This suggests that there is no significant difference, based on the input spectra, between the groups. However, in the loading plots that correspond to these two principal components there are areas of the spectrum that appear to have more contribution to the variance than others. These regions are highlighted in the red boxes in Figure 4.7.

Selecting a threshold value in the loading plot, which was 20% of the absolute value of maximum/minimum, the data was winnowed to remove the low contribution features in higher m/z ranges (above ~1000 m/z in this case). PCA was again run on the winnowed

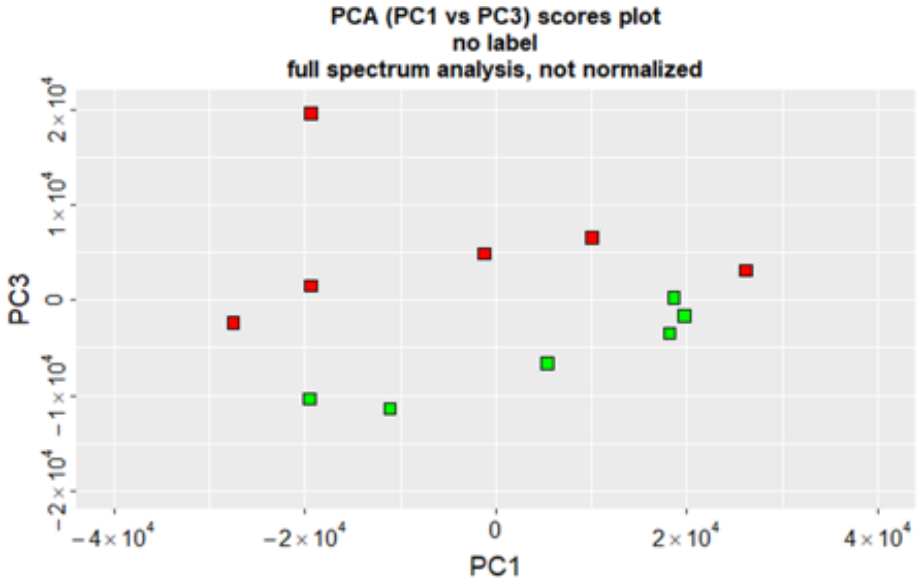

Figure 4.8: PCA on the same data shown in Figure 4.6: with the winnowing approach from Figure 4.7 reveals two groups corresponding to undifferentiated (red dots) and differentiated (green dots) cells. Discussion of data detail is in Section 4.5.

data, and the resulting PCA scatter plot in Figure 4.8 shows two groupings corresponding to the known difference in the sampled media, which was differentiation state.

4.5 Detecting Cell State

The ability to determine, in real-time, cells' health, therapeutic potential, or developmental state is paramount to developing effective feedback control for cellular therapy production (e.g. immunotherapies, biologics, regenerative medicines). Whether or not a cell has differentiated is an important aspect of the cell's state. For example, clinically relevant cells such as mesenchymal stromal cells (MSCs) have their therapeutic potential drastically altered depending on their differentiation state.[69, 70] As a first step towards real-time monitoring of primary cell cultures, DSP was applied to MC3T3 cells for rapid ESI-MS, followed by PCA of the collected spectra to determine if features in the raw spectra corresponded to differences in the secretome, and therefore the cell state.

The MC3T3 cells used in this study served as a proxy to clinically relevant cells due to their predictable differentiation behavior, with a developmental sequence similar to osteoblasts in bone tissue.[71] As cells grow and differentiate, the molecules they secrete have the highest concentration near the cell membrane, while the concentration of these secreted biomolecules in the bulk media grows slowly with time due to substantial dilution. Therefore, these experiments were designed so that sampling was done just before media changes, when the biomolecules would be at the highest concentration in the bulk media, to investigate if localized sampling provides a different analytical outcome than bulk sampling. At each of the six time points triplicate samples of bulk and local (Figure 4.4, inset) were taken for both cell groups (i.e., differentiated and undifferentiated).

Representative data from the first and last time point for both the undifferentiated and differentiated cell groups is shown in Figure 4.5. As discussed, detecting any differences in the spectral data required statistical analysis. The data processing approach outlined in section 4.4 enabled PCA to identify differences between the spectra and to identify m/z values that contribute most to variance between data. These selected m/z values were then later used to for comparison with offline high performance liquid chromatography (HPLC) data.

Due to the small number of sample replicates at each time point, data from multiple time points were grouped to increase the robustness of PCA. For each time point, PCA is carried out on bulk and local samples to study localized sampling enrichment. Figure 4.9 shows the resulting PCA scatter plots for bulk samples taken from time points 5 and 6 grouped together for the undifferentiated and differentiated groups. These are the last two time points measured using DSP with direct ESI-MS analysis. The cells in the differentiated group are expected to have begun differentiation by time point 4 and completed by time point 5, while the cells in the undifferentiated group remained undifferentiated throughout the experiment. Time points 5 and 6 were therefore grouped to represent the cells in their fully undifferentiated or differentiated state, respectively, and to omit earlier time points where the cells were still expanding or undergoing the differentiation process. Subsequent staining in Figure 4.3 of both the undifferentiated and differentiated cell lines confirmed that the cells had either remained in the undifferentiated state or had completed differentiation after time point 6.

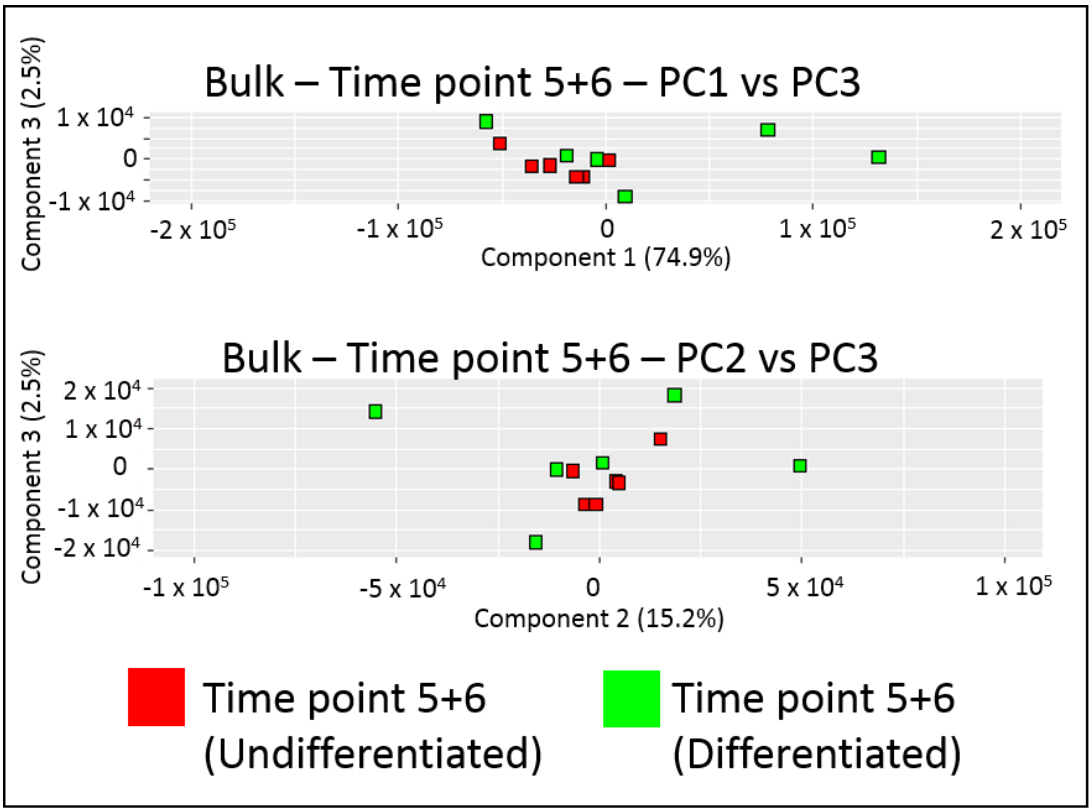

Figure 4.9: Principal component analysis (PCA) cluster plots for bulk samples taken from time points 5 and 6 of the undifferentiated cell group vs time points 5 and 6 of the differentiated cell group reveals no clustering.

The clusters in the PCA plot based on bulk sampling in Figure 4.9 are not well segregated, which suggests that there is no significant difference in the spectra in the bulk sampling case. Localized sampling, on the other hand, reveals a strong clustering of the two groups, shown in Figure 4.10. This indicates that localized sampling is important for the detection of differences in cell differentiation state. Both cell groups were given different media throughout the culture process, but these differences are not revealed by the bulk samples which suggests that the differences observed in the local samples are due to secreted biomarkers captured near the cells, and not due to differences in the cell culture media composition. Additionally, the DSP selectively removes smaller molecules from

treated samples while retaining larger biomolecules. The additives given to the differentiated cell group have molecular weights below 300 g/mol (Da), and were likely removed during DSP treatment [72] .

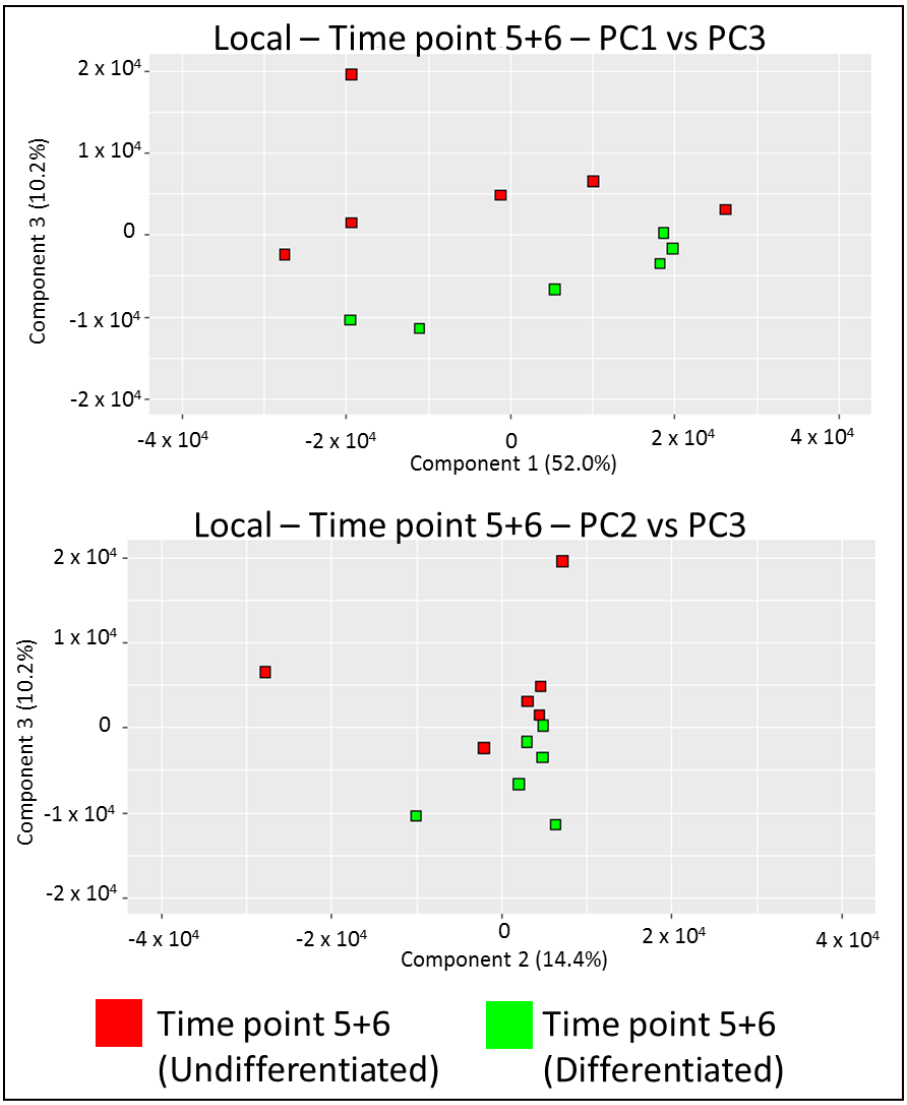

Figure 4.10: Principal component analysis (PCA) cluster plots for local samples taken at time points 5 and 6 of the undifferentiated cell group vs time points 5 and 6 of the differentiated cell group. Localized sampling reveals clusters for the two groups, indicating that localized sampling captures the cells' differentiation state.

In order to observe if the same cell culture exhibited differences with time, and to remove the contribution of cell culture conditions to the variance in data, the same differentiated cell culture, i.e., the culture given the osteogenic factors to induce differentiation, was analyzed alone. Time points 1 and 2 were grouped and compared to time points 5 and 6. These groupings compare the cells in early time points, when they

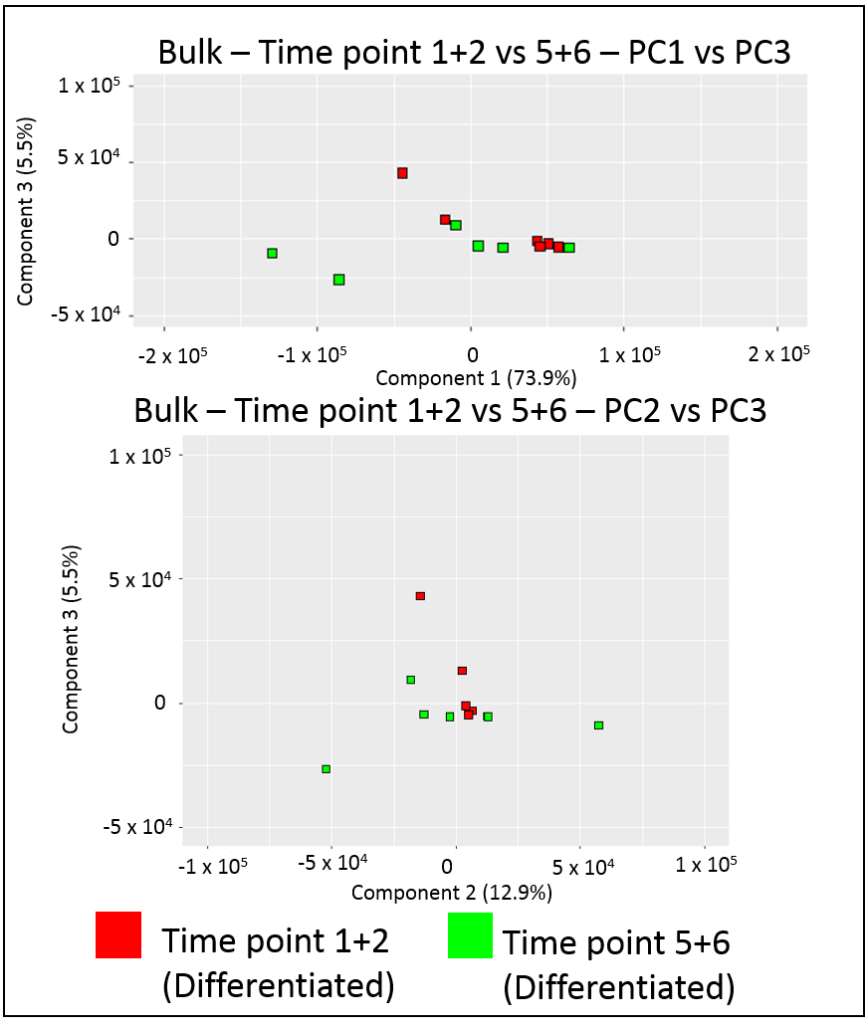

Figure 4.11: Principal component analysis (PCA) cluster plots for bulk samples taken from the differentiated cell line at time points 1 and 2 versus time points 5 and 6. Cells were expected to begin differentiation between time points 3 and 4, with differentiation completed by time point 5. Bulk sampling does not exhibit any clustering.

have not completed differentiation, to the cells in a fully differentiated state. Because all of the data was taken from the same cell culture in the same continuously performed cell growth and development experiment, this approach also removes the possibility that

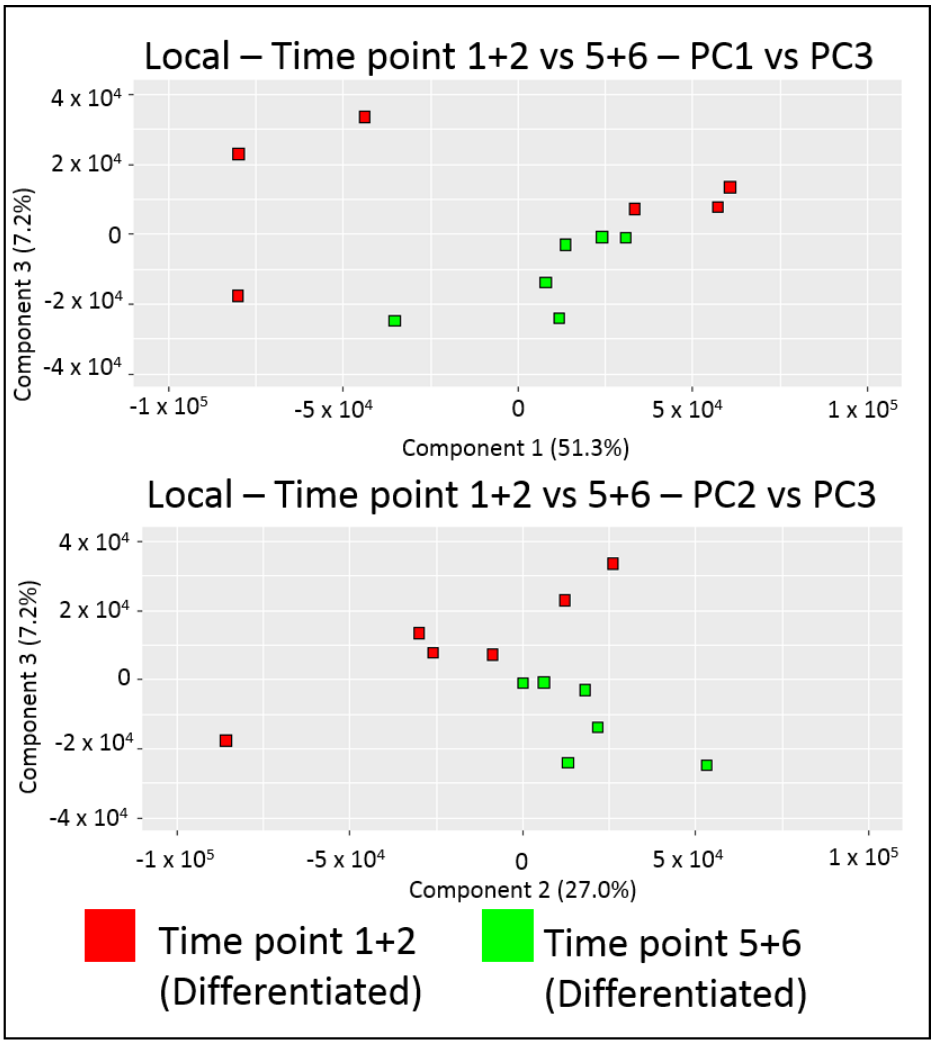

Figure 4.12 Principal component analysis (PCA) cluster plots for local samples taken from the differentiated cell line at time points 1 and 2 versus time points 5 and 6. Cells were expected to begin differentiation between time points 3 and 4, with differentiation completed by time point 5. With localized sampling, clusters are observed indicating that DSP detects differences between undifferentiated and differentiated cell lines by probing the near cell enriched secretome.

different culture conditions (e.g., seeding density, media type, etc.) contributed to the differences observed.

Figure 4.11 shows the resulting PCA plots for bulk samples taken from the differentiated cell group at early and late time points. Once again, the spectra do not exhibit significant clustering for bulk sampling, which suggests that the spectra do not contain features contributing to differences between groups. Figure 4.12 shows that again localized sampling is paramount for detecting cell state. In these cluster plots, the early and late stage groupings correlate with cell differentiation status. The top cluster plot in Figure 4.12 also exhibits clear subgroup separation between the early stage cells represented by red boxes, which was confirmed to correspond with time point 1 and time point 2. This suggests that not only does localized sampling capture clear differences in cell types, such as whether or not they have differentiated, but also more subtle aspects of cell state, e.g., whether the cells are in a proliferative or confluent states.

PCA was performed as previously described (i.e., time points 1 and 2 vs time points 5 and 6) for the data from the undifferentiated cell group. In this case, bulk sampling once again resulted in no separation (Figure 4.13) and for local sampling (Figure 4.14) the separation between the two groups is not obvious, though some grouping is evident. The localized sampling data suggests some changes in the undifferentiated cells with time. Staining at the end of the experiment (Figure 4.3) confirmed that this group remained in an undifferentiated state, and therefore these differences are not due to differentiation. One possible explanation is that the differences observed are due to a change in the cell secretome during expansion, which has been shown to correlate with preosteoblasts in a state of proliferation (early) or confluence (late).[73] Another possibility is that the cells

underwent another phenotypical change, such as apoptosis. Further studies will explore DSP determination of cell secretome correspondence to cellular state, from early

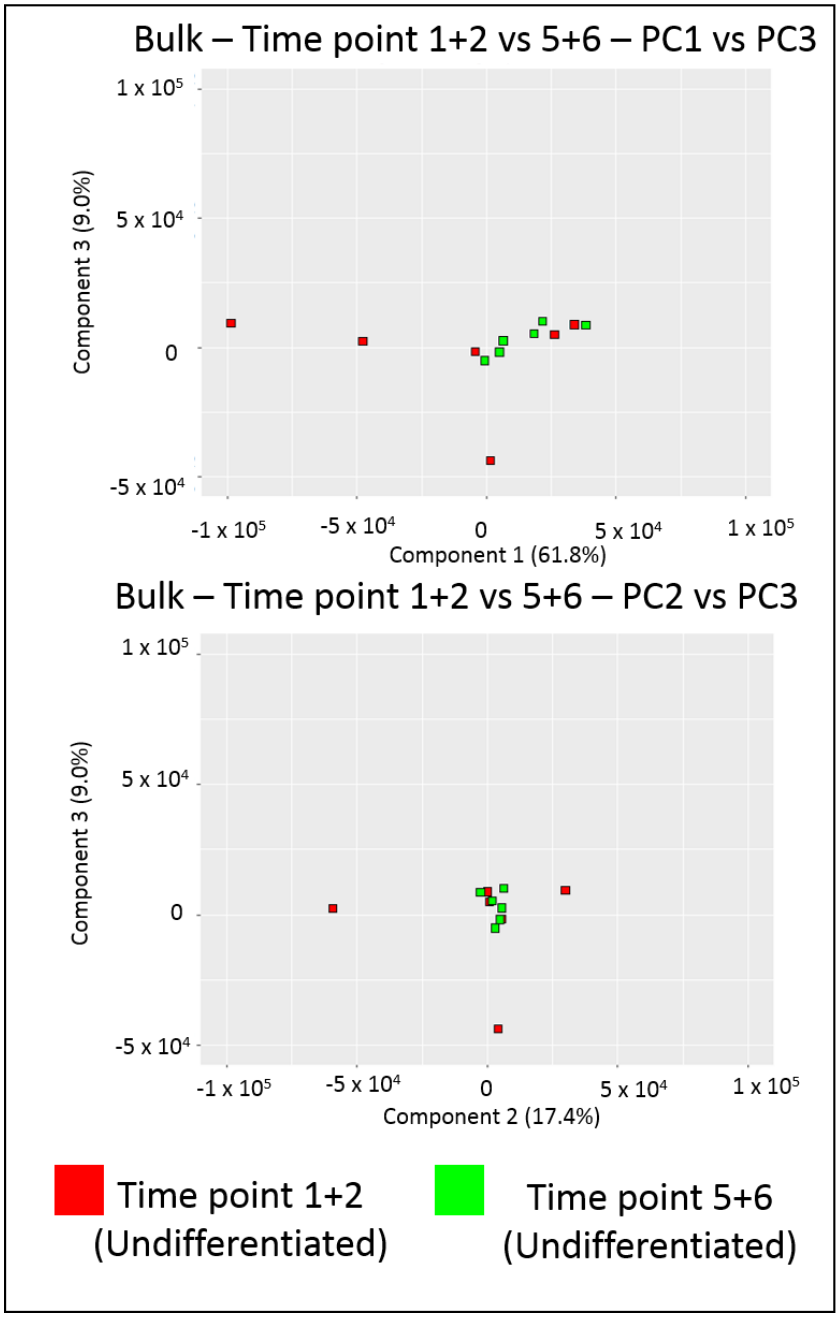

Figure 4.13: Principal component analysis (PCA) of bulk samples taken from the undifferentiated cell group at time points 1 and 2 versus 5 and 6. Bulk sampling shows no separation between groups.

proliferation, later confluence, and in certain cases final differentiation. Once biomarkers are correlated with cell state, DSP will provide the unprecedented ability to monitor cells

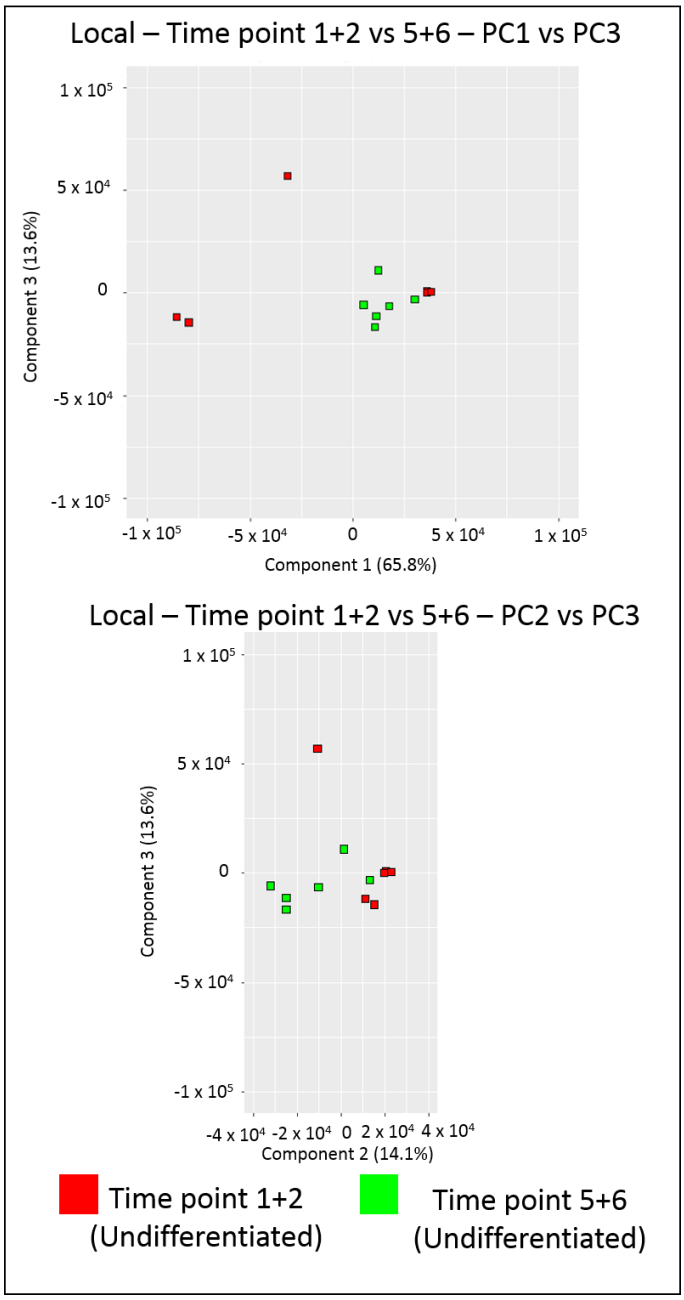

Figure 4.14: Principal component analysis (PCA) of bulk samples taken from the undifferentiated cell group at time points 1 and 2 versus 5 and 6. Local sampling reveals moderate separation, indicating a difference between the groups such as proliferative (early time point) vs confluent (late time point).

in real-time. This approach will enable improved quality assurance and reduced batch-to-batch variability with closed-loop feedback control.

To enhance biochemical interpretation of the PCA analysis, offline HPLC-MS was performed on aliquots of conditioned media which were gathered during media change and frozen at -40 °C until the end of the study. HPLC was carried out on media from both cell types at time points 1, 2, 5, and 6 to identify candidate differentiation biomarkers and to quantify differences in biomolecules between time points. The candidate biomolecules identified with HPLC were then manually compared to m/z values with the highest contribution to variance in the PCA data that are hypothesized to correlate with cell state (i.e., differentiated vs undifferentiated). The mass spectrometer used for direct-from-culture DSP analysis was not equipped with tandem mass spectrometry (MS-MS) capability, therefore fragmentation patterns could not be matched to the HPLC-MS data. As a result, the m/z values from the PCA loading data were matched to potential chemicals from HPLC-MS based on accurate mass alone, resulting in tentative IDs only. A large number of candidate molecules were identified using this approach, but only those which

Table 4.1: List of potential chemicals identities based on HPLC matches to DSP-MS based PCA loading plots.

Chemical Name	HPLC Result
LysoPC(24:1(15Z))	Increased
1-stearoyl-sn-glycero-3-phosphoethanolamine	Increased
1-arachidonoyl-sn-glycero-3-phosphocholine	Increased
1-Oleoyl-2-Stearoyl-sn-Glycero-3-Phosphocholine	Decreased
Militarinone A	Decreased
Folate	Decreased

had been cited in literature are presented in Table 4.1.[71, 74-79] These results demonstrate that DSP serves to not only generate cell culture "fingerprint" spectra, but to also identify which detected biomolecules correlate with cell state. For more complete identification of biomolecules, DSP can be used with MS^n for fragmentation to generate candidate IDs before HPLC is carried out. Further studies will elucidate the manner in which PCA loading data correlates with HPLC-MS data for independent identification of CQA biomarkers using DSP based analysis. Integrating DSP directly into workflows with MS instruments with tandem MS capabilities will also ensure that instrument-to-instrument variability is reduced as fragmentation patterns can be used as in addition to accurate mass for comparison.

CHAPTER 5.
CONCLUSIONS AND FUTURE WORK

The Dynamic Sampling Platform (DSP) is a new technology for real-time quality monitoring and CQA discovery for biomanufacturing. This thesis focuses on DSP development and applications in the growing field of cellular based therapies, which include immunotherapies such as the CAR-T cell treatment, regenerative medicines, and other promising therapeutics for previously untreatable ailments. DSP is designed as a drop-in sensor with broad applicability. Therefore, well established biomanufacturing industries can also adopt the DSP enabled analytical capabilities, including the biologics field which would benefit from the ability to characterize large and complex proteins in their native state.[4, 5, 18, 38, 80, 81] The DSP is capable of probing bioreactors with high spatial and temporal resolution to capture the transient and spatial heterogeneities which correlate with cell state and therapeutic potential. These secreted biomolecules are in high concentration near where the cells are located, so the ability to capture the CQA biomarkers where they are produced unlocks a new method for quality monitoring in biomanufacturing. Importantly, DSP will provide real-time feedback on the cell state based on its secretome evolution, a current void in process analytical technologies (PATs) that is considered as the primary bottleneck for bringing promising advanced therapies to a wide patient population.[6]

In CHAPTER 2, the fully integrated DSP PAT for integration with good manufacturing practice (GMP) workflows is presented. For clinical applications, especially GMP workflows, the cell bioreactor, DSP, and mass spectrometer are expected to be spatially separated which confounds the application of the DSP sensor system to advanced

workflows. To overcome these barriers, the DSP is designed to couple with a novel sample uptake system, the dynamic sampling interface (DSI), and an ion transfer interface for analyte transport. The DSI is a minimally invasive sampling technology for direct from culture sampling with minimal loss of sensitivity due to sample dispersion effects. Central to the DSP technology is the microfabricated mass exchanger which is produced in a scalable format. The microfabrication approach is used for precise feature size control that enables DSP's inline sample treatment. A novel clog-resistant counterbore inlet/outlet geometry allows monolithic integration of the sampling interface and an ESI outlet. For application to GMP workflows, the sampling interface, mass exchanger, and ESI outlet are positioned near the cell culture, while an ion transfer interface couples the MS instrument to the DSP for real-time analysis. The ion transfer interface is introduced for the transfer of analyte ions in gas phase over many meter distance from the DSP system to the mass spectrometer without significant loss in signal. Importantly, the fully integrated system is capable of maintaining sterility and minimally disturbing the cell culture. Finally, an optimization study for the DSP mass exchanger is presented, and a simple change in device mass exchanger operation from counterflow to crossflow orientation improves device efficiency. This improved design is critical for enabling clinical workflows where the sample treatment requirements are burdensome such as those explored in CHAPTER 4.

CHAPTER 3 demonstrates that the DSP active sample conditioning approach enables a broad range of CQA biomolecule detection. During sample treatment, a size selective membrane allows for the transport of interfering species (salt) out of the sample and the infusion of signal enhancing chemicals into the sample. A reduced effective diffusion coefficient for larger biomolecules enhances the retention of CQAs in the sample while

effectively removing small (high diffusion coefficient) salt molecules through the nanoscale pores of a dialytic membrane, enabling real-time ESI-MS with improved sensitivity. Active sample conditioning is shown to enhance MS performance, including improved limit of detection, multi-component detection, and increased dynamic range for high molecular weight biomolecule detection. The experiments presented in this chapter serve as proxies to clinically relevant testbeds and demonstrated the DSP's capability for real-time ESI-MS bioreactor monitoring.

Application of DSP to living cell cultures demonstrated the key capability to detect cell state during the cell development trajectory in CHAPTER 4. First, comparing local and bulk samples from NHLF cells revealed a biochemical signature in the microenvironment that was qualitatively different from bulk samples, suggesting the need for localized sampling to detect cell state. Two other clinically relevant cells (MSCs, HUVECs) were compared to the local NHLF samples for cell-type fingerprinting, demonstrating DSP's key ability to detect cell state. To detect more subtle aspects of cell states, such as differentiation, a longitudinal study was carried out on preosteoblast MC3T3-E1 cells. DSP was applied to cells throughout their entire cycle without affecting culture sterility or final cell state. Post hoc analysis of the 21 day study revealed that localized sampling was paramount to detecting cells in their proliferative, confluent, undifferentiated, and differentiated states. Using PCA as an input, orthogonal HPLC analysis was used to identify potential CQA biomolecules, establishing the workflow for DSP as not only a spectral fingerprint monitoring tool, but as a tool for detailed discovery of critical process parameters and unambiguous molecular identification of cell state predictors.

5.1 Original Contributions

This PhD research made several important contributions to fundamental science and to the engineering practice as stated next.

Fundamental Science

1. A new analytical concept (DSP – Dynamic Sampling Platform) for process monitoring of bioreactors has been introduced, including the key enabling technology components and an integration approach for applications in emerging cell therapy development. The core element of the DSP is the microfluidic mass exchanger that was developed using new design and microfabrication approaches, which ultimately led to significant analytical advances. Using a combination of active sample conditioning including dialytic salt removal, sample acidification, and chemical conditioning via supercharging molecules the DSP micro-mass exchanger i) improves ESI-MS sensitivity to low concentration biomolecules by an order of magnitude in samples with high salt content, ii) enables multicomponent detection of protein biomarkers of significance to cell therapy quality and potency assessment, and iii) expands the mass range for high molecular weight protein detection through the use of carefully optimized sample conditioner. These results prove that DSP active sample conditioning fundamentally improves ESI-MS analysis due to several chemical mechanisms (e.g., supercharging, acidification, protein conformation) that previously were unexplored in real-time applications.
2. DSP provides a pioneering methodology for in situ probing of the rich biochemical microenvironment in cell bioreactors locally, in a transient

manner. Samples taken directly from bioreactors with subsequent DSP active sample conditioning and inline ESI-MS measurement are shown to correlate directly with cell state. A longitudinal study of living cells demonstrates that the DSP's ability to detect cell proliferation, confluence, and differentiation are enhanced by localized sampling and active conditioning.

3. DSP enables a novel approach to statistically significant correlation of dynamically acquired MS spectral signature of secreted CQA biomolecules (molecular fingerprinting) with the cell biochemical state. When used in combination with HPLC-MS as a complimentary offline identification approach, it establishes DSP as a powerful biosensing technology for both real-time process monitoring and new therapy discovery applications in biomanufacturing.

Engineering Practice

1. Development of a scalable, transferable microfabrication process for a microfluidic ESI-MS platform technology based on a micro-mass exchanger with integrated sampling and electrospray ionization capabilities. Design rules for enhanced mass transfer in counterflow and crossflow orientations of the mass exchanger have been identified and used to achieve an enhanced analytical performance.
2. Demonstration and optimization of a sterile sampling method for direct-from-culture sampling with the dynamic sampling interface (DSI) for isolated sample uptake and infusion capabilities; design rules for mitigating the

detection sensitivity penalty due to dispersion during sampling/sample transport to MS analysis.

3. System level integration of a long distance gas-phase ion transfer interface with the DSP platform and mass spectrometer to enable real-time quality monitoring of cell bioreactors in GMP facilities, where cell culture and analysis must take place in physically separated locales.

5.2 Research Areas for Future Work

With the advances made in this dissertation research, DSP was advanced to the market readiness level (MRL) 4-5 for application to biomanufacturing workflows, but additional studies will aid improving DSP performance in application to salient testbeds. The size selective membrane, which is monolithically integrated into the DSP mass exchanger, has an average pore size of approximately 50 nm. The effective diffusion coefficient of a biomolecule in a small pore is inversely proportional to the ratio of the molecule diameter to the pore diameter, so therefore decreasing the size of pores improves the retention of smaller molecular weight biomarkers in the sample.[82] DSP's effectiveness at removing/retaining a specific molecule is a function of the molecule's effective diffusion coefficient through the nanoporous membrane, which is shown in Figure 5.1. Three graphs show the effect of reducing pore size on selectivity of separation of different molecular weight compounds. Currently, at the 50 nm pore size, DSP effectively removes ~70% of the IL-8 content, which explains why this molecule was not visible during active sample treatment in section 3.4. By reducing the pore size to 15 nm, or even lower to 6 nm, DSP should remove approximately 50% or 10% of the IL-8 content; this improved selectivity

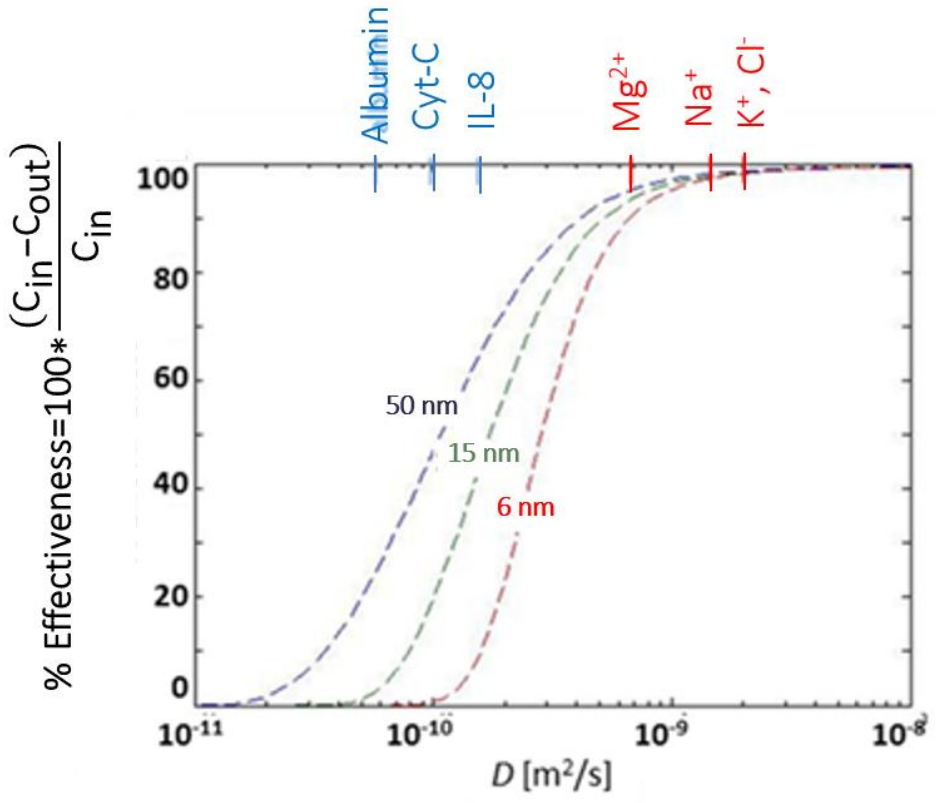

Figure 5.1: DSP is less effective at removing larger biomolecules with a reduction in nanoporous membrane pore size. The current DSP system has 50 nm pores, and reducing the pore size further would increase DSP selectivity to larger CQA biomolecules.

will enable DSP to detect smaller signaling molecules with little detrimental effect on the removal of small salt ions, as DSP's effectiveness at removing very small salt ions is nearly independent of pore size.

Some work was done to reduce the pore size by changing the electrolyte from oxalic acid to sulfuric acid and changing anodization potential during the Al_2O_3 fabrication, which was observed to reduce pore size to approximately 10 nm. These devices did not remove salts, which is thought to be due to incomplete anodization, residual barrier layers, or

unexpected tortuosity within the porous structure that increased mass transfer resistance. By reducing the pore size far below the 10 nm level, the mass transfer resistance across the membrane may increase significantly. This will increase the time necessary to remove the same amount of interfering salt ions, which may be of some concern depending on the application. Alternative designs can reduce characteristic lengths in all areas of mass transfer to improve the performance, i.e., reducing sample channel height, membrane thickness, and conditioner channel height.

Retaining molecules with weights below ~15 kDa is of interest because the signaling molecules that correlate with cell state are in this mass range. On the other hand, larger molecules like albumin, which are in very high abundance in cell media, are retained very effectively. The presence of these heavy proteins will dominate the MS spectra masking other important analytes. For some workflows, such as those involving biologics or monoclonal antibodies, this may be desirable, but in initial experiments with bulk monitoring of low concentration additives in some types of cell culture media it was found

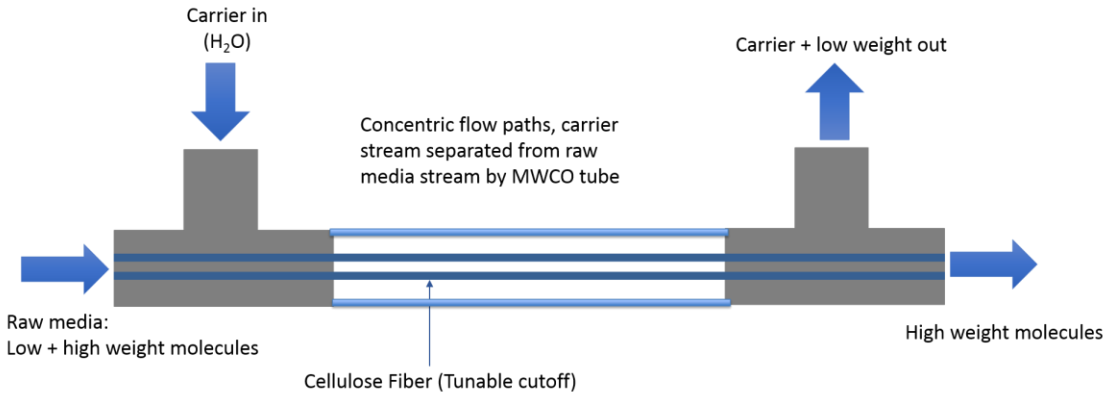

Figure 5.2: Inline filter for high MW cutoff based on prior designs by Olivero et. al. Two separate output flows will allow for parallel analysis (via DSP) of effluent with high MW content and low MW content.

that signal from serum albumin overwhelms the spectra. In cell culture media, serum is orders of magnitude higher in concentration than CQA biomolecules, and accordingly serum masks the signal of most biomarkers. Therefore, additional separators may be placed inline with DSP to serve as a low molecular weight pass filter. One possibility is to design a continuous inline filter, similar to the one used by Olivero et. al, to separate raw cell culture media into high MW and low MW streams.[33] Other possibilities are inline digestion, precipitation, or modified chromatographic columns for selective removal of larger proteins.

Coupling DSP to clinical workflows that take place within GMP regulated facilities requires careful design of the interfacing components, namely, the DSI and the ion transfer interface. For adherent, 2D cell cultures that are common in research settings, obtaining minimally invasive samples intermittently was easily accomplished with the iteration of DSI presented in CHAPTER 2. Producing cells at scale necessitates the use of bioreactors. These bioreactors may be fed batch, stirred tank, cell stacks, or other geometries that are not amenable to direct sampling. Therefore, an effective sampling interface should be able to extract sample from these complex bioreactors without affecting culture sterility or bioreactor function. For example, coupling DSP with an N-degree of freedom "snake" robot for highly resolved inlet manipulation can enable DSP to probe the spatial and temporal heterogeneities within commercially relevant bioreactors. Alternatively, designing the bioreactors to allow for one-way sample uptake (e.g., a check valve sampling port) is another approach for DSI integration. In addition to sampling concerns, transporting the sample from DSP to analysis is a critical area for DSP improvement.

The ion transfer interface presented in CHAPTER 2 was based on prior art by Garimella et al. This system was shown, in agreement with literature, to reduce sensitivity and to preferentially transmit lower charge state ions.[42] Optimizing the transfer interface such that it does not hinder the DSP approach to bioreactor monitoring is a critical area of further research. Exploring positive pressure systems, i.e., higher pressure at the ion transfer inlet vs MS inlet, will allow for higher flow rate operation. It was reported that ions are generally transmitted more effectively at higher flow rates in larger diameter transfer tubes, but in fully turbulent regimes it is expected that enhanced mixing would lead to loss of ions due to wall collisions. Additionally, a large portion of the ion loss comes in the first meter of transmission. The counter electrode geometry presumably affects ion trajectory, as does the entry region to the interface where flow is developing hydrodynamically. Therefore, a holistic approach to the ion transfer interface should study the interplay between inertial forces, viscous forces, and space charge effects on ion transmission efficiency.

Relevant testbeds for exploration with DSP should mirror clinically relevant areas of interest. Two immediate test beds are the concentration gradients in T-cell cultures and the transient nature of MSC cultures. The first FDA approved cell-based therapy, CAR-T cell therapy, has over 50% of the production cost tied up in materials and supplies alone. With price tags of single therapy dose well over $0.5M, the burden of material costs is substantial.[80] IL-2 is added during production in high abundance, from 1 to 100 U/mL, and then left unmonitored. As the production scale increases, the spatial heterogeneities that exist in research grade bioreactors are likely exacerbated on larger scales. DSP can probe

local and bulk concentrations of additives, such as IL-2, and also monitor the transient secretion of IL-15, which is known to indicate cell subtype.[38]

MSCs have yet to reach clinical relevance, although it is known that they secrete a number of anti-inflammatory signaling molecules as well as growth factors associated with angiogenesis. A common method used to prime MSCs is the addition of interferon-gamma (INFγ) or tumor necrosis factor alpha (TNFα).[39, 83] The transient behavior of MSCs after priming, as well as the molecules which are released at different levels of priming, are both important research questions which will help unlock the therapeutic potential of these promising cell types. MSC and T-cell therapies are just a very small subset of the range of applications that DSP will prove useful both as a CMC (Chemistry/Manufacturing/Control) tool for biochemical mechanism discovery and product manufacturing monitoring and validation.

As a platform technology, DSP can also be modified to couple with other sensing techniques. Mass spectrometry has advantages in being label free and highly sensitive, but it is also highly dependent on sample preparation and a relatively costly analysis method. Exploring other sensing techniques in conjunction with DSP, especially very fast and readily available methods such FTIR, Raman, and NMR, which also require a special care of sample treatment for improved selectivity and sensitivity of detection, will enable new transient analysis modes for applications in a broader engineering ecosystem.

APPENDIX A. DEVICE MICROFABRICATION

This appendix provides specific details microfabrication process used to create the DSP mass exchanger. This was developed using instruments within the shared user GT cleanroom facilities and therefore the specific parameters may vary depending on the instrument condition.

A.1 Detailed Microfabrication Workflow

The purpose of this section is to outline in detail each fabrication step and provide insight as well as options for producing the DSP. In general, having the ability to transition between instruments can be helpful when navigating scheduling and maintenance issues in a shared-user facility, so multiple options are presented where they were found to work. Since the entire process relies on photolithography alignment, and eventually wafer level alignment, it is important to make sure the alignment mark system utilized will function on every instrument used. As a last note, the entire fabrication process should be walked through with an experienced user/staff member since there are compliance issue with certain instruments and some of the processes pushed the limits of the instruments.

A.1.1 Wafer Selection and Preparation (A1, B1)

The material properties of the starting silicon wafers do not affect the fabrication steps or final device performance, so double-side polished silicon wafers with any crystalline orientation and doping would function as the feedstock material for DSP, as long as the structural integrity of the device is maintained. With the specific workflow developed in the GT facilities, wafer alignment relied on IR microscopy and necessitated

that the wafers have IR transparency and be polished on both sides. Therefore, wafers with a resistivity of at least 0.05 ohm-cm were used, although any double-side polished silicon wafer should be adequate so long as alignment does not rely on IR transparency, for instance if external alignment marks with optical cameras are used. Wafers were acquired from Polishing Corp of America (PCA) that were 100 mm diameter, <100> orientation, double-side polished, 500 μm thick +/- 20 μm, p-type doped (boron), with resistivity between 1-20 ohm-cm.

The first step of process flows A and B (Figure 2.13 and Figure 2.14) is thermal oxidation. Before oxidizing, the wafers underwent a standard CMOS piranha etch in batches of 25 wafers with a common use wet bench. Before beginning the etch, wafers were transferred into a Teflon wafer cassette for material compatibility with Piranha. The bath used for this cleaning step was initially filled with 3 liters of 98% H_2SO_4 (sulfuric acid) and each time the common use bath was used 100 mL of 60% H_2O_2 (hydrogen peroxide) was added, which means that the exact composition of the bath varied, but the resulting cleans were observed to be highly repeatable assuming the wet bench was operated per established protocols. The batch of wafers were placed in the bath before heating the bath to 120 °C, at which point the wafers were left in for a minimum of 10 minutes. After the bath, the wafer cassette was removed and rinsed in the quick-dump rinser contained within the CMOS wet bench. This rinse process sprayed DI H_2O on top of the wafer cassette until the tops of each wafer were submerged, followed by a quick dump of the bath; this fill/drain cycle completed five times. After rinsing, the wafers were placed in the spin rinse drier with the H-bar of the wafer cassette oriented inward and the standard cycle was used to again rinse the wafers before finally drying them by rapidly

spinning the cassette and blowing N_2 across the wafers. At this stage, visual inspection of the wafers was carried out to confirm that no solid or liquid particles were left behind and that the polished surfaces of the wafers were free of imperfections. If any splotches, liquid pools, or solid particles were observed the entire cleaning process was repeated. Any imperfections at this stage affected oxidation of the wafer surface, and therefore the entire DSP fabrication flow was compromised by imperfections at this stage.

Immediately after cleaning and inspection, each wafer was transferred from the Teflon cassette to a quartz cassette using a plastic vacuum "wand" wafer holder to avoid scratching the surface of the wafers. Wafers were oxidized at 1100 ^{o}C for 18 hours and 45 minutes in a Tystar^{TM} Mini furnace in a wet oxidation environment, resulting in an ~3 μm thick layer of SiO_2 that was confirmed with reflectometry. Final thickness of the SiO_2 is not critical from a device performance perspective, but uniformity and the lack of pinhole defects is important to prevent bulk Si etching in later steps. The presence of pinholes resulted in inadvertent through etches during deep-reactive ion etching (DRIE). The presence of pinholes caused final device fracture or leaking while nonuniformity changed etch rates for plasma based reactive ion etch (RIE) steps across the wafer, leading to device-to-device variation due to incomplete etching of key features. Additionally, variations in thickness can affect surface reflectivity and absorptivity that will change photolithographic dosage requirements that must be accounted for. Although SPR 220 was found to perform properly regardless of SiO_2 film quality, the SU-8 3005 layer that served as the adhesion layer for the DSP was observed to be highly sensitive to any changes in substrate properties.

A.1.2 SPR 220 Lithography and AMI Cleaning (A2, A4, B2)

Megaposit^{TM} SPR 220 is a positive photoresist with a thickness range of 1-10 μm with sensitivity to 405 nm wavelength. It was found to have excellent selectivity for both Si and SiO_2 during etch steps and is easily removed with acetone or piranha. In the DSP workflow, care was taken to position any SPR 220 developing steps before aluminum was deposited since the developer used for SPR 220 (MF-319) etches aluminum, which can affect the aluminum film quality before anodization and induce delamination of Al_2O_3 after anodization.

Before spin coating SPR 220 the substrate was cleaned with a standard acetone, methanol, isopropyl alcohol (IPA) rinse. Both sides of the wafer were rinsed for 5 seconds with each solvent (first acetone, then methanol, then IPA) followed by N_2 drying of the surface *not to be patterned* by holding the wafer at an angle above a low particle count towel/wipe until visually dry before placing the wafer patterned side up on a low-particle count wipe, blowing N_2 directly into the wafer, and moving in circular patterns from the inside to the outside to ensure that the side to patterned is completely dry without any splotches or solid particles. *The consecutive rinsing of a sample with acetone, then methanol, then IPA for 5-30 seconds with each solvent is called AMI (acetone, methanol, IPA), which will be used throughout the rest of this thesis for brevity. The order in which the solvents are used and the use of pure solvents for each step is unique to this process. For instance, using equal parts of each solvent mixed together will not have the same effect.*

After AMI, additional cleaning of the side to be patterned is recommended for best results, especially for step A4 in Figure 2.13. Due to the ease of processing multiple wafers at once, a standard 30 second O_2 plasma etch in the Vision RIE with the side to be processed placed up was used most often (parameters shown in Table A.1). Alternatively, a piranha

etch was found to be as effective. The CMOS wet bench piranha etch can process multiple wafers at once but requires 1-2 hours for the entire process. An alternative is to make a small volume bath in a glass dish (ensure the dish is not contaminated or shared use). The IEN facilities at GT set a limit that the ratio is to be 3:1 H_2SO_4:H_2O_2 (96% H_2SO_4 and 60% H_2O_2). **The sulfuric acid should be added to the dish prior to adding hydrogen peroxide, and all proper PPE should always be worn. Consult staff members and do not carry this step out until given clearance by qualified personnel.** After mixing the two chemicals a small amount of vapor will be released that will subside within ~30 seconds at which point the wafer can be placed in the bath for 10 minutes with the patterned side up. After the bath is complete, rinse the wafer in H_2O and follow the drying procedure above. Allow the piranha bath to come to room temperature before disposal and follow all necessary safety precautions during use. Note, piranha aggressively etches a wide range of materials and is not compatible with metals or photoresists, so this cleaning procedure is not recommended as a general clean procedure but can be used to intentionally remove deposited titanium, aluminum, Al_2O_3, and in some cases SU-8 (underdeveloped or underexposed SU-8).

After cleaning the wafer, 2 mL of SPR 220 was pipetted onto the pattern side and spincoated with a two-step process (Table A.6). The first step was 500 RPM for 5 seconds with a 1 second ramp up and the second step was 2500 RMP for 40 seconds with a 2 second ramp up, which produced films with ~7 μm thickness. For SPR 220 only a "soft" bake at 110 °C on a hotplate for 3 minutes before exposure is required, *post exposure bakes (PEB) caused the lithography to fail even though the datasheet recommends them.* Any bubbles or imperfections resulted in pinhole defects during etching, so if the areas affected could

be covered with Kapton tape before etching then the process could proceed. If the imperfections are abundant or overlapping critical features, the SPR 220 was removed by soaking in acetone for ~5 minutes prior to an AMI clean and repeated SPR 220 spincoating.

Both manual lithography (Karl Suss Mask Aligner) and laser mask-writing (Heidelberg MLA150) exposure were explored for the SPR 220 lithography step that worked equally well. Using the manual Karl Suss mask aligner system, the film was exposed to 500 mJ/cm^2 at 405 nm. For process A2, the alignment marks were oriented with the horizontal pattern on the left side of the wafer and the vertical pattern on the right side. For process B2, the alignment marks were flipped. This ensured that when the wafers were positioned for bonding in later processes that all critical features aligned. The hard mask designs for DSP were symmetric except for the alignment marks. During mask production the entire patterns were shifted due to the asymmetric alignment mark design so care was taken to reverse the orientation of one of the exposures. For these reasons, the Heidelberg was the preferred method of exposure.

The Heidelberg MLA150 is a maskless aligner that uses a 375 or 405 nm wavelength laser to write a digital mask directly onto a substrate. The advantage of this instrument is that no hard masks are required and, more importantly, the digital mask design comes with alignment marks that allow auto-alignment with ultra-high precision with the automated software, alleviating a source of human error during manual alignment. The symmetric mask design was centered on each wafer using the Heidelberg approach, which drastically improved the final device alignment and enabled easy wafer alignment in step C1. For the SPR 220, the pattern was written on the “fast setting” for 650 mJ/cm^2. *Note that for both the Karl Suss system and the Heidelberg system, overexposure is*

acceptable for SPR 220. Aiming for higher dosages will result in slightly larger features, but also ensures that the films will develop without residue left behind.

After exposure, the wafers were held for 5-10 minutes at ambient conditions and then were developed in MF-319 at room temperature for 2-3 minutes, rinsed in H_2O, and dried off with N_2. Consistently agitating the bath by hand for the entire development process helped to keep the bath homogenized and developer rates constant. Visual inspection of critical features was carried out on an optical microscope, any residual SPR 220 was removed by developing for another 15 seconds. A final oxygen descum (Table A.1) was carried out for 30 seconds to remove any remaining SPR 220. Before etching masks in steps A3 and A4, the wafers were baked in an oven at 100 °C for 15 minutes. Before step A4, the sample was baked at 100 °C in an oven for 12-24 hours. Before moving onto etch steps, especially when using manual alignment via Karl Suss, final wafer alignment was checked on the IR microscope to make sure that the features on each device would align. More than a 2 mm offset at the wafer level resulted in fracture during bonding, so if the overall alignment was wrong the entire SPR 220 was stripped and adjustments to the initial mask offset were made. For instance, while using the hard masks designed and fabricated at the GT-IEN facilities, a 1.5 mm offset on the mask for step A2 was found to be necessary. It is important to note that when using the Heidelberg with symmetric mask design there was no need to offset designs.

A.1.3 SiO_2 Mask Etching (A3, B3)

Reactive ion etching (RIE) and inductively coupled plasma (ICP) etching are both effective options for etching SiO_2. Both approaches use a fluorocarbon gas plasma for etching SiO_2 although the etch rates and feature side wall profiles differ. RIE uses CHF_3

as a plasma precursor, and it is a near isotropic etch which makes it ideal for etching thin layers of SiO_2. During longer etches, RIE will etch horizontally under the photoresist mask to increase the patterned feature size, causing the features that are ultimately etched with deep reactive ion etching (DRIE) to have slightly different dimensions than what was patterned in the photoresist. During the anisotropic ICP process, which uses C_4F_8 as the source for plasma, the ions are accelerated towards the surface with a strong electric field and therefore features etched into the SiO_2 mask have more vertical walls with precise dimension control. Additionally, ICP is a much faster process *for a single wafer*, etching thermal oxide at 67 nm/min vs 200 nm/min for RIE based on the specific approaches used in the DSP fabrication workflow.

Before any etch of the SiO_2 masking layer (Figure 2.13 step A3 and Figure 2.14 step B3), all noticeable bubbles or defects in the bulk photoresist film were covered with Kapton tape. Without covering these defects, the mask would be etched, which caused the DRIE step to etch these areas. As a result, trough-hole defects in the final device caused device fracture or fluidic leaking. Care was taken to avoid any coverage of patterned features with Kapton tape by visually inspecting the features on an optical microscope before etching.

The specific instrument available (Plasma Therm^{TM} ICP) for ICP etching at Georgia Tech required that ~5 mm of photoresist be removed from the edge of the wafer with an acetone-soaked swap. This prevented the wafer from sticking to the wafer clamp, which would cause the sample to break. A significant draw back of the ICP approach was that part of the SiO_2 layer was inadvertently removed around the wafer edge where photoresist was removed, which had to be covered with Kapton tape before later DRIE steps. The ICP

approach is significantly faster for a single sample, so for some prototypes it was used for rapid iterations of device design. For reference, the etch parameters for the ICP are shown in Table A.2.

Up to four wafers could be etched simultaneously for increased output using the RIE approach, and the risk of breaking the wafer was nonexistent. These advantages alone made the Vision RIE the preferred method of etching SiO_2. When multiple samples are placed inside the RIE, the etch rate becomes less uniform and slower for the features. For this reason, the etch was designed to "over-etch" such that all features were etched through. The etch parameters for the Vision RIE were the same for both single and multiple samples, which is shown in Table A.3. *To ensure that the SiO_2 layer is etched through (with either etch method used), the SiO_2 features were checked on a NanoSpec™ Reflectometer with the "SiO_2 on Silicon" program. Fit parameters should be less than ~0.5 and the thickness should measure <10 Å.*

A.1.4 Bulk Silicon DRIE (A4, A5, C2)

Deep Reactive Ion Etching (DRIE) is an anisotropic, inductively coupled plasma (ICP) based approach used for generating high aspect ratio features with utility for a range of materials, including silicon. The process alternates the deposition of a uniform passivation layer for masking generated from a C_4F_8 plasma and an anisotropic ICP etch step with an SF_6 based plasma. During etching, the ICP system accelerates ions to the bottom of features for higher etch rates vertically than horizontally, resulting in near vertical walls and high aspect ratio. For the DSP process, DRIE is used for processing the counterbore capillary interface (Figure 2.13 steps A4, A5) and the conditioner channel (Figure 2.15 step C2). The specific instrument used for all DSP processing was the

STS™ ICP with the parameters shown in Table A.5. For this process, it was found that the position of the butterfly valve (Automatic Pressure Control, displayed as APC % setting in the control software) for maintaining chamber pressure was critical. The valve position was found to be best for stable plasma between 65-69%. To verify if the position is correct, the plasma was observed through the viewing windows to check that the plasma did not flicker except for between the etch and passivation step. If the plasma was flickering, the most likely cause was found to be the APR position. Adjusting the valve position in 1% increments either up or down until the plasma was steady was found to be the most effective method for stabilizing the process.

For all DRIE steps a "carrier wafer" was used for processing. The process wafer was mounted on a 500 μm thick Si carrier wafer with at least 1 μm of SiO_2 on top. This carrier wafer ensured that if the DRIE process etched completely through the process wafer, the STS ICP chuck would not experience any damage. Traditionally, a type of Silicone based "cool-grease" is used to mount process wafers to carrier wafers, but this grease caused clogs in the final DSP device. Therefore, three pieces of Kapton tape were placed at equal angles around the edge of the wafer stack and wrapped from the top of the process wafer to the bottom of the carrier wafer. Using a razor blade, the pieces were trimmed to ~2 mm in length on the carrier wafer bottom side so that the tape covering the carrier wafer did not touch the chuck seal. On the top of the process wafer, small pieces of Kapton tape were used to cover the alignment marks so they did not get etched through during the processing. After covering all defects and alignment marks, and mounting the wafer, inspection of all features was carried out to make sure that no features were inadvertently covered/exposed.

The counterbore geometry used for capillary integration (inset, Figure 2.13) was achieved using a novel two-step masking process without backside alignment. Prior reports of this geometry required backside alignment and patterning, which was found to not be compatible with the DSP microfabrication workflow since patterning on the backside of the capillary interface wafer caused the wafers to delaminate after bonding in later steps.

Prior to the first DRIE counterbore step in A4, the SPR layer patterned directly on top of the patterned SiO_2 layer was baked in an oven set to 100 °C for at least 12 hours, with best results after a 24 hour bake. Note, baking can occur before or after mounting the wafer but the Kapton tape adhesive was more likely to leave a residue which was cleaned afterward when the entire mounted wafer was baked. Without baking, the photoresist can cause micromasking effects, which occurs when the SPR 220 is ablated from the surface and subsequently redeposited inside features. Increasing the O_2 flow rate can help with these micromasking effects, but it also increases the bulk etch rate, reduces selectivity, and results in more isotropic etching. The wafer was then processed for a partial through etch by processing for 650 cycles with the parameters outlined in Table A.5.

After etching, Kapton tape was removed and the wafer was soaked in acetone for 10-20 minutes to remove bulk SPR 220. After, the wafer was place in a 3:1 piranha bath at room temperature for 60 minutes to remove all residual SPR 220 and passivation layers. The wafer was rinsed in H_2O, then dried off and mounted on a carrier wafer as described above. The alignment marks were again covered with Kapton tape before the next counterbore DRIE step. For the final through etch, care was taken not to over-etch so the sample was etched for 325 cycles using the parameters in Table A.5 to start. After completing the etch, the wafer was removed from the carrier wafer and a white LED was

placed behind the wafer to confirm whether the etch had gone through. If light was visible through all features, a backlit microscope was used to inspect the feature quality. If some features required additional etching while others were through, pieces of Kapton tape were placed over the finished features to prevent over etching effects and the wafer was etched for another 15 cycles until breakthrough was observed.

After all features were completed, the device was sonicated for 15 minutes in separate baths of acetone, methanol, and then IPA. A small droplet of H_2O was placed on a flat surface and the wafer was then pressed down on top of the droplet by hand to confirm that through flow was observed. At this stage, the wafer was cleaned in a piranha bath at 120 °C for 30 minutes and rinsed in H_2O to remove all residue from inside the counterbore interfaces.

A.1.5 Membrane Metallization and Anodization (B4)

After finishing the patterning of SiO_2 on the process B wafer (Figure 2.14, step B3) an AMI clean process was carried out on both sides of the wafer followed by either a piranha clean or a batch O_2 descum in the Vision RIE (Table A.1) with the unpatterned side placed up. Any defects or imperfections at this stage directly impacted the final device performance, so care was taken to ensure the side for metallization was free of defects.

The metallization process developed by Tibavinsky et. al utilized a custom sample holder that increased the deposition rate and final thickness of evaporated materials in the CHA™ E-Beam Evaporator tool.[34, 43] The modified sample holder was attached to the standard 3 wafer holder by attaching clamps to the standard holder and suspending the custom holder by chain as shown in Figure A.1.[43] The wafers were lowered from their standard height to a distance approximately 200 mm lower, which corresponded to 5 links

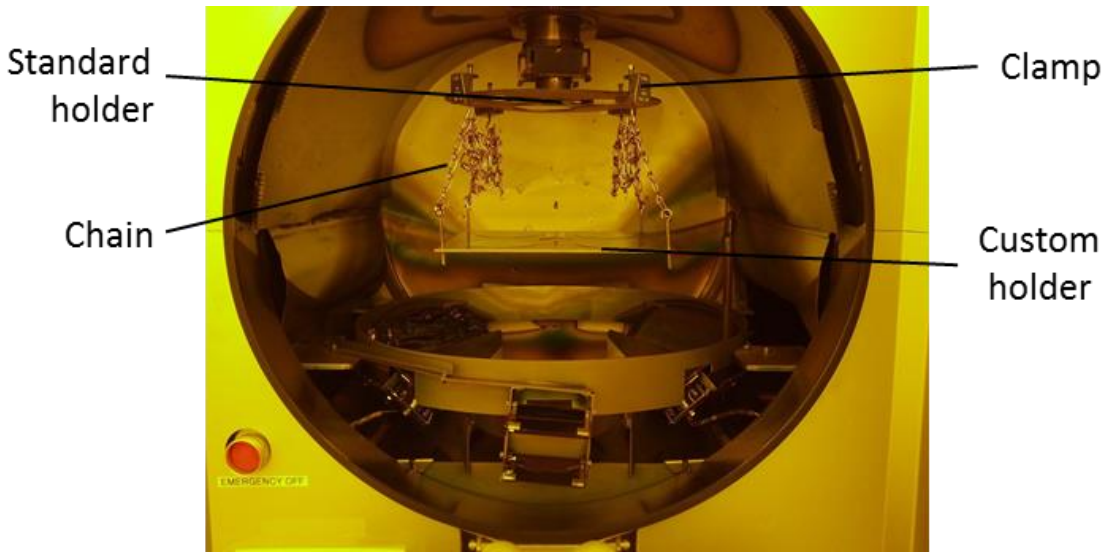

Figure A.1: Custom mounting setup for increased deposition rate and final metal thickness in the CHA E-Beam. Adapted, with permission, from Tibavinsky, I.A., *A microfabricated rapid desalting device for integration with electrospraying tip*. 2014, Georgia Institute of Technology.

in the chain. A hole in the center of the custom sample holder allowed for the evaporated material to pass through for deposition rate monitoring via quartz crystalline microbalance. Although the monitored deposition rates and final thickness did not represent the actual deposition rates, by monitoring the measured values each deposited film was similar.

The metallization was done in three steps. First, an adhesion layer of Ti was deposited by programming 250 Å at 1 Å/s followed by two steps of bulk Al deposited for 12,500 Å at 5 Å/s. Between each step the instrument was given time to cool down so the crucibles did not break by holding for 15 minutes. The final thickness of the stack was not completely uniform, so when mounting the wafers the flats were placed facing the inner cut out so the thickness varied from the bottom to the top of the wafer. The final thickness was approximately 4 μm at the top of the wafer and 7 μm at the bottom. Note that at this

stage piranha cleans were not compatible with the sample as they etched the Ti and Al layers. If the aluminum films appeared highly dull/non-reflective or had bulk defects, a piranha etch was used to remove the Ti and Al layers. This piranha etch was carried out in a separate bath due to the incompatibility with the CMOS wet-bench processes, and all waste from the bath was placed in a secondary container after cooling to room temperature.

After deposition, the samples were anodized to produce a uniform, nanoporous alumina (Al_2O_3) membrane. Depending on the type of electrolyte used and the voltage applied, pore size can be controlled from 5 to 500+ nm in diameter.[44, 82, 84-86] For the prototype DSP, oxalic acid was used as the electrolyte to produce 50 nm pores. A continuously stirred 4 liter bath of 0.1 M oxalic acid maintained at 0 °C in a chilled jacketed beaker was used for the anodization process. The cathode was the wafer itself, held by the positive lead alligator clip of the power supply, and the anode was a 30 cm graphite rod with carbon tape used to attach the ground lead of the power supply. Once the bath was at temperature, the wafer was placed in 1.5% chromic acid and 5% phosphoric acid at 65°C for 30 minutes to remove the native oxide layer. The wafer was rinsed in DI H_2O and secured to the alligator clip and lowered into the oxalic acid bath such that all the conditioner channels patterned on the far side were submerged. A 40 V potential was applied between the wafer and graphite rod, which was observed to produce a current of 80 mA. The sample was anodized for 45 minutes before the power was shut off and the sample was rinsed with H_2O before being placed in the 1.5% chromic acid and 5% phosphoric acid bath at 65 °C for 30 minutes to etch the thin layer of Al_2O_3. This step exposes the preferred nucleation steps for the through pore anodization process. The wafer

was removed from this bath, rinsed again in H_2O, and placed back into the oxalic acid bath with the same 40V potential for approximately 8 hours.

To confirm the end-point anodization, the current was monitored. Generally, the measured current decreased throughout the anodization process from 80 mA to 5 mA. The current value gradually reduced until it reached a steady state level, at which point it was left to anodize for at least another hour to confirm the current does not change. If the wafer was removed before the anodization was completed, DSP mass exchanger device is not functional because if the pores do not penetrate the entire film thickness, the sample channel and conditioner channel are fluidically decoupled. If the device is "over-anodized" it can lead to delamination and bulk Al_2O_3 etching but was only observed after 15+ hour long anodization steps. After anodization was completed, the wafer was rinsed in H_2O and then AMI. The integrity of the pore structure was confirmed using an SEM, as shown in the inset of Figure 2.14.

A.1.6 SU-8 Lithography (B5)

SU-8 is a biocompatible, negative type photoresist which is used to define the side walls of the DSP sample channel and to serve as the adhesive for sealing the final device.[87-92] This processing step is critical in the DSP fabrication process and required extensive optimization. Importantly, steps B5 and C1 (SU-8 lithography and bonding respectively) should be carried out within ~30 minutes of each other for optimal bonding performance.

The anodized wafer was cleaned with AMI and then descammed for 30 seconds using the parameters outlined in Table A.1. Before beginning spincoating, the ambient temperature and humidity were recorded. Note that if the humidity is below 25% or above 40% during SU-8 processing, the bonding process will fail (*humidity values may measure*

low near hot plates). The wafer was placed anodized side up in a spincoating instrument and ~3 mL of SU-8 3005 was poured directly on the wafer from the bottle. A 3 step spin process was carried out with the parameters in Table A.8. The first step was 500 RMP, 1 second ramp, 5 second hold, the second was 3000 RPM, 2 second ramp, 40 second hold, and finally 4500 RPM, 0.5 second ramp, 3 second hold. The final high spin rate step was used to reduce edge bead, which will affect final bonding performance. Immediately after spincoating, the wafer was soft baked at 95 °C on a hotplate for 2 minutes and 30 seconds before backside alignment and exposure (no hold times or delays can occur from spin coating to exposure).

Two alignment/exposure procedures, the manual EVG 620 backside aligner and the Heidelberg MLA150 maskless aligner, were explored for DSP fabrication that both worked effectively, although the Heidelberg MLA150 approach was far more repeatable. Using the EVG, the SU-8 layer was exposed to 195 mJ/cm^2 dosage at 365 nm. The measured light intensity used to calculate exposure time was not adjusted, i.e., without the mask absorptivity taken into account. *For hard mask exposure, a soda-lime masking material is recommended because it filters out high wavelength UV light that causes lateral cross-linking under darkfield patterns in the mask.* After exposure, the sample was immediately post exposure baked at 95 °C for 2 minutes and 30 seconds before holding for 10 minutes.

For Heidelberg MLA150 exposure, the same spincoating and soft bake procedure was carried out before loading the sample for backside alignment. The optimal exposure dosage was 760 mJ/cm^2 on the Heidelberg in "high quality" mode. This dosage differs drastically from the mask aligner dosage because the wavelength is 375 nm for the maskless aligner vs 365 nm for the EVG. After exposure, the sample was soft baked on a

hotplate at 95 °C for 2 minutes and 30 seconds. The sample was not held between exposure and development for the Heidelberg approach.

Development was the same for both exposure processes. Prior to development the wafer was rinsed with DI H_2O for 20 seconds to aid in the reabsorption of water into the film. The sample was then developed with agitation in SU-8 developer (MicroChem^{TM}) for 90 seconds, followed immediately but rinsing with IPA for 30 seconds. After IPA rinse the sample was again developed for 30 seconds in SU-8 developer before another 30 second IPA rinse, followed by a 15 second rinse in DI H_2O and, finally, a 15 second rinse in IPA. Note that SU-8 is not compatible with acetone, so AMI rinses are not recommended. Additionally, for the rest of the processes the wafer carrier was covered in aluminum foil when not in yellow-light environments to avoid exposure to any broad spectrum light, which can overexpose the SU-8 layer and cause bonding to fail.

A.1.7 Wafer Alignment & Bonding (C1)

Since it relies so heavily on the SU-8 processing. aligning and bonding the wafers in DSP fabrication were also the processing steps that required extensive optimization. It was found that if the SU-8 was deposited on the capillary inlet wafer (separate prototype workflow, not presented here) bonding failed. It is hypothesized this is because the rough Al_2O_3 surface did not bond effectively to the smooth SU-8 surface. When the SU-8 was spun on the Al_2O_3 surface, the SU-8 penetrated into the porous surface and the smooth top surface of the spincoated SU-8 bonded well to the polished surface of the capillary interface wafer.

Alignment of the wafers was carried out using an infrared (IR) microscope. As discussed, IR transmissibility was a critical material property for the stock Si wafers used

for DSP fabrication for this reason. Before alignment, both wafers were cleaned in the appropriate manner; for the process A wafer, full AMI and piranha cleaning or O_2 descum was used and for the process B wafer a simple IPA rinse was used since SU-8 is sensitive to most cleaning processes. The process B wafer was prepared for bonding by placing three ~8 mm pieces of Kapton tape on the conditioner channel side and then inverting the sample such that the adhesive side of the tape and the nanoporous membrane were facing up. In this orientation, the wafer was placed onto the IR microscope plate and the process A wafer was placed on top for alignment. With the backlight on the lowest setting, the IR sensitive microscope allowed for easy viewing of the patterned SU-8 features and all alignment marks through the Si layers. The wafers were first aligned using large alignment marks, at which point a single piece of the tape was folded over to secure the stack. The alignment could then be adjusted using a disparate feature, such as an alignment mark or an inlet hole. Once alignment was confirmed the final two pieces of tape were folded to secure the wafer. The entire stack was carefully lifted and 5 additional pieces of tape were added around the circumference of the wafer such that all 8 had approximately equal spacing. The alignment was double checked on the IR microscope before bonding.

Bonding was carried out using the Obducat Nanoimprinter. The entire wafer stack was placed in the 4" wafer chuck with the inlet/outlet holes up and a sheet of polycarbonate was placed on top of the chuck before the o-ring holder was placed to secure the stack. The bonding program consisted of two steps. In the first step, pressure was set to 10 bar and temperature to 25 °C for 60 seconds and in the second step pressure was maintained at 10 bar and temperature was increased to 130 °C for 30 minutes. The measured pressure increased to ~12.5 bar during this process due to thermal expansion effects. After bonding,

the polycarbonate sheet should be completely transparent and free of polymer residue. The presence of an opaque film indicates that the SU-8 was not cross-linked completely, and the final device would either delaminate or clog due to SU-8 reflow. *Under-exposed SU-8 will reflow and clog the final DSP devices, while over-exposed SU-8 will not bond. After bonding, the wafer stack was checked on the IR microscope to ensure none of the internal channels had clogged or changed in dimension.*

A.1.8 Membrane Release (C2)

Membrane release is comprised of three main steps. First, the bulk Si is removed with a DRIE process, then the SiO_2 and Ti layers are removed with a C_4F_8 RIE, and finally the barrier layer of Al and pores are opened with a CF_4 RIE step. The DRIE process is carried out after bonding is completed. The wafer stack was mounted to a carrier wafer with tape to protect the capillary interface surface. Once again the alignment marks were covered with Kapton tape, and the DRIE process was run for 475 cycles with the parameters in Table A.5. If bulk silicon was left on the bottom of the conditioner channel, an additional 50 cycles were added until all the conditioner channels appeared to have a reflective finish due to the SiO_2, Ti, Al_2O_3 layers underneath. Bubbles in the SiO_2 surface indicate poor bonding, which can be attributed to localized defects or over-exposed SU-8.

After the DRIE step was completed, the bonded wafer was removed from the carrier wafer and transferred to the Vision RIE for a 3 hour etch according to the parameters in Table A.3. After the etch, the sample channels were visible through the remaining layers of Al and Al_2O_3 and the bulk of the membrane appeared dull; the presence of a reflective layer or the inability to make out the sample channel indicated an incomplete SiO_2 etch.

The final etch step was used to remove the barrier layer from the anodization process. Multiple options were explored, including the wet etch utilized by Tibavinsky, but the most effective and repeatable method was a CF_4 RIE etch. This step was found to be the least repeatable of the entire fabrication process, which is likely due to a non-uniform Al_2O_3 layer. For this reason, the devices were diced prior to the final CF_4 etch release of the membrane. Over etching the membrane in this step resulted in bulk leaks and device failure, while under-etching prevented efficient transfer between the sample and conditioner channels. The etch was carried out on the Unaxis™ RIE with the parameters in Table A.4. For most devices, the optimal etch time was found to be 13 minutes and 45 seconds, but bulk defects were observed with as little as 10 minutes and some devices were found to require 20 minutes of etching before performing well.

A.1.9 Dicing

Dicing was carried out on an ADT™ 7100 dicing saw. The wafer was mounted on the tape with the conditioner channel facing up. To protect the membrane, Kapton tape was placed over each conditioner channel to prevent the high flow-rate H_2O, used for keeping the blade cooled, from depositing debris or fracturing the membrane. Dicing was found to be successful independent of blade type, although a nickel type blade with a 100 μm thickness was used predominantly. After dicing, each device was removed and the tape was carefully removed.

A.1.10 Inlet & Outlet Capillary Integration (C3)

A Dymax™ PC-3D light welder with the included photo-sensitive epoxy were used to glue the inlet/outlet capillaries into the counterbores of the bonded mass exchanger

device. A 360 μm OD capillary was placed tangent to the SiO_2 surface and slid gently into the counterbore opening. Once the capillary was self-supporting, epoxy was dispensed around the entire capillary interface and immediately exposed to the UV source for 20 seconds for complete cross-linking. For the inlet, a 360 μm OD 50 μm ID PEEK tube from Upchurch Scientific™ was used, while the outlet was an ESI capillary, generally a 30 μm tapered fused silica emitter from NewObjective™.

A.2 RIE, ICP, and DRIE Parameters

The Vision RIE (renamed the CTRL Layer RIE) was used for descum (Table A.1) and SiO_2 etching (Table A.3).

Table A.1. Vision RIE O_2 descum/clean parameters

Pressure	60 mTorr
Power	150 W
Temperature	25 ° C
O_2	50 sccm
Time	15-60s

The Plasma Therm™ ICP was an alternative to the Vision RIE. The standard SiO_2 etch parameters are shown in Table A.2

Table A.2. Plasma Therm ICP Etch Parameters

Pressure	5 mTorr
Ar flow rate	5 sccm
C_4F_8 flow rate	15 sccm

CO_2 flow rate	28 sccm
ICP power	800 W
Chuck power	40 W
Time	45 min

The Vision RIE was the preferred method for etching masking layers of SiO_2 and the layer of SiO_2 on the backside of the membrane, the etch parameters are shown in Table A.3.

Table A.3. Vision RIE Parameters

Pressure	40 mTorr
CHF_3 flow rate	45 sccm
O_2 flow rate	5 sccm
Power	250 W
Time	0-3 hours

The Unaxis^{TM} RIE was used for CF_4 etching of the membrane for pore opening. The parameters are shown in Table A.4.

Table A.4. Unaxis RIE Etch Parameters

Pressure	100 mTorr
Power	250 W
CF_4	18 sccm
O_2	8 sccm
Time	10-20 min

The STS ICP was used for etching bulk features in Si. The parameters are shown in Table A.5

Table A.5. STS ICP Bosch (DRIE) Parameters

	Passivation	Etch
SF_6 flow rate	0	130 sccm
C_4F_8 flow rate	85 sccm	0
O_2	0 sccm	13 sccm
Coil Power	800 W	800 W
Platen Power	0 W	10 W
Pressure	0.1 mTorr	0.1 mTorr
Time	9 s	11 s

A.3 SPR 220 Spincoat and Exposure Parameters

SPR 220 is a positive type photoresist used for masking purposes in process A (**Error! R eference source not found.**) and process B (**Error! Reference source not found.**).

Table A.6: SPR 220 Spincoat Parameters

Step	RPM	Ramp (s)	Hold (s)
1	500	1	5
2	2500	1	40

Soft Bake	3 min @ 110 °C

Table A.7: SPR 220 Exposure and Post Exposure Bake (PEB) Parameters

Instrument	Dosage	PEB
Karl Suss	500 mJ/cm^2 @ 405 nm	Not required; hold 5-10 min before development
Heidelberg MLA150	650 mJ/cm^2 @ 405 nm, fast setting OK	

A.4 SU-8 3005 Spincoat and Exposure Parameters

SU-8 3005 is a negative type photoresist with excellent biocompatibility used to define the sidewalls of the DSP sample channel and to serve as an adhesive layer for bonding.

Table A.8: SU-8 3005 Spincoat parameters

Step	RPM	Ramp (s)	Time (s)
1	500	1	5
2	3000	2	40
3	4500	0.5	3
Soft Bake		2 min 30 s @ 95 °C	

Table A.9: SU-8 3005 Exposure and Post Exposure Bake (PEB) Parameters

Instrument	Dosage	PEB
EVG 620	195 mJ/cm^2 @ 365 nm	Bake @ 95 °C 2 min 30s ; hold 15 min before development
Heidelberg MLA150	760 mJ/cm^2 @ 405 nm, high quality only	

FLUIDIC INTERFACE PACKAGE PRODUCTION

The fluidic interface package design had two iterations: one for counterflow used in early experiments and one for crossflow used in later experiments. Although the notes in the drawings indicate polycarbonate stock material for the machined top, PEEK was also used. PEEK is not transparent and therefore care should be taken to monitor bubble formation in the conditioner channel. The bottom portion of the DSP fluidic package was machined out of PEEK. The gasket was laser machined by generating a .DXF trace of the groove in the package drawings. Different offsets from the inner to outer traces were used depending on the laser power (multiple lasers used). The final width of the gasket should be less than 0.5 mm to fit into the machined recess.

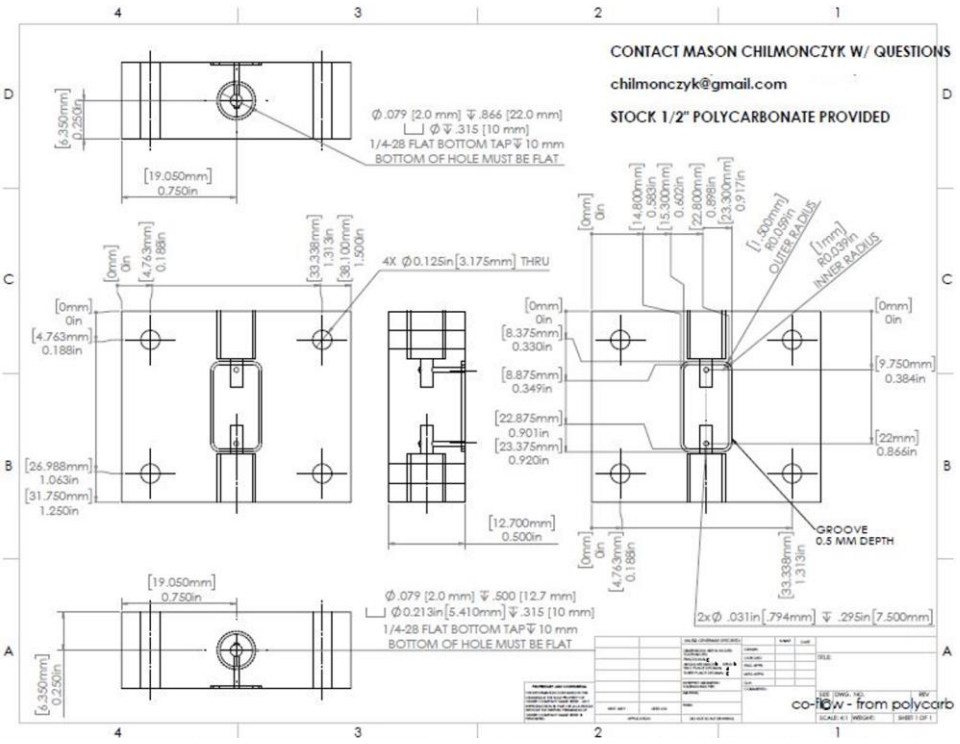

Figure 0.1: Production drawing for counterflow fluidic interface top.

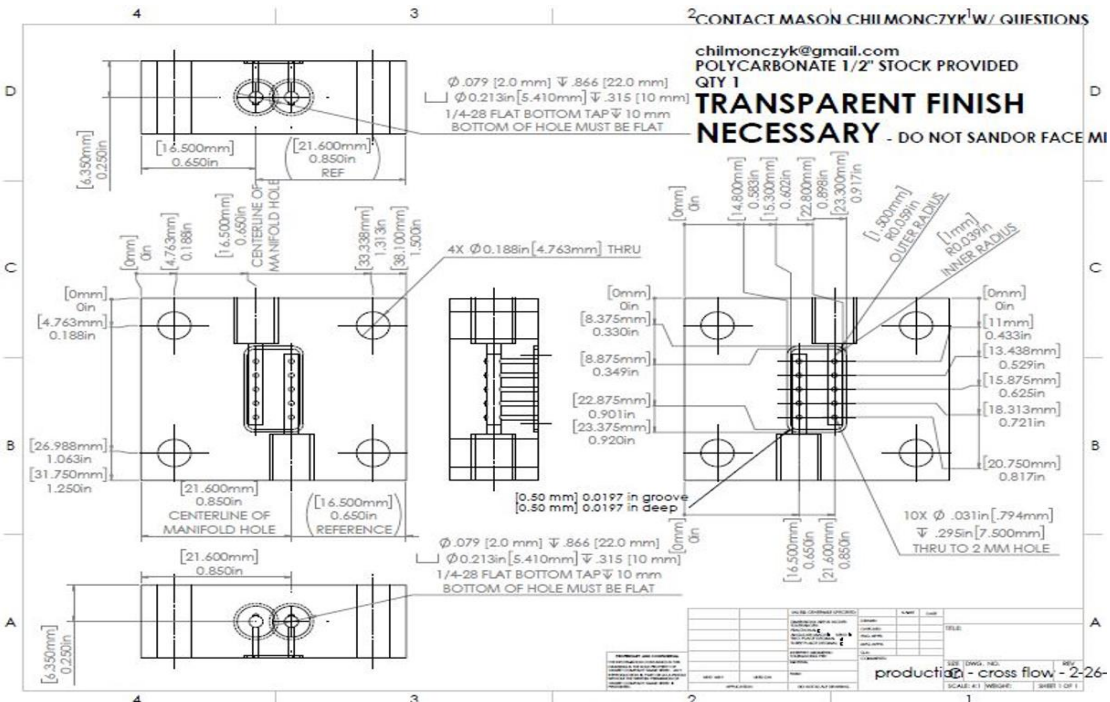

Figure 0.2: Production drawing for crossflow fluidic interface top.

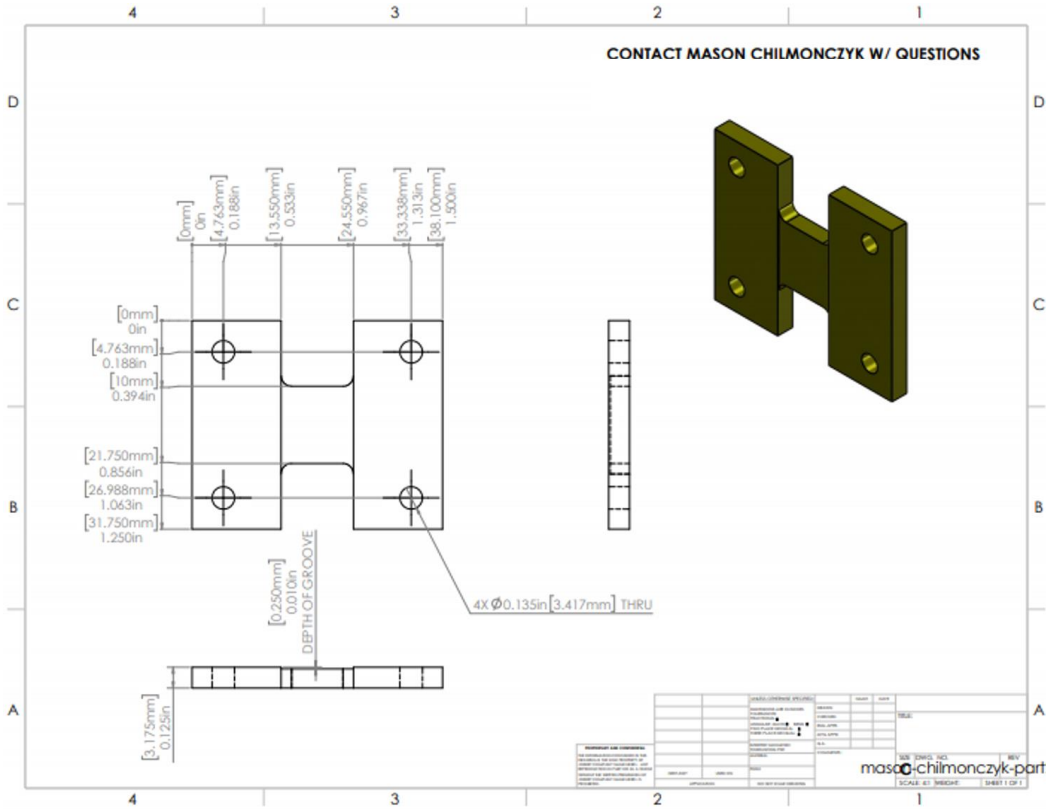

Figure 0.3: Production drawing for bottom of fluidic package.

ION TRANSFER INTERFACE DRAWINGS

The production drawings for the ion transfer interface used for the Q-Exactive Plus are shown in this appendix. The polycarbonate pieces the gasket, and the spacer are assembled to form the box assembly. The bushing bar assembly was attached to the MS box with hand tightened fasteners before fixed on the front of the MS to ensure proper fit. The MS side supports have build in compliance in the form of slotted holes for all fittings. The left side support shaft has a small recess to allow for the ball detent safety override.

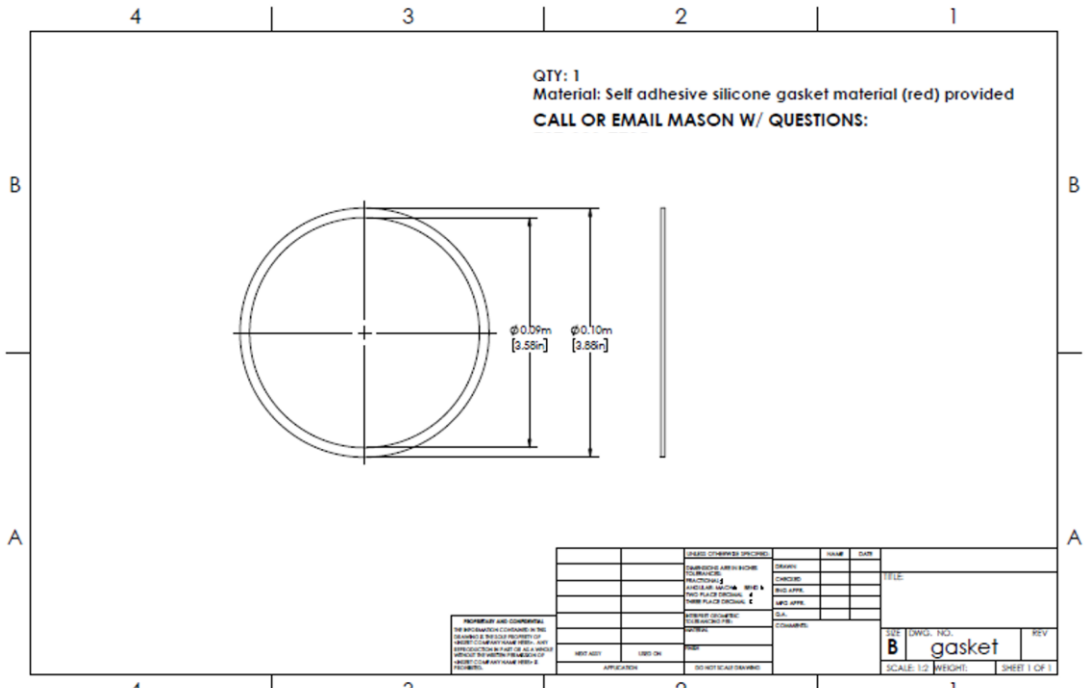

Figure 0.1: Gasket used to seal ion transfer box to the front of the MS system.

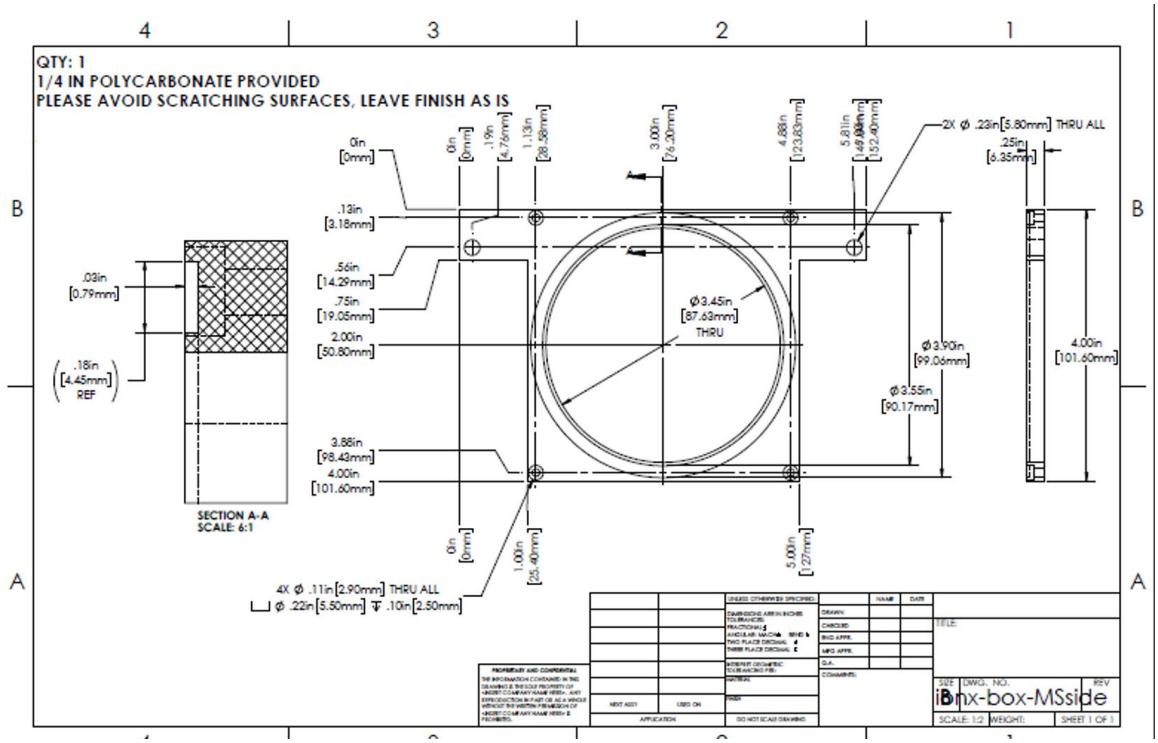

Figure 0.2: MS side of the ion transfer box; gasket designed to fit into recess.

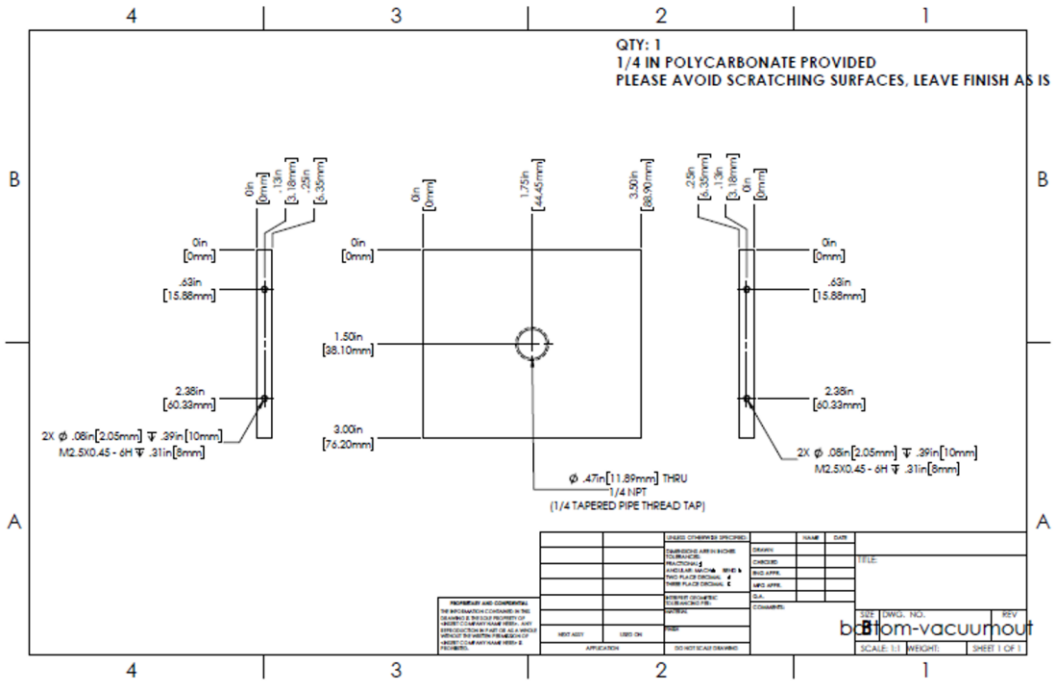

Figure 0.3: Bottom of ion transfer box, for interfacing with vacuum system.

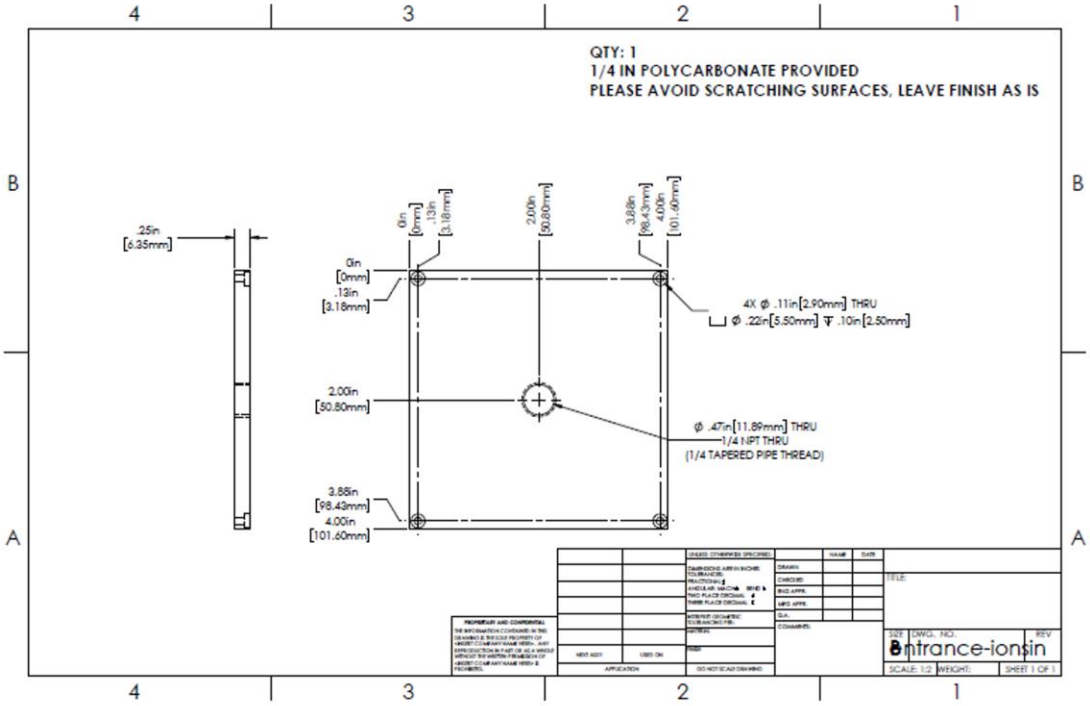

Figure 0.4: Front of ion transfer box, where ions enter system.

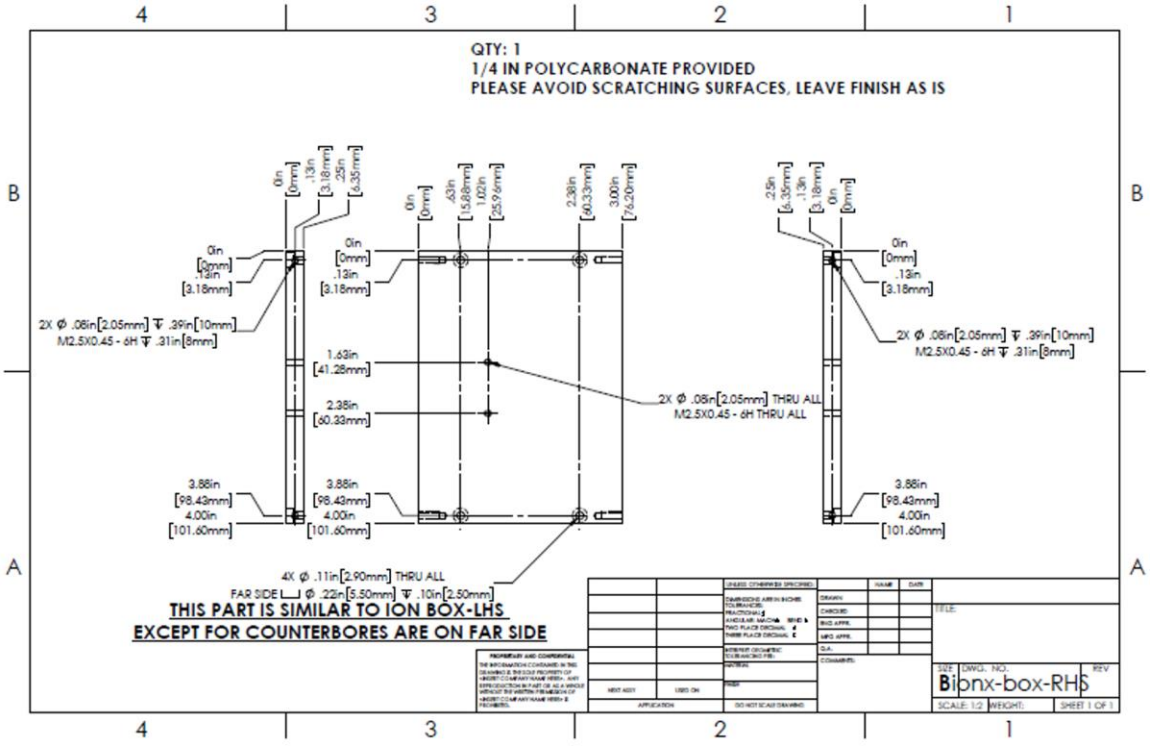

Figure 0.5: Right hand side of the ion transfer box.

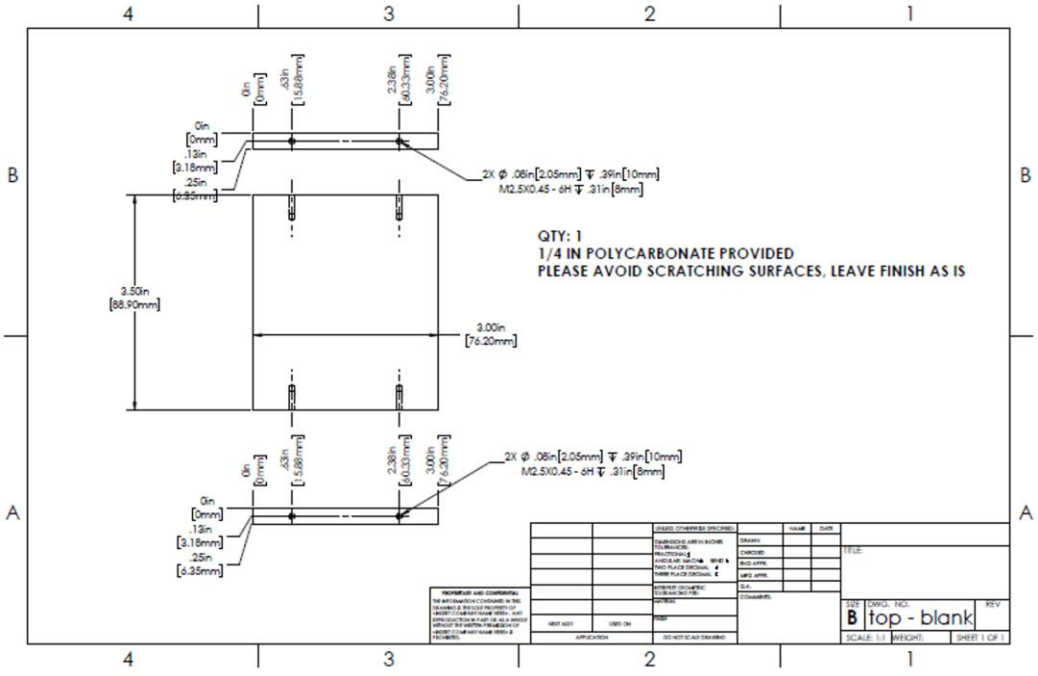

Figure 0.6: Top of the ion transfer box.

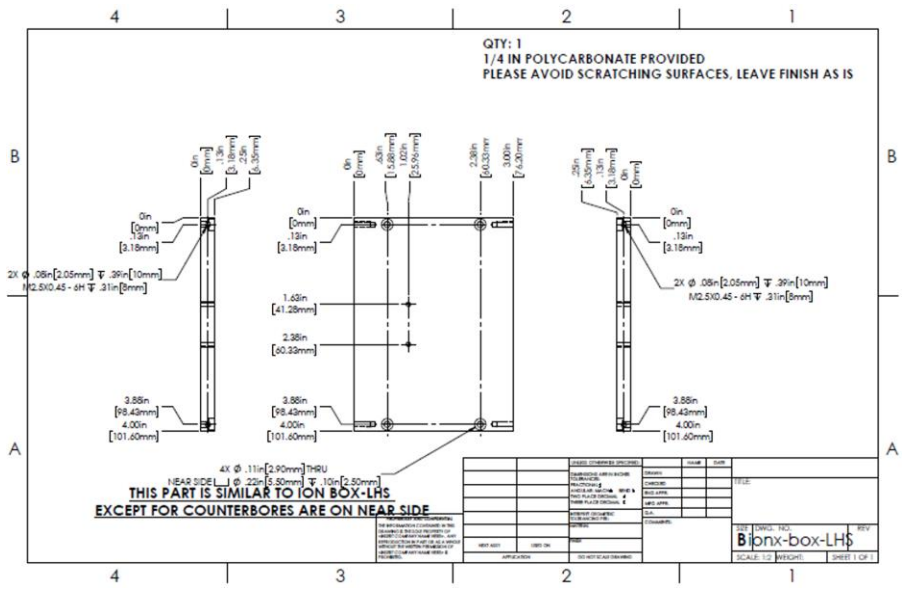

Figure 0.7: Left hand side of the ion transfer box.

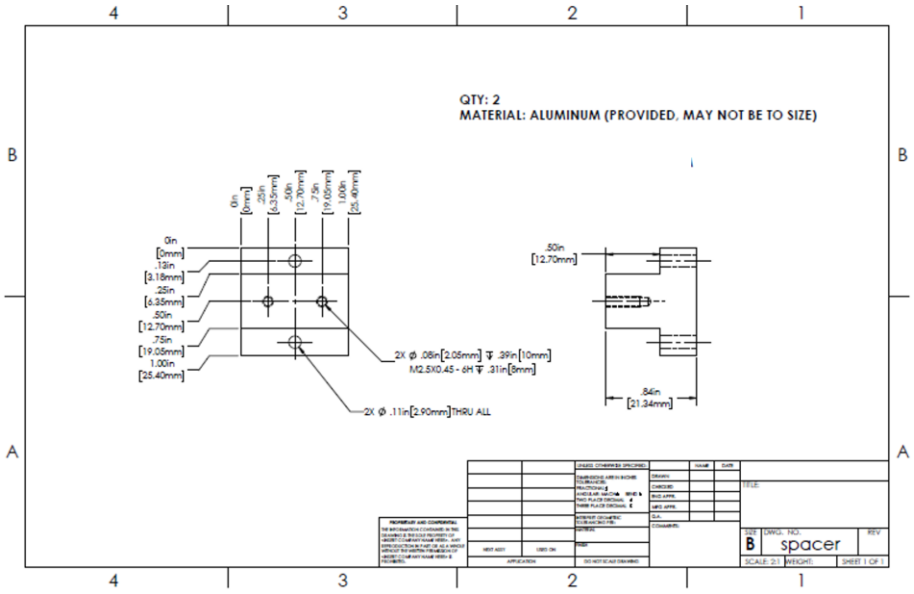

Figure 0.8: Spacer used to attach to left/right hand side of ion transfer box to support a commercially available latch which spanned from spacers to catch plates, where the latch catch was fixed.

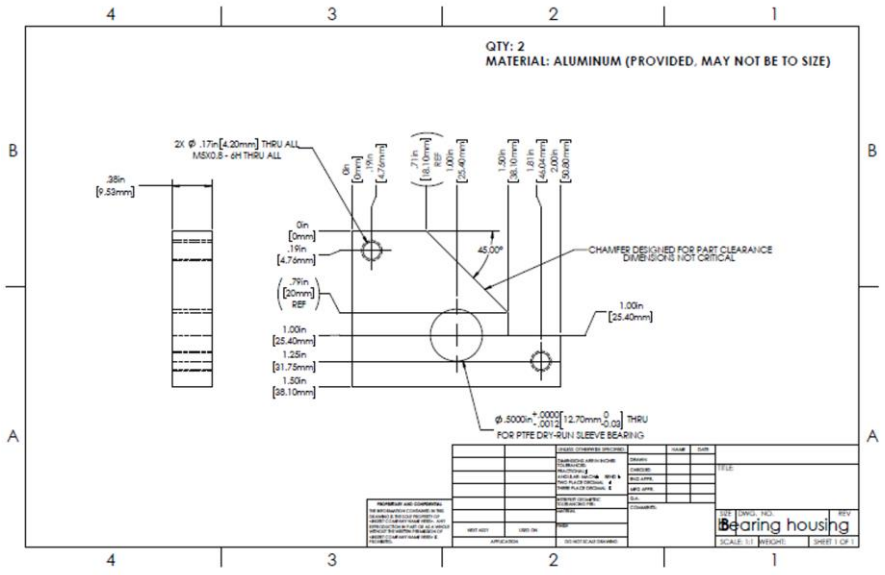

Figure 0.9: Bushing housing, for pressfit of plastic bushing. Two of these parts attach to the bearing cross bar.

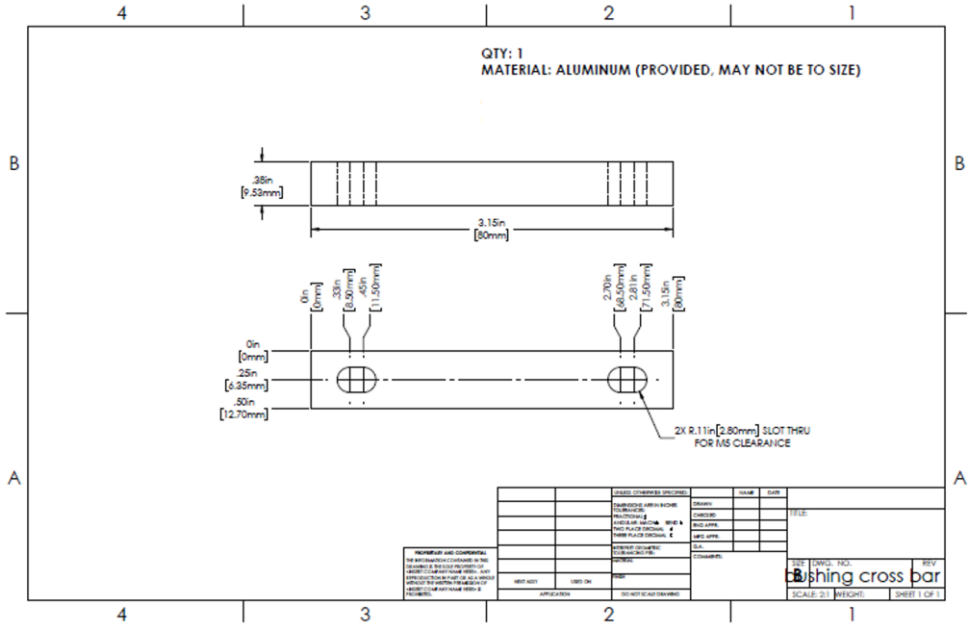

Figure 0.10: Bushing cross bar, used to allow for adjustments of the mounting interface after installation.

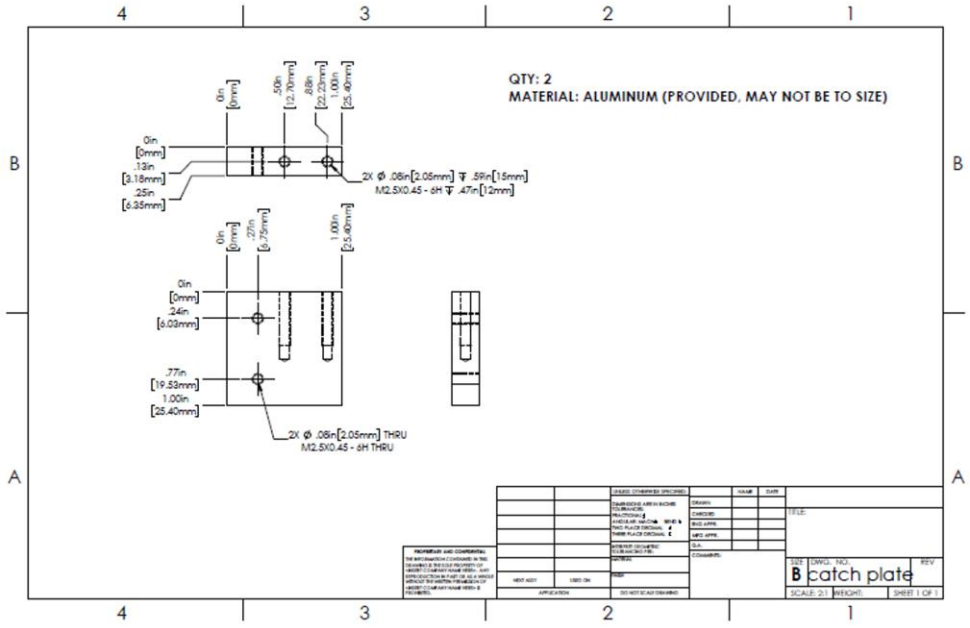

Figure 0.11: Catch plate used to mount latch catch to MS supports.

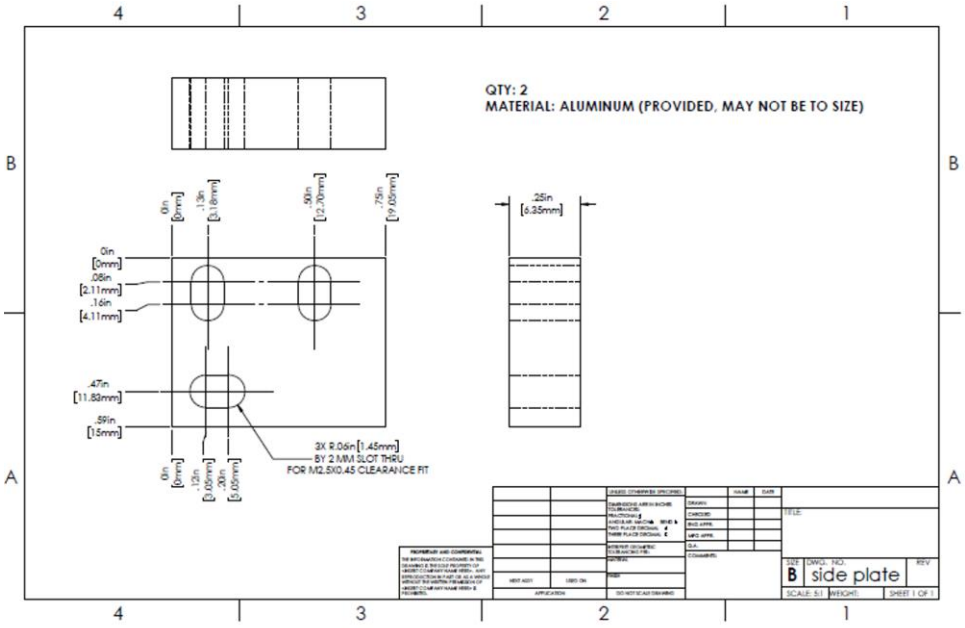

Figure 0.12: Side plate used to attach to vertical shafts and to support catch plate with build in adjustment capability in the form of slotted holes.

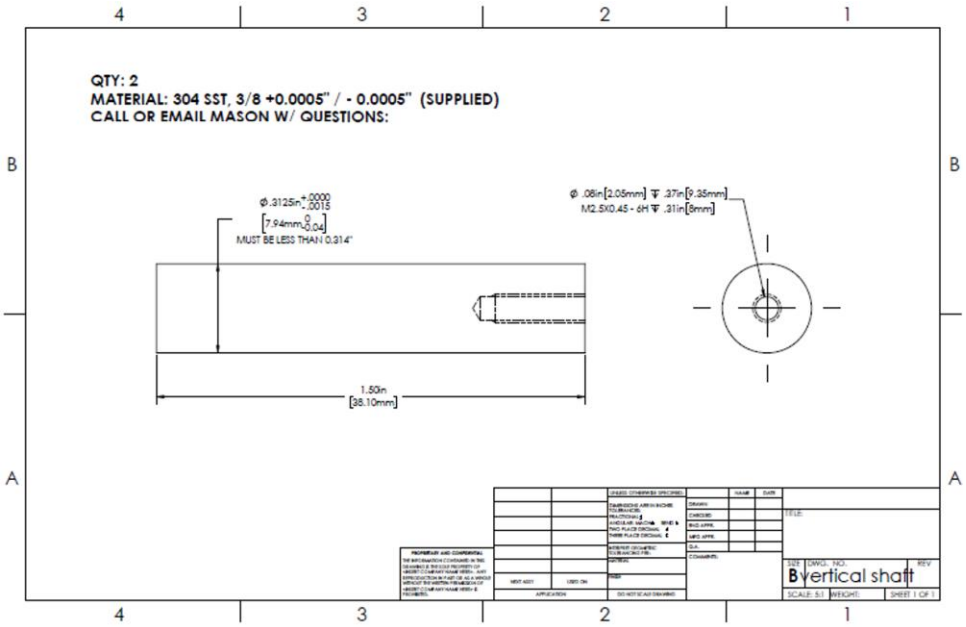

Figure 0.13: Shaft used to support ion transfer box on MS side. This shaft functions in slot without safety override ball detent.

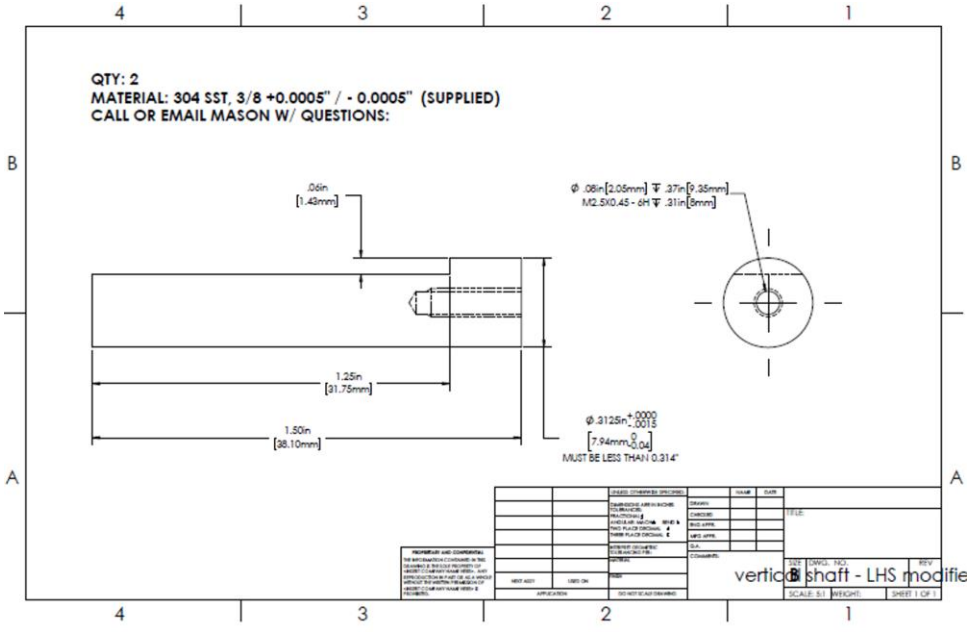

Figure 0.14: This modified version of the shaft is used to allow room for the ball detent safety override in the QE plus model.

REFERENCES

1. Thiel, K.A., *Biomanufacturing, from bust to boom... to bubble?* Nature biotechnology, 2004. **22**(11): p. 1365.

2. Iyer Nisha, R., S. Wilems Thomas, and E. Sakiyama-Elbert Shelly, *Stem cells for spinal cord injury: Strategies to inform differentiation and transplantation.* Biotechnology and Bioengineering, 2016. **114**(2): p. 245-259.

3. Kaiser, A.D., et al., *Towards a commercial process for the manufacture of genetically modified T cells for therapy.* Cancer Gene Therapy, 2015. **22**: p. 72.

4. Oettgen, P., *Cardiac Stem Cell Therapy.* Circulation, 2006. **114**(4): p. 353.

5. Poulos, J., *The limited application of stem cells in medicine: a review.* Stem Cell Research & Therapy, 2018. **9**(1): p. 1.

6. Aijaz, A., et al., *Biomanufacturing for clinically advanced cell therapies.* Nature Biomedical Engineering, 2018. **2**(6): p. 362.

7. Mucida, D., et al., *Reciprocal T_H17 and Regulatory T Cell Differentiation Mediated by Retinoic Acid.* Science, 2007. **317**(5835): p. 256.

8. Agarwal, S. and A. Rao, *Modulation of Chromatin Structure Regulates Cytokine Gene Expression during T Cell Differentiation.* Immunity, 1998. **9**(6): p. 765-775.

9. Albrecht, S., et al., *Proteomics in biomanufacturing control: Protein dynamics of CHO-K1 cells and conditioned media during apoptosis and necrosis.* Biotechnology and Bioengineering, 2018. **115**(6): p. 1509-1520.

10. Abu-Absi, N.R., et al., *Real time monitoring of multiple parameters in mammalian cell culture bioreactors using an in-line Raman spectroscopy probe.* Biotechnology and bioengineering, 2011. **108**(5): p. 1215-1221.

11. Biechele, P., et al., *Sensor systems for bioprocess monitoring.* Engineering in Life Sciences, 2015. **15**(5): p. 469-488.

12. Zhao, L., et al., *Advances in process monitoring tools for cell culture bioprocesses.* Engineering in Life Sciences, 2015. **15**(5): p. 459-468.

13. Forcinio, H., *Pharmaceutical industry embraces NIR technology.* Spectroscopy, 2003. **18**(9).

14. Odeleye Akinlolu Oyekunle, O., et al., *Development of an optical system for the non-invasive tracking of stem cell growth on microcarriers.* Biotechnology and Bioengineering, 2017. **114**(9): p. 2032-2042.

15. Rice, W.L., D.L. Kaplan, and I. Georgakoudi, *Two-Photon Microscopy for Non-Invasive, Quantitative Monitoring of Stem Cell Differentiation.* PLOS ONE, 2010. **5**(4): p. e10075.

16. Wang, M., et al., *Microarray-based gene expression analysis as a process characterization tool to establish comparability of complex biological products: Scale-up of a whole-cell immunotherapy product.* Biotechnology and Bioengineering, 2009. **104**(4): p. 796-808.

17. Kirouac, D.C. and P.W. Zandstra, *The Systematic Production of Cells for Cell Therapies.* Cell Stem Cell, 2008. **3**(4): p. 369-381.

18. Levine, B.L., et al., *Global manufacturing of CAR T cell therapy.* Molecular Therapy-Methods & Clinical Development, 2017. **4**: p. 92-101.

19. Duncan, M.W., et al., *Applications of MALDI Mass Spectrometry in Clinical Chemistry.* Clinical Chemistry, 2016. **62**(1): p. 134-143.

20. El-Aneed, A., A. Cohen, and J. Banoub, *Mass spectrometry, review of the basics: electrospray, MALDI, and commonly used mass analyzers.* Applied Spectroscopy Reviews, 2009. **44**(3): p. 210-230.

21. Feng, X., et al., *Mass spectrometry in systems biology: an overview.* Mass spectrometry reviews, 2008. **27**(6): p. 635-660.

22. Fenn, J.B., et al., *ELECTROSPRAY IONIZATION FOR MASS-SPECTROMETRY OF LARGE BIOMOLECULES.* Science, 1989. **246**(4926): p. 64-71.

23. Vaughn Cecily, P., et al., *Identification of proteins released by follicular lymphoma-derived cells using a mass spectrometry-based approach.* PROTEOMICS, 2006. **6**(10): p. 3223-3230.

24. Matallana-Surget, S., B. Leroy, and R. Wattiez, *Shotgun proteomics: concept, key points and data mining.* Expert review of proteomics, 2010. **7**(1): p. 5-7.

25. Doerr, A., *Navigating the negative-mode proteome.* Mol. Cell. Proteomics, 2015.

26. Kebarle, P., *A brief overview of the present status of the mechanisms involved in electrospray mass spectrometry.* Journal of mass spectrometry, 2000. **35**(7): p. 804-817.

27. Kebarle, P. and U.H. Verkerk, *Electrospray: from ions in solution to ions in the gas phase, what we know now.* Mass spectrometry reviews, 2009. **28**(6): p. 898-917.

28. Sterling, H.J., et al., *Effects of Buffer Loading for Electrospray Ionization Mass Spectrometry of a Noncovalent Protein Complex that Requires High Concentrations of Essential Salts.* Journal of the American Society for Mass Spectrometry, 2010. **21**(6): p. 1045-1049.

29. Stubblefield, E. and G.C. Mueller, *Effects of Sodium Chloride Concentration on Growth, Biochemical Composition, and Metabolism of HeLa Cells.* Cancer Research, 1960. **20**(11): p. 1646-1655.

30. Tubaon, R.M., P.R. Haddad, and J.P. Quirino, *Sample Clean-up Strategies for ESI Mass Spectrometry Applications in Bottom-up Proteomics: Trends from 2012 to 2016.* PROTEOMICS, 2017. **17**(20): p. 1700011-n/a.

31. Xiang, F., et al., *An Integrated Microfabricated Device for Dual Microdialysis and On-Line ESI-Ion Trap Mass Spectrometry for Analysis of Complex Biological Samples.* Analytical Chemistry, 1999. **71**(8): p. 1485-1490.

32. Paul, S.K., *Culture Media.* Language, 1980.

33. Olivero, D., M. LaPlaca, and P.A. Kottke, *Ambient Nanoelectrospray Ionization with In-Line Microdialysis for Spatially Resolved Transient Biochemical Monitoring within Cell Culture Environments.* Analytical Chemistry, 2012. **84**(4): p. 2072-2075.

34. Tibavinsky, I.A., P.A. Kottke, and A.G. Fedorov, *Microfabricated Ultrarapid Desalting Device for Nanoelectrospray Ionization Mass Spectrometry.* Analytical Chemistry, 2015. **87**(1): p. 351-356.

35. Karmacharya, J.B., *Good Manufacturing Practices (GMP) for Medicinal Products.* Promising Pharmaceuticals, 2014: p. 101-148.

36. Teixeira, A.P., et al., *Advances in on-line monitoring and control of mammalian cell cultures: Supporting the PAT initiative.* Biotechnology Advances, 2009. **27**(6): p. 726-732.

37. Lai, Y., A. Asthana, and W.S. Kisaalita, *Biomarkers for simplifying HTS 3D cell culture platforms for drug discovery: the case for cytokines.* Drug Discovery Today, 2011. **16**(7): p. 293-297.

38. Maude, S.L., et al., *CD19-targeted chimeric antigen receptor T-cell therapy for acute lymphoblastic leukemia.* Blood, 2015. **125**(26): p. 4017.

39. Coronel, A., et al., *Cytokine production and T-cell activation by macrophage–dendritic cells generated for therapeutic use.* British Journal of Haematology, 2001. **114**(3): p. 671-680.

40. *Dispersion of soluble matter in solvent flowing slowly through a tube.* Proceedings of the Royal Society of London. Series A. Mathematical and Physical Sciences, 1953. **219**(1137): p. 186.

41. Kirby, B.J., *Micro-and nanoscale fluid mechanics: transport in microfluidic devices*. 2010: Cambridge university press.

42. Garimella, S., et al., *Gas-flow assisted ion transfer for mass spectrometry.* Journal of Mass Spectrometry, 2012. **47**(2): p. 201-207.

43. Tibavinsky, I.A., *A microfabricated rapid desalting device for integration with electrospraying tip*. 2014, Georgia Institute of Technology.

44. Jessensky, O., F. Müller, and U. Gösele, *Self-organized formation of hexagonal pore arrays in anodic alumina.* Applied Physics Letters, 1998. **72**(10): p. 1173-1175.

45. Hoofnagle, A.N. and M.H. Wener, *The fundamental flaws of immunoassays and potential solutions using tandem mass spectrometry.* Journal of immunological methods, 2009. **347**(1-2): p. 3-11.

46. Yates, J.R., C.I. Ruse, and A. Nakorchevsky, *Proteomics by mass spectrometry: approaches, advances, and applications.* Annual review of biomedical engineering, 2009. **11**: p. 49-79.

47. Iavarone, A.T. and E.R. Williams, *Supercharging in electrospray ionization: effects on signal and charge.* International Journal of Mass Spectrometry, 2002. **219**(1): p. 63-72.

48. Teo, C.A. and W.A. Donald, *Solution Additives for Supercharging Proteins beyond the Theoretical Maximum Proton-Transfer Limit in Electrospray Ionization Mass Spectrometry.* Analytical Chemistry, 2014. **86**(9): p. 4455-4462.

49. Iavarone, A.T. and E.R. Williams, *Mechanism of Charging and Supercharging Molecules in Electrospray Ionization.* Journal of the American Chemical Society, 2003. **125**(8): p. 2319-2327.

50. Keller, B.O., et al., *Interferences and contaminants encountered in modern mass spectrometry.* Analytica Chimica Acta, 2008. **627**(1): p. 71-81.

51. Liu, C., et al., *On-Line Microdialysis Sample Cleanup for Electrospray Ionization Mass Spectrometry of Nucleic Acid Samples.* Analytical Chemistry, 1996. **68**(18): p. 3295-3299.

52. Jakubowski Jennifer, A., G. Hatcher Nathan, and V. Sweedler Jonathan, *Online microdialysis-dynamic nanoelectrospray ionization-mass spectrometry for monitoring neuropeptide secretion.* Journal of Mass Spectrometry, 2005. **40**(7): p. 924-931.

53. Cech, N.B. and C.G. Enke, *Practical implications of some recent studies in electrospray ionization fundamentals.* Mass Spectrom Rev, 2001. **20**(6): p. 362-87.

54. Konerman, L., *Addressing a Common Misconception: Ammonium Acetate as Neutral pH "Buffer" for Native Electrospray Mass Spectrometry.* Journal of The American Society for Mass Spectrometry, 2017. **28**(9): p. 1827-1835.

55. Abbassi-Ghadi, N., et al., *A Comparison of DESI-MS and LC-MS for the Lipidomic Profiling of Human Cancer Tissue.* Journal of The American Society for Mass Spectrometry, 2016. **27**(2): p. 255-264.

56. Rush Michael, D. and B. Breemen Richard, *Role of ammonium in the ionization of phosphatidylcholines during electrospray mass spectrometry.* Rapid Communications in Mass Spectrometry, 2016. **31**(3): p. 264-268.

57. Cassou, C.A. and E.R. Williams, *Desalting protein ions in native mass spectrometry using supercharging reagents.* Analyst, 2014. **139**(19): p. 4810-4819.

58. Lomeli, S.H., et al., *New Reagents for Increasing ESI Multiple Charging of Proteins and Protein Complexes.* Journal of the American Society for Mass Spectrometry, 2010. **21**(1): p. 127.

59. Pinho, S.P. and E.A. Macedo, *Solubility of NaCl, NaBr, and KCl in Water, Methanol, Ethanol, and Their Mixed Solvents.* Journal of Chemical & Engineering Data, 2005. **50**(1): p. 29-32.

60. Hogan Jr, C.J., et al., *Ion mobility–mass spectrometry of phosphorylase B ions generated with supercharging reagents but in charge-reducing buffer.* Physical Chemistry Chemical Physics, 2010. **12**(41): p. 13476-13483.

61. Pavlovic, Z., et al. *A synthetic anti-Frizzled antibody engineered for broadened specificity exhibits enhanced anti-tumor properties*. in *MAbs*. 2018. Taylor & Francis.

62. Kshitiz, et al., *Dynamic secretome of bone marrow-derived stromal cells reveals a cardioprotective biochemical cocktail.* Proceedings of the National Academy of Sciences, 2019: p. 201902598.

63. Siegel, G., et al., *Phenotype, donor age and gender affect function of human bone marrow-derived mesenchymal stromal cells.* BMC medicine, 2013. **11**(1): p. 146.

64. Gregory, C.A., et al., *An Alizarin red-based assay of mineralization by adherent cells in culture: comparison with cetylpyridinium chloride extraction.* Analytical biochemistry, 2004. **329**(1): p. 77-84.

65. Martens, L., et al., *mzML—a community standard for mass spectrometry data.* Molecular & Cellular Proteomics, 2011. **10**(1): p. R110. 000133.

66. Holman, J.D., D.L. Tabb, and P. Mallick, *Employing ProteoWizard to convert raw mass spectrometry data.* Current protocols in bioinformatics, 2014. **46**(1): p. 13.24. 1-13.24. 9.

67. Hrdlickova Kuckova, S., et al., *Evaluation of mass spectrometric data using principal component analysis for determination of the effects of organic lakes on*

protein binder identification. Journal of Mass Spectrometry, 2015. **50**(11): p. 1270-1278.

68. Cejnar, P., et al., *Principal component analysis of normalized full spectrum mass spectrometry data in multiMS-toolbox: An effective tool to identify important factors for classification of different metabolic patterns and bacterial strains.* Rapid Communications in Mass Spectrometry, 2018. **32**(11): p. 871-881.

69. Chang, C.-P., et al., *Hypoxic preconditioning enhances the therapeutic potential of the secretome from cultured human mesenchymal stem cells in experimental traumatic brain injury.* Clinical Science, 2013. **124**(3): p. 165-176.

70. Paul, G. and S.V. Anisimov, *The secretome of mesenchymal stem cells: potential implications for neuroregeneration.* Biochimie, 2013. **95**(12): p. 2246-2256.

71. Quarles, L.D., et al., *Distinct proliferative and differentiated stages of murine MC3T3-E1 cells in culture: An in vitro model of osteoblast development.* Journal of Bone and Mineral Research, 1992. **7**(6): p. 683-692.

72. Chilmonczyk, M.A., et al., *Dynamic mass spectrometry probe for electrospray ionization mass spectrometry monitoring of bioreactors for therapeutic cell manufacturing.* Biotechnology and bioengineering, 2019. **116**(1): p. 121-131.

73. Siddhanti, S.R. and L.D. Quarles, *Molecular to pharmacologic control of osteoblast proliferation and differentiation.* Journal of cellular biochemistry, 1994. **55**(3): p. 310-320.

74. Choi, J.Y., et al., *Expression patterns of bone-related proteins during osteoblastic differentiation in MC3T3-E1 cells.* Journal of cellular biochemistry, 1996. **61**(4): p. 609-618.

75. Coetzee, M., M. Haag, and M.C. Kruger, *Effects of arachidonic acid and docosahexaenoic acid on differentiation and mineralization of MC3T3-E1 osteoblast-like cells.* Cell Biochemistry and Function: Cellular biochemistry and its modulation by active agents or disease, 2009. **27**(1): p. 3-11.

76. Kriebitzsch, C., et al., *1, 25-dihydroxyvitamin D3 influences cellular homocysteine levels in murine preosteoblastic MC3T3-E1 cells by direct regulation of cystathionine β-synthase.* Journal of Bone and Mineral Research, 2011. **26**(12): p. 2991-3000.

77. Wang, D., et al., *Isolation and characterization of MC3T3-E1 preosteoblast subclones with distinct in vitro and in vivo differentiation/mineralization potential.* Journal of Bone and Mineral Research, 1999. **14**(6): p. 893-903.

78. Xu, Z., et al., *Isolation and Characterization of Peptides from Mytilus edulis with Osteogenic Activity in Mouse MC3T3-E1 Preosteoblast Cells.* Journal of agricultural and food chemistry, 2019. **67**(5): p. 1572-1584.

79. Yokota, K., et al., *Stimulation of prostaglandin E2 synthesis in cloned osteoblastic cells of mouse (MC3T3-E1) by epidermal growth factor.* Journal of Biological Chemistry, 1986. **261**(33): p. 15410-15415.

80. Harrison, R.P., et al., *Chimeric antigen receptor–T cell therapy manufacturing: modelling the effect of offshore production on aggregate cost of goods.* Cytotherapy, 2019. **21**(2): p. 224-233.

81. Galipeau, J., et al., *International Society for Cellular Therapy perspective on immune functional assays for mesenchymal stromal cells as potency release criterion for advanced phase clinical trials.* Cytotherapy, 2016. **18**(2): p. 151-159.

82. Adiga, S., et al., *Nanoporous materials for biomedical devices.* JOM, 2008. **60**(3): p. 26-32.

83. Parameswaran, N. and S. Patial, *Tumor necrosis factor-α signaling in macrophages.* Critical reviews in eukaryotic gene expression, 2010. **20**(2): p. 87-103.

84. O'Sullivan, J.P. and G.C. Wood, *The Morphology and Mechanism of Formation of Porous Anodic Films on Aluminium.* Proceedings of the Royal Society of London. Series A, Mathematical and Physical Sciences, 1970. **317**(1531): p. 511-543.

85. Zhang, F., et al., *Nano-porous anodic aluminium oxide membranes with 6–19 nm pore diameters formed by a low-potential anodizing process.* Nanotechnology, 2007. **18**(34): p. 345302.

86. Thompson, G.E. and G.C. Wood, *Porous anodic film formation on aluminium.* Nature, 1981. **290**(5803): p. 230-232.

87. Jokinen, V. and S. Franssila, *Capillarity in microfluidic channels with hydrophilic and hydrophobic walls.* Microfluidics and Nanofluidics, 2008. **5**(4): p. 443-448.

88. Li, S., et al., *Fabrication of micronozzles using low-temperature wafer-level bonding with SU-8.* Journal of Micromechanics and Microengineering, 2003. **13**(5): p. 732.

89. Tuomikoski, S. and S. Franssila, *Free-standing SU-8 microfluidic chips by adhesive bonding and release etching.* Sensors and Actuators A: Physical, 2005. **120**(2): p. 408-415.

90. Nemani, K.V., et al., *In vitro and in vivo evaluation of SU-8 biocompatibility.* Mater Sci Eng C Mater Biol Appl, 2013. **33**(7): p. 4453-9.

91. Carlier, J., et al., *Integrated microfabricated systems including a purification module and an on-chip nano electrospray ionization interface for biological analysis.* Journal of Chromatography A, 2005. **1071**(1–2): p. 213-222.

92. Tao, S.L., et al., *Surface Modification of SU-8 for Enhanced Biofunctionality and Nonfouling Properties.* Langmuir, 2008. **24**(6): p. 2631-2636.